

Doctoral Thesis

**Analysis of TRP channel functions in sensory neurons
and microglia**

Nishimoto, Rei

SOKENDAI (The Graduate University for Advanced Studies)

School of Life Science

Department of Physiological Sciences

2016

Table of contents

| | |
|-------------------------------|---|
| 1. Summary | 3 |
| 2. Overall introduction | 5 |

Chapter I.

| | |
|---|----|
| Propofol-induced pain sensation involves multiple mechanisms in sensory neurons | 8 |
| I-1. Introduction | 9 |
| I-2. Materials and Methods | 12 |
| I-2-1. Animals | 12 |
| I-2-2. Isolation of dorsal root ganglion (DRG) cells | 12 |
| I-2-3. Electrophysiology | 13 |
| I-2-4. Ca²⁺ imaging | 14 |
| I-2-5. Pain-related behaviors using Wt and V1A1DKO mice | 14 |
| I-2-6. Chemicals | 15 |
| I-2-7. Statistical analysis | 16 |
| I-3. Results | 17 |
| I-3-1. Patch-clamp studies of propofol-evoked TRP channel currents | 17 |
| I-3-2. The effects of propofol on mouse DRG cells | 18 |
| I-3-3. Involvement of GABA_A receptors and voltage-gated Ca²⁺ channels in propofol-induced [Ca²⁺]_i increases in V1A1DKO DRG cells | 20 |
| I-3-4. Propofol-induced depolarization of mouse DRG cells through GABA_A receptor activation | 21 |
| I-3-5. Effects of propofol on pain-related behaviors in mice | 22 |
| I-4. Discussion | 24 |
| I-5. Figure Legends | 28 |
| I-6. Figures | 31 |

Chapter II.

| | |
|---|----|
| Temperature-dependent microglia movement and the involvement of thermosensitive TRP channels | 37 |
| II-1. Introduction | 38 |
| II-2. Materials and Methods | 44 |

| | |
|---|----|
| II-2-1. Animals | 44 |
| II-2-2. Construction of expression vectors | 44 |
| II-2-3. Cell culture | 45 |
| II-2-4. Time-lapse imaging and quantitative analysis of microglia movement | 48 |
| II-2-5. Electrophysiology | 50 |
| II-2-6. siRNA knockdown of TRPM4 expression in primary microglia | 51 |
| II-2-7. Immunostaining | 51 |
| II-2-8. RT-PCR and quantitative RT-PCR | 53 |
| II-2-9. Chemicals | 54 |
| II-2-10. Statistical analysis | 54 |
| II-3. Results | 56 |
| II-3-1. Confirmation of the purity of microglia cultures | 56 |
| II-3-2. Temperature-dependent microglia movement revealed by time-lapse imaging | 56 |
| II-3-3. The screening of thermosensitive TRP channels expressed in microglia ... | 58 |
| II-3-4. Time-lapse imaging using <i>Trpm2</i> - and <i>Trpv4</i> -knockout microglia | 59 |
| II-3-5. The expression of TRPM4 in microglia assessed by immunocytochemistry | 60 |
| II-3-6. The channel properties of TRPM4 in a heterologous expression system | 61 |
| II-3-7. 9-phenanthrol inhibits heat-evoked currents in microglia in the presence of high intracellular free Ca ²⁺ | 62 |
| II-3-8. The 9-phenanthrol effects on microglia movement | 64 |
| II-3-9. Evaluation of the involvement of voltage-gated proton channels in microglia movement | 66 |
| II-4. Discussion | 68 |
| II-5. Figure Legends | 76 |
| II-6. Figures | 82 |
| | |
| 3. Abbreviations | 94 |
| 4. Acknowledgements | 97 |
| 5. References | 98 |

1. Summary

Sensing is a fundamental ability of all the organisms. Regardless of the character of the signals we sense, they bring us beneficial information to make decisions, such as ‘Go’ or ‘No Go’. Similarly, sensing environmental changes is an essential function at the cellular level. Transient receptor potential (TRP) channels are involved in a wide variety of sensing functions in the human body, including pain and temperature sensations. I focused on TRP channel functions involved in the mechanism of pain sensation induced by propofol, a general anesthetic drug (Chapter I) and the mechanism of temperature-dependent microglial motility (Chapter II).

Chapter I.

Propofol-induced pain sensation involves multiple mechanisms in sensory neurons

Propofol, a commonly used intravenous anesthetic agent, is known to sometimes cause pain sensation upon injection in humans. However, the molecular mechanisms underlying this effect are not fully understood. Although propofol was reported to activate human TRP ankyrin 1 (TRPA1), its action on human TRP vanilloid 1 (TRPV1), another nociceptive receptor, is unknown. Furthermore, whether propofol activates TRPV1 in rodents is controversial. In this study, I found that propofol activated human and mouse TRPA1. In contrast, I did not observe propofol-evoked human TRPV1 activation, whereas the ability of propofol to activate mouse TRPV1 was very small. I also found that propofol caused increases in intracellular Ca^{2+} concentrations in a considerable portion of dorsal root ganglion (DRG) cells from mice lacking both TRPV1 and TRPA1, indicating the existence of TRPV1- and TRPA1-independent mechanisms for propofol action. In addition, propofol produced action potentials in a manner dependent on a type A γ -amino butyric acid (GABA_A) receptor. Finally, I found that both T-type and L-type voltage-gated Ca^{2+} channels were activated downstream of

GABA_A receptor activation by propofol. Thus, propofol may cause pain sensation through multiple mechanisms involving not only TRPV1 and TRPA1 but also voltage-gated channels downstream of GABA_A receptor activation. These findings might provide effective approaches for the prevention of propofol-induced pain sensation and the development of treatments.

Chapter II.

Temperature-dependent microglia movement and the involvement of thermosensitive TRP channels

Microglia are resident immune cells in the brain that play important roles in its maintenance. Under physiological conditions, they survey the surrounded area where neurons and other glial cells exist with highly motile processes. They also transform into the activated phenotype in response to the environmental changes under pathological conditions such as brain damage, injury or inflammations. Therapeutic hypothermia is an effective treatment for neural protection in the clinical field and also suppresses microglial functions such as cytokine release. However, there are few studies focusing on the molecular basis involved in the changes of microglial function in therapeutic hypothermia. Here, I found that microglia movement is temperature-dependent. In addition, I found suggestions that TRPM4 activation was involved in the temperature-dependent microglia movement. First, I observed TRPM4 expression in mouse microglia not only at the mRNA level by RT-PCR but also at the protein level by immunocytochemistry. Next, heat-evoked currents in microglia were inhibited by 9-phenanthrol, a TRPM4 inhibitor, in a dose-dependent manner. Finally, I observed that the temperature-dependency of microglia movement was diminished by 9-phenanthrol treatment. These novel findings regarding microglia movement might expand the development of therapeutic disciplines for diseases involving TRPM4.

2. Overall introduction

TRP ion channels serve as cellular sensors

Transient receptor potential (TRP) channels are non-selective cation channels that play important roles in both physiological and pathological conditions. The *trp* gene was identified by genetic screening of a phototransduction mutant of *Drosophila melanogaster* that showed an abnormal response to light stimulus (Gees *et al.*, 2012). The TRP channel superfamily is conserved in yeast, invertebrates and vertebrates and is composed of 28 members that are divided into 7 subfamilies based on their protein sequence homology: canonical or classic (C), vanilloid (V), melastatin (M), polycystin or polycystic kidney disease (P), mucolipin (ML), ankyrin (A) and NO mechanopotential (N), which is only identified in invertebrates (Vennekens *et al.*, 2012). The TRP proteins are constituted by six transmembrane domains and a pore region between the fifth and sixth transmembrane domains with N- and C-termini inside the cytoplasm. The structure was confirmed by recent work showing the 3D structures of TRPV1 and TRPA1 at a higher resolution (~ 4 Å) by single particle analysis with an electron cryo-microscopy (Liao *et al.*, 2013; Paulsen *et al.*, 2015).

The mechanisms activating TRP channels are highly diversified: activation by temperature, by chemical molecules or activation downstream of signal transduction pathways (Vennekens *et al.*, 2012). Additionally, the selectivity and permeability of TRP channels to cations (Na^+ , K^+ , Ca^{2+} , Mg^{2+}) vary depending on the individual channel. Among TRP channels, TRPM4 and TRPM5 are impermeable to divalent cations, whereas TRPV5 and TRPV6 are highly selective for Ca^{2+} (Zheng, 2013). Basically, activation of TRP channels allows a cation flux across the plasma membrane in accordance with the concentration gradient. Due to the much higher extracellular calcium concentration (Islam, 2012) than that inside the cell, activation of TRP channels causes a Ca^{2+} influx, inducing subsequent activation of Ca^{2+} -dependent proteins that

are key molecules in Ca^{2+} -dependent signal pathways (Gees *et al.*, 2010). Simultaneously, such a cation influx itself can cause a depolarization of the membrane, leading to activation of voltage-dependent proteins including voltage-gated channels (Waxman *et al.*, 2014) consecutively. In addition, it is noteworthy that TRP channels are polymodal receptors. When different types of activators exist at the same time, synergistic effects on TRP channel activation can be observed. Namely, the temperature threshold of TRPV1 activation could be lower (35°C) in the presence of a proton (another activator of TRPV1) than in its absence ($\sim 43^{\circ}\text{C}$) (Tominaga *et al.*, 1998). Such a synergistic potentiation of TRP channel activity by diverse stimuli is another intrinsic feature shared by many TRP channels.

TRP channels are widely distributed in a variety of tissues and cell types not only in invertebrates but also in vertebrates as mentioned above (Vennekens *et al.*, 2012; Zheng, 2013). They can be found in the plasma membrane and intracellular membrane of organelles such as lysosomes (Dong *et al.*, 2010; Zheng, 2013). From the perspective of cell types, they can be found in excitable cells such as neurons and non-excitable cells including pancreatic β cells, skin keratinocytes, urothelial cells and macrophages (Talavera *et al.*, 2005; Sokabe *et al.*, 2010; Kashio *et al.*, 2012; Zhou *et al.*, 2013; Kashio *et al.*, 2015; Takayama *et al.*, 2015; Watanabe *et al.*, 2015). In those cells, TRP channels function as sensors for diverse stimuli such as temperature, osmotic pressure and a variety of endogenous molecules such as Ca^{2+} , phosphatidylinositol 4,5-bisphosphate ($\text{PI}(4,5)\text{P}_2$), nucleotides, as well as exogenous stimuli including components of foods or plants (Zheng, 2013). The detection of those stimuli through activation of TRP channels can lead to not only modulation of the homeostatic functions of the cells but also organization of the phenotype from a cellular level to an individual. TRP channels are cellular sensors essential for fundamental functions in living creatures (Vennekens *et al.*, 2012; Zheng, 2013).

In mammals, TRPV1 was discovered as the first ion channel that responded to a thermal stimulus ($>43^{\circ}\text{C}$) (Caterina *et al.*, 1997). Thereafter, some TRP channels were reported as thermosensitive channels that were activated or modulated by physiological range of temperatures. Besides TRPV1, TRPV2 is activated by extremely high temperature ($>52^{\circ}\text{C}$) (Caterina *et al.*, 1999). TRPV3 ($>30\text{-}39^{\circ}\text{C}$) (Peier *et al.*, 2002b; Smith *et al.*, 2002; Xu *et al.*, 2002) and TRPV4 ($\sim 25\text{-}34^{\circ}\text{C}$) (Watanabe *et al.*, 2002; Guler *et al.*, 2002) are involved in the perception of warm temperatures (Benham *et al.*, 2003). TRPM2 ($>35^{\circ}\text{C}$), TRPM4 and TRPM5 ($15\text{-}35^{\circ}\text{C}$) also exhibit temperature-dependency (Talavera *et al.*, 2005; Togashi *et al.*, 2006; Uchida *et al.*, 2013). On the other hand, TRPM8 ($<28^{\circ}\text{C}$) and TRPA1 ($<15^{\circ}\text{C}$) are reportedly cold sensors (Peier *et al.*, 2002a; McKemy *et al.*, 2002), although activation of TRPA1 in mammals by cold temperature is still controversial. The temperature threshold for TRP channel activation is within a physiological range to which the individuals can be exposed. In other words, TRP channels play an important role in sensing the temperature changes at a molecular level as well as an individual level, initiating the modulation of cellular functions and individual behaviors such as avoiding reflexes against noxious heat (Gees *et al.*, 2010). Thus, TRP channels serve as cellular sensors for detecting diverse stimuli. They convert such environmental inputs to electrical signals with cation fluxes across the plasma membrane to modulate cellular functions, leading to considerable changes in functional properties from a cellular level to an individual level.

Chapter I

Propofol-induced pain sensation involves multiple mechanisms in sensory neurons

I-1. Introduction

Propofol (2,6-diisopropylphenol) is one of the most common intravenous drugs in the clinical field used to induce a loss of consciousness (Dundee, 1979). It is known as a modulator and an activator of GABA_A receptors in the central nervous system (Franks, 2006; Alkire *et al.*, 2008), but is also reported to affect the function of glycine receptors in the spinal cord (Yevenes *et al.*, 2011). Many clinicians, including anesthesiologists, use it for sedation and induction or maintenance of general anesthesia in hospitals because of its rapid onset and short-acting duration (Dundee, 1979; Jalota *et al.*, 2011). Although it is valuable for its safe use in clinical medicine, it has a serious side-effect, namely, the production of intense pain upon injection that patients feel along the limbs where propofol flows after injection into the vein (Klement *et al.*, 1991). This distressing effect occurs in more than 20% of adult patients and at a higher rate in children (Tan *et al.*, 1998). In my clinical experience, much more adult patients have complained propofol-induced pain sensation upon its injection. Although many clinical trials have been conducted in efforts to attenuate this side-effect, a solution to reduce such pain has not been established because the precise mechanism of propofol-evoked pain sensation has not been determined (Jalota *et al.*, 2011).

Recent work indicates that TRP channels, especially TRP vanilloid 1 (TRPV1) and TRP ankyrin 1 (TRPA1), which are expressed in peripheral neurons detecting noxious stimuli such as thermal and irritant chemical stimuli (Caterina *et al.*, 1997; Story *et al.*, 2003), are involved in propofol-evoked pain sensation (Fischer *et al.*, 2010; Matta *et al.*, 2008). TRP channels are non-selective cation channels and play important roles in nociception under physiological and pathological situations (Chung *et al.*, 2011). TRPV1 is a polymodal receptor that responds to noxious heat (above 42°C), capsaicin (Cap, a main ingredient of hot chili peppers) and low-pH (Tominaga *et al.*, 1998) at peripheral nerve endings. TRPV1 function is important for the

development of hyperalgesia since mice genetically lacking TRPV1 displayed a decrease in behavioral responses to inflammatory mediator-induced hypersensitivity, such as ATP-induced thermal hyperalgesia (Moriyama *et al.*, 2003). Studies have revealed that TRPV1 function is enhanced by certain kinases such as protein kinase C epsilon (PKC ϵ) (Mandadi *et al.*, 2006; Numazaki *et al.*, 2002) and phosphoinositide 3-kinase (PI3K) (Stein *et al.*, 2006), causing a sensitization of TRPV1 activity. In contrast, the membrane lipid phosphatidylinositol 4,5-bisphosphate (PIP₂) negatively modulates TRPV1 activity (Cao *et al.*, 2013), although basal PIP₂ activity was reported to be essential for TRPV1 activation (Klein *et al.*, 2008). Additionally, it is known that a Ca²⁺-binding protein, calmodulin, is involved in the desensitization of TRPV1 in an extracellular Ca²⁺-dependent manner (Numazaki *et al.*, 2003; Rosenbaum *et al.*, 2004). Overall, TRPV1 has become an intriguing target in the pain research field. In comparison, TRPA1 is a chemical-detecting receptor that responds to irritants and pungent chemicals such as allyl isothiocyanate (AITC) and cinnamaldehyde, which activate TRPA1 via covalent modification of cytosolic cysteine residues (Hinman *et al.*, 2006; Macpherson *et al.*, 2007). TRPA1 is also activated by formalin, which is known to induce tissue damage and inflammation. Furthermore, bradykinin, one of the inflammatory mediators, also activates TRPA1 through activation of bradykinin 2 receptors linked to phospholipase C activation (Chung *et al.*, 2011). It is also reported that TRPA1 is directly activated or modulated by intracellular Ca²⁺ (Zurborg *et al.*, 2007; Wang *et al.*, 2008). Thus, TRPA1 has a polymodal nature to detect various stimuli as does TRPV1. Consequently, these two TRP channels have become important targets in pain research especially for the development of innovative drugs.

Previous studies reported that TRPA1 could be activated by propofol in mice and humans although the involvement of TRPV1 activation in propofol-evoked pain sensation is still

controversial (Matta *et al.*, 2008; Fischer *et al.*, 2010). While propofol was reported to activate GABA_A receptors in mouse dorsal root ganglion (DRG) neurons to increase intracellular Ca²⁺ concentrations ([Ca²⁺]_i), the precise mechanism for [Ca²⁺]_i increases downstream of GABA_A receptor activation remains unclear. In this study, I tried to clarify the molecular mechanisms of propofol-induced pain sensation by focusing on TRPA1, TRPV1 and GABA_A channels. The results were published (Nishimoto *et al.*, 2015).

I-2. Materials and Methods

All procedures involving the care and use of animals were approved by the Institutional Animal Care and Use Committee of the National Institutes of Natural Sciences and carried out in accordance with the National Institutes of Health Guide for the care and use of laboratory animals (NIH publication no. 85-23. Revised 1985).

I-2-1. Animals

C57BL/6Ncr (Wt) mice (5- to 8-weeks-old, SLC) were used as a control. *Trpv1/Trpa1* double-knockout (V1A1DKO) mice were obtained from a mating between *Trpv1*-knockout (V1KO) and *Trpa1*-knockout (A1KO) mice (both were generously provided by Dr. David Julius, UCSF, San Francisco, CA, USA) (Caterina *et al.*, 2000; Bautista *et al.*, 2006), which were backcrossed on a C57BL/6Ncr background. Mice were housed in a controlled environment (12 hrs light/12 hrs dark cycle; room temperature, 22 to 24°C; 50 to 60% relative humidity) with free access to food and water. The genotyping of V1A1DKO mice used for the experiments in Figures 4, 5 and 6 was performed by PCR.

I-2-2. Isolation of dorsal root ganglion (DRG) cells

Mouse DRG (at thoracic and lumbar levels) from each genotype were rapidly dissected and dissociated by incubation at 37°C for 20 min in a solution of culture medium that contained Earle's balanced salts solution (Sigma-Aldrich), FBS (10%, BioWest or Gibco), penicillin-streptomycin (50 mg/mL and 50 units/mL respectively, Gibco), GlutaMAX (2 mM, Gibco), and vitamin solution (1%, Sigma-Aldrich), with 0.25% collagenase type XI (Sigma-Aldrich). Cells were gently triturated using fire-polished Pasteur pipettes and centrifuged in culture medium to separate cells from debris. Cells were resuspended and

plated onto 12-mm cover slips coated with poly-D-lysine (Sigma-Aldrich). The patch-clamp recordings were performed 12 to 24 hrs after the incubation of isolated DRG cells as described in I-2-3. Ca^{2+} -imaging experiments were performed 12 to 20 hrs after the incubation of isolated DRG cells as described in I-2-4.

I-2-3. Electrophysiology

HEK293T cells and isolated mouse DRG cells were used for patch-clamp recordings. HEK293T cells were maintained in D-MEM (Wako) supplemented with 10% FBS (BioWest), penicillin-streptomycin (50 mg/mL and 50 units/mL, respectively, Gibco), and GlutaMAX (2 mM, Gibco) and seeded at a density of 5×10^5 cells per 35-mm dish 24 hrs before transfection. For patch-clamp recordings of HEK293T cells, either 1 μg human TRPA1 (hTRPA1), human TRPV1 (hTRPV1), mouse TRPV1 (mTRPV1), or mouse TRPA1 (mTRPA1) channel expression vector and 0.1 μg pGreen-Lantern 1 vector were transfected into HEK293T cells using Lipofectamine and Plus reagents (Invitrogen). Patch-clamp recordings of HEK293T cells were performed 18 to 36 hrs after the transfection. Mouse DRG cells were prepared as described above. The extracellular solution contained 140 mM NaCl, 5 mM KCl, 2 mM MgCl_2 , 2 mM CaCl_2 , 10 mM HEPES, and 10 mM glucose at pH 7.4 adjusted with NaOH. The intracellular solution for the experiments with HEK293T cells contained 140 mM KCl, 5 mM EGTA, and 10 mM HEPES at pH 7.4 adjusted with KOH. For the recordings of mouse DRG cells, the intracellular solution contained 67 mM KCl, 65 mM K-gluconate, 1.0055 mM CaCl_2 , 1 mM MgCl_2 , 4 mM Mg-ATP, 1 mM 2Na-GTP, 5 mM EGTA, and 10 mM HEPES at pH 7.3 adjusted with KOH. The free Ca^{2+} concentration was 20 nM (calculated by CaBuf; www.kuleuven.be/fysio/trp/cabuf). A Ca^{2+} -free bath solution used in the Ca^{2+} -free experiments was made by removing 2 mM CaCl_2 and adding 5 mM EGTA to the standard bath

solution. Data for analysis were sampled at 10 kHz and filtered at 5 kHz for whole-cell recordings and 2 kHz for single-channel recordings (Axopatch 200B amplifier with pCLAMP software, Molecular Devices). In the experiments with mouse DRG cells at a current-clamp mode, the cells in which the resting potential was under -40 mV were selected. All of the patch-clamp experiments were performed at room temperature. The coverslips were mounted in a chamber connected to a gravity flow system to deliver various stimuli. Chemical stimulation was applied by running a bath solution containing various chemical reagents.

I-2-4. Ca²⁺-imaging

Mouse DRG cells on coverslips were incubated at 37°C for 30 min in culture medium containing 5 μM Fura-2-acetoxymethyl ester (Molecular Probes). The cover slips were washed with a standard bath solution identical to the extracellular solution in the patch-clamp recordings and a Ca²⁺-free bath solution identical to the extracellular solution used in the patch-clamp experiments. Fura-2 fluorescence was measured in a standard bath solution. Fura-2 was excited with 340- and 380-nm wavelength lights and the emission was monitored at 510 nm with a CCD camera, CoolSnap ES (Roper Scientific/Photometrics) at room temperature. Chemical stimulations were applied as described above for the patch-clamp recordings. Data were acquired using IPlab software (Scanalytics) and analyzed with ImageJ software (National Institutes of Health) and Excel software (Microsoft). Ionomycin (5 μM, Sigma-Aldrich) was applied to confirm cell viability and values were normalized to those evoked by ionomycin for each experiment. Cells in which an increase in normalized intensity during propofol application was over 0.2 were considered activated.

I-2-5. Pain-related behaviors using Wt and V1A1KO mice

Male mice (5- to 6-weeks-old) of Wt and V1A1DKO genotypes were used and housed as described above. Mice were placed individually in transparent cages (19.5 x 12 x 12 cm) for at least 30 min before experiments. Ten microliters of 10% dimethyl sulfoxide (DMSO) or propofol (50 mM) was injected into the dorsum of the left hind paw using a 30 G needle (Becton Dickinson) connected with a polyethylene tube (42740, Becton Dickinson) and a 25 μ L Hamilton syringe. DMSO and propofol solutions were prepared for each subject in saline using stock solutions of 100% DMSO and 500 mM propofol, respectively. The mouse behavior was monitored and recorded for 60 min with a digital video camera (HDR-XR520V, Sony Corporation). The time spent licking and biting the injected paw was measured for 2 min after injection. Subjects with prolonged bleeding at the injected site were excluded from analysis.

I-2-6. Chemicals

Chemicals used in this study were purchased as described below. Propofol (2,6-diisopropylphenol), HC-030031, capsaicin, ionomycin, nifedipine, γ -amino butyric acid (GABA), and (+)-bicuculline were from Sigma-Aldrich. Allyl isothiocyanate (AITC) was from Kanto Chemical. Picrotoxin, verapamil hydrochloride, flunarizine dihydrochloride and NNC 55-0396 dihydrochloride were from Tocris. Propofol, picrotoxin, flunarizine, nifedipine, and (+)-bicuculline were dissolved in DMSO as stock solutions. Capsaicin and AITC were dissolved in ethanol and methanol, respectively. The others were dissolved in water. All of the dissolved chemicals were diluted (from 1:10000 to 1:1000) into the solution for the patch-clamp and Ca^{2+} -imaging experiments. The concentration of DMSO did not exceed 0.15%.

I-2-7. Statistical analysis

Data are presented as means \pm standard error of mean (SEM). The abbreviation n indicates the number of data points. The Mann-Whitney *U* test, unpaired *t*-test, Chi-square test, and non-parametric multiple comparison were applied for statistical analyses. P values less than 0.05 were considered significant. Data from the propofol-evoked hTRPA1 current recordings were fitted with a Hill's equation to generate a dose-response curve and EC₅₀ values were calculated. Data related to the inhibitory effect of HC-030031 on propofol-evoked humanTRPA1 currents were fitted by a logistic curve to calculate the IC₅₀ value. All statistical analyses were performed using Origin software (OriginLab).

I-3. Results

I-3-1. Patch-clamp studies of propofol-evoked TRP channel currents

First, I utilized a patch-clamp method to examine propofol actions in HEK293T cells expressing either hTRPA1, mTRPA1, hTRPV1 or mTRPV1. As shown in Figure 1A, 100 μ M of propofol activated both hTRPA1 and mTRPA1 with an outwardly rectifying current-voltage relationship although an increase in currents upon propofol washout was observed in the case of mTRPA1, probably due to the bimodal effects of the compound on mTRPA1. Once large current responses were observed upon propofol application, the following AITC responses were small as previously reported (Lee *et al.*, 2008). Propofol-evoked current activation was observed in relation to mTRPV1, but not hTRPV1, although both hTRPV1 and mTRPV1 responded similarly to capsaicin (Cap, 1 μ M) with clear outward rectification in the same cells, indicating that propofol actions on TRPV1 differ depending on species.

Next, I tried to determine the dose-dependency for the propofol effects on the four TRP channels at -60 mV (Fig. 1B). When I analyzed propofol-evoked currents during the propofol application, I found that propofol was most effective at hTRPA1, in which propofol effects were almost saturated at 100 μ M. The effects of propofol on mTRPA1 exhibited a bell-shape curve, possibly due to its bimodal action. High concentrations of propofol caused small but significant mTRPV1 activation at -60 mV although the current activation looked negligible in Fig. 1A. When the curve of the dose-dependent activation of hTRPA1 by propofol was fitted with a Hill equation, Hill co-efficient and EC_{50} value were 3.3 and 65.4 μ M, respectively (Fig. 1C), representing attainable concentrations in the clinical setting (Doenicke *et al.*, 1996). Surprisingly, 100 μ M propofol did not cause measurable hTRPA1 activation at -60 mV in the absence of extracellular Ca^{2+} , suggesting that propofol-induced hTRPA1 activation requires extracellular Ca^{2+} , similar to the extracellular Ca^{2+} -dependent activation of green anole lizard

TRPA1 by heat (Kurganov *et al.*, 2014) and to the very small propofol-induced inward currents in HEK293 cells expressing rat TRPA1 in the absence of extracellular Ca^{2+} (Matta *et al.*, 2008). Propofol-evoked currents were inhibited reversibly by HC-030031, a specific TRPA1 antagonist, with an IC_{50} value of 1.2 μM , further supporting the notion that propofol activates hTRPA1 (Fig. 1D).

In order to examine whether hTRPA1 is directly activated by propofol in a membrane-delimited manner, I performed single-channel recordings in an inside-out mode of a membrane excised from a HEK293T cell expressing hTRPA1. Clear single-channel openings at a membrane potential of +60 mV were observed upon application of propofol (30 μM), and robust hTRPA1 channel activation by 30 μM AITC was induced in the same patch membrane (Fig. 2A), confirming the hTRPA1 activation by propofol. I next analyzed unitary amplitudes of the single-channel currents activated by propofol by fitting the amplitude histogram with a Gaussian equation, which provided 4.3 ± 0.4 pA and 2.8 ± 0.1 pA at +60 and -60 mV, respectively (Fig. 2B) without measurable currents at 0 mV (data not shown), leading to conductances of 71.7 and 46.7 pS at positive and negative potentials, respectively. These results indicate that propofol can activate hTRPA1 directly and that the intracellular component is not necessary for the mechanism of propofol-induced hTRPA1 activation.

I-3-2. The effects of propofol on mouse DRG cells

Thus far, propofol was shown to directly activate hTRPA1 at a concentration attainable in a clinical setting. To further confirm the ability of propofol to activate TRPA1, I performed Ca^{2+} -imaging experiments using mouse DRG cells. A previous report showed that propofol-induced $[\text{Ca}^{2+}]_i$ increases were not observed in TRPA1-deficient DRG cells (Matta *et al.*, 2008) while another report showed that propofol-induced $[\text{Ca}^{2+}]_i$ increases were still

observed in DRG cells from V1A1DKO mice (Fischer *et al.*, 2010). Some DRG cells from Wt mice responded to propofol (50 μM), and a greater number of cells responded to AITC (100 μM) and/or Cap (1 μM) (Fig. 3A). Such propofol-induced $[\text{Ca}^{2+}]_i$ increases were abolished completely in the absence of extracellular Ca^{2+} (Fig. 3B), indicating that propofol induced $[\text{Ca}^{2+}]_i$ increases through Ca^{2+} influx from outside of the cells. Next, in order to confirm the involvement of TRPV1 and/or TRPA1 in the propofol-induced $[\text{Ca}^{2+}]_i$ increases, I compared the propofol-induced $[\text{Ca}^{2+}]_i$ increases in DRG cells from Wt, A1KO, V1KO and V1A1DKO mice. My patch-clamp studies using HEK293T cells (Fig. 1) suggested that propofol could induce $[\text{Ca}^{2+}]_i$ increases through both TRPV1 and TRPA1 in mouse DRG cells although the TRPA1 contribution looked greater. The propofol-induced $[\text{Ca}^{2+}]_i$ increases were observed in A1KO, V1KO and V1A1DKO DRG cells (Fig. 3C) although the percentage of the propofol-responsive DRG cells was significantly smaller in V1A1DKO compared with Wt, A1KO and V1KO DRG cells (Fig. 3D). This result suggests that propofol actions on mouse DRG cells are almost similar even if either TRPA1 or TRPV1 is genetically abolished, and that both TRPA1 and TRPV1 might be involved in propofol-induced $[\text{Ca}^{2+}]_i$ increases. In this regard, I might underestimate the TRPA1 and TRPV1 activation by 50 μM propofol in mouse DRG cells because my results in Fig. 1 indicate that 50 μM of propofol activates mTRPA1 and mTRPV1 to a much lesser degree than 100 μM AITC and 1 μM Cap, respectively.

To know what kind of differences exist in propofol-induced $[\text{Ca}^{2+}]_i$ increases across each genotype, I compared the maximal intensities of propofol-induced $[\text{Ca}^{2+}]_i$ increases. When the propofol-induced $[\text{Ca}^{2+}]_i$ increases were normalized to the values induced by ionomycin, the values were significantly smaller in A1KO and V1A1DKO DRG cells compared with V1KO DRG cells. This result indicated that TRPA1 is more profoundly involved in propofol-induced $[\text{Ca}^{2+}]_i$ increases compared with TRPV1 (Fig. 3E), consistent with data obtained in the

patch-clamp experiments using HEK293T cells expressing either mTRPV1 or mTRPA1 (Fig. 1). The fact that the propofol-induced $[Ca^{2+}]_i$ increases were still observed in the V1A1DKO DRG cells indicates the existence of another mechanism causing $[Ca^{2+}]_i$ increases by propofol. In order to examine what kinds of DRG cells respond to propofol, I compared cell sizes between propofol-responsive Wt and V1A1DKO DRG cells, the former of which should contain TRPA1- and/or TRPV1-expressing cells. The mean size of the propofol-responsive V1A1DKO DRG cells was $24.9 \pm 0.5 \mu\text{m}$, which was significantly larger than those of the propofol-responsive Wt DRG cells ($21.4 \pm 0.4 \mu\text{m}$). This result suggested that propofol-responsive DRG cells not expressing TRPA1 or TRPV1 are a little larger and could contain A δ fiber neurons.

I-3-3. Involvement of GABA_A receptors and voltage-gated Ca²⁺ channels in propofol-induced $[Ca^{2+}]_i$ increases in V1A1DKO DRG cells

Because propofol is known to act on GABA_A receptors (Orser *et al.*, 1994), GABA_A receptor activation by propofol in DRG cells could cause depolarization. It is well known that intracellular chloride concentrations in DRG cells are quite high due to the lack of potassium chloride cotransporter 2 (KCC2) expression (Mao *et al.*, 2012). Therefore, I hypothesized that depolarization involving GABA_A receptor activation would activate voltage-gated Ca²⁺ channels to cause $[Ca^{2+}]_i$ increases upon propofol application, although such membrane depolarization should also activate voltage-gated Na⁺ channels. In order to confirm the hypothesis, I performed Ca²⁺-imaging experiments using DRG cells from V1A1DKO mice, the use of which excludes the involvement of TRPA1 or TRPV1 in propofol-induced $[Ca^{2+}]_i$ increases. Propofol-induced $[Ca^{2+}]_i$ increases were drastically and reversibly inhibited by picrotoxin (Pic, 100 μM), a GABA_A receptor antagonist (Fig. 4A and D). Another GABA_A

receptor antagonist, (+)-bicuculline (Bic, 30 μM), also inhibited propofol-induced $[\text{Ca}^{2+}]_i$ increases almost completely, indicating that a majority of the TRPV1/TRPA1-independent component of the propofol-induced $[\text{Ca}^{2+}]_i$ increases is caused by GABA_A receptor activation (Fig. 4A and D). Among the voltage-gated Ca^{2+} channels that could be activated by depolarization downstream of GABA_A receptor activation, I first tested two kinds of L-type voltage-gated Ca^{2+} channel inhibitors, verapamil (Ver) and nifedipine (Nif). Both Ver (50 μM) and Nif (10 μM) significantly inhibited propofol-induced $[\text{Ca}^{2+}]_i$ increases while the inhibition by Ver was significantly greater than that by Nif and to the level obtained by Pic (Fig. 4B and D). These data indicated that L-type voltage-gated Ca^{2+} channels are activated downstream of GABA_A receptor activation, although Ver is also known to inhibit T-type voltage-gated Ca^{2+} channels. Therefore, I next examined the effects of T-type voltage-gated Ca^{2+} channel inhibitors flunarizine (Flu) and NNC 55-0396 (NNC) on propofol-induced $[\text{Ca}^{2+}]_i$ increases. Both Flu (50 μM) and NNC (10 μM) reduced propofol-induced $[\text{Ca}^{2+}]_i$ increases, albeit to a lesser extent compared with Ver. Moreover, co-application of Nif and NNC further inhibited propofol-induced $[\text{Ca}^{2+}]_i$ increases compared with Nif or NNC treatment alone (Fig. 4C and D), suggesting that both L-type and T-type voltage-gated Ca^{2+} channels are activated by depolarization upon GABA_A receptor activation.

I-3-4. Propofol-induced depolarization of mouse DRG cells through GABA_A receptor activation

Given that propofol exhibited an ability to cause intracellular $[\text{Ca}^{2+}]_i$ increases in DRG cells through GABA_A receptor activation (as shown in Fig. 4), I performed patch-clamp recordings of GABA-responsive V1A1DKO DRG cells to confirm whether GABA_A receptor activation by propofol causes depolarization of DRG cells. As shown in Fig. 5A, propofol (50 μM) induced

inward currents repeatedly, which could cause depolarization, in a GABA-responsive cell at -60 mV. The propofol-induced inward current was completely inhibited by picrotoxin (100 μ M, n = 4). Furthermore, not only GABA but also propofol depolarized isolated V1A1DKO DRG cells (Fig. 5B upper panel and C, n = 4) followed by action potential generation, whereas such propofol-induced action potential generation observed in V1A1DKO DRG cells was inhibited by picrotoxin (Fig. 5B lower panel, n = 4). These results obtained in my preparations indicate that GABA_A receptor activation by propofol causes action potential generation in mouse DRG cells, suggesting that TRPA1 and TRPV1 are not the sole targets for propofol actions as expected from the results presented in Fig. 3.

I-3-5. Effects of propofol on pain-related behaviors in mice

I attempted to evaluate pain-related behaviors in Wt and V1A1DKO mice given propofol. I chose the method of subcutaneous injection into the mouse hind paw. I selected 50 mM propofol for the behavioral experiments after several preliminary trials with various concentrations. However, I did not find significant differences in licking and biting behaviors among the control groups (10% DMSO) and the propofol-injected groups (50 mM, 10 μ L/site) in Wt and V1A1DKO mice according to an ANOVA analysis over the two minutes following subcutaneous propofol injection (Fig. 6). However, there was a significant difference between WT mice given DMSO and WT mice given propofol with a Student *t*-test (the average \pm SEM of licking and biting time (sec), Wt-DMSO (n = 13): 11.7 \pm 2.9, Wt-prop (n = 14): 21.4 \pm 3.2, V1A1DKO-DMSO (n = 7): 16.3 \pm 2.7, V1A1DKO-prop (n = 7): 17.9 \pm 3.4). Therefore, I am not completely sure whether propofol causes pain sensations in mice upon injection into their hind paw although it appears that it might. This could be due to the limited ability of propofol to activate mouse TRPA1 as shown in Fig. 1, and this could be the reason why there are few

reports of propofol-induced pain-related behaviors in mice injected with propofol in the hind paw.

I-4. Discussion

In the present study, I found that propofol, a widely used anesthetic drug in the clinical field, activates human and mouse TRPA1. On the other hand, I did not observe propofol-evoked human TRPV1 activation although the ability of propofol to activate mouse TRPV1 was very small. In addition, I also found that propofol caused increases in intracellular Ca^{2+} concentrations in a considerable portion of DRG cells from mice lacking both TRPV1 and TRPA1, indicating the existence of TRPV1- and TRPA1-independent mechanisms for propofol action. Finally, I found that both T-type and L-type voltage-gated Ca^{2+} channels were activated downstream of GABA_A receptor activation by propofol, which might be an alternative pathway evoked by propofol in sensory neurons.

Species-dependent variations of propofol effects on TRPV1 and TRPA1 activation

I found that the effects of propofol on TRPV1 varied in a species-dependent manner and that the ability of propofol to activate hTRPV1 is negligible (Fig. 1). These *in vitro* data indicate that hTRPV1 is not involved in propofol-induced pain sensation in humans. Regarding propofol-evoked TRPA1 activation, the ability of propofol to activate hTRPA1 was much greater than mTRPA1, consistent with many reports of propofol-induced pain sensation in humans (Jalota *et al.*, 2011) while there are few reports regarding propofol-induced pain-related behaviors in mice injected with propofol in their hind paws. I also for the first time observed activation of hTRPA1 by propofol at a single-channel level (Fig. 2), indicating the activation of hTRPA1 in a membrane-delimited manner.

Multiple pathways of propofol-induced intracellular Ca^{2+} increases in DRG cells

Propofol-induced pain sensation in patients arises immediately after injection (Jalota *et al.*,

2011; Tan *et al.*, 1998). I hypothesized that such an acute response could be mediated by activation of ion channels expressed in peripheral neurons. Previous reports showed that TRP channels, especially TRPV1 and TRPA1, might be involved in the propofol-induced $[Ca^{2+}]_i$ increases in Ca^{2+} -imaging studies using DRG neurons (Matta *et al.*, 2008; Fischer *et al.*, 2010). However, I found alternative components that responded to propofol in Ca^{2+} -imaging studies using V1A1DKO DRG cells, suggesting that other targets might be involved in the mechanism of propofol-induced $[Ca^{2+}]_i$ increases as well. Regarding the involved molecules mediating propofol-induced $[Ca^{2+}]_i$ increases, I determined that both T-type and L-type voltage-gated Ca^{2+} channels are activated upon depolarization caused by propofol-induced GABA_A receptor activation. T-type voltage-gated Ca^{2+} channels are known to be expressed in small- and medium-sized DRG neurons (Scroggs *et al.*, 1992; Aptel *et al.*, 2007), corresponding to the size of propofol-responsive V1A1DKO DRG cells as shown in Fig. 3F. After depolarization by GABA_A receptor activation, T-type voltage-gated Ca^{2+} channels are expected to be more activated than L-type voltage-gated Ca^{2+} channels, and propofol may thereby induce considerable amounts of depolarization. The effects of verapamil (which inhibits both L-type and T-type voltage-gated Ca^{2+} channels) were similar to effects caused by picrotoxin, indicating that L-type and T-type voltage-gated Ca^{2+} channels are the main targets downstream of depolarization by GABA_A receptor activation, although I cannot rule out the possibility that other proteins are inhibited by verapamil. I examined the effects of strychnine (a glycine receptor inhibitor), ω -agatoxin IVA (an inhibitor for P and Q type voltage-gated Ca^{2+} channels) and ω -conotoxin (an inhibitor for N type voltage-gated Ca^{2+} channel) on the propofol-induced $[Ca^{2+}]_i$ increases, and no effects were observed (unpublished data), ruling out the involvement of those ion channels in the propofol actions.

The proposed mechanism of depolarization of DRG cells by propofol

It is widely believed that many general anesthetics activate GABA_A receptors to produce their anesthetic effects in the brain (Franks, 2006; Alkire *et al.*, 2008; Rudolph *et al.*, 2004; Garcia *et al.*, 2010). In spinal cord neurons, chloride concentrations can be changed dynamically depending on tissue conditions such as injury or inflammation to reduce the expression of Cl⁻ transporters, including KCC2 (Coull *et al.*, 2003). Intracellular Cl⁻ concentrations in neurons are also known to be high in early developmental stages when GABA may excite neurons (Kakazu *et al.*, 1999). In the case of peripheral sensory neurons such as DRG neurons, intracellular Cl⁻ concentrations are high owing to the low expression of KCC2 (Mao *et al.*, 2012), indicating that Cl⁻ channel openings cause depolarization with Cl⁻ efflux. Whether GABA_A receptor activation could cause excitatory responses of peripheral neurons in rodents depends on the intracellular Cl⁻ concentrations (Ault *et al.*, 1994; Stein *et al.*, 2003; Funk *et al.*, 2008). In this regard, it is possible that DRG neurons could be depolarized, followed by action potential generation, through GABA_A receptor activation due to high intracellular Cl⁻ concentrations. Indeed, I clearly observed action potential generation in some V1A1DKO DRG cells during application of propofol, which was drastically reduced by antagonizing GABA_A receptor activity as shown in Fig. 5. Additionally, my *in vitro* study shows that propofol activated hTRPA1 with an EC₅₀ value of 65.4 μM, which is close to the previously reported values of 48 μM in the oocyte system (Usala *et al.*, 2003) and 23 μM in HEK293 cells (Mohammadi *et al.*, 2001) using human GABA_A receptor containing β2 subunits, suggesting that propofol activates not only TRPA1 but also GABA_A receptors within the same concentration ranges if it can reach peripheral nerve endings across blood vessels. Propofol-induced anesthetic effects are mediated by activation of GABA_A receptors containing β2 or β3 subunits, and such effects vary depending on the subunit components of GABA_A

receptors (Jurd *et al.*, 2003; Garcia *et al.*, 2010; Zeller *et al.*, 2005). It was reported that a subset of GABA_A receptors containing $\beta 2/\beta 3$ subunits was expressed in unmyelinated sensory fibers (Carlton *et al.*) and that bilateral effects of GABA_A receptor activation were observed in formalin-induced pain behaviors, meaning that low concentrations of muscimol attenuated while higher concentrations enhanced pain behaviors (Carlton *et al.*, 1999; Funk *et al.*, 2008). Although I did not evaluate the effects of GABA_A receptor activation by propofol on central terminals of DRG neurons or spinal cord neurons, it is possible that propofol might have a considerable influence on peripheral nociception by activating peripheral GABA_A receptors and voltage-gated Ca²⁺ channels in addition to voltage-gated Na⁺ channels.

In conclusion, my study showed that the pain-producing effects of propofol may relate to its actions on both TRPA1 and GABA_A receptors. However, I could not obtain solid evidence supporting the involvement of TRPA1 in the propofol-induced pain behaviors at an *in vivo* level in mice. Importantly, compounds acting on GABA_A receptors in the periphery may be expected to exhibit similar abilities to induce pain sensation through activation of voltage-gated channels.

I-5. Figure Legends

Figure 1.

Effects of propofol on human and mouse TRPA1 and TRPV1

(A) Representative whole-cell current traces in HEK293T cells expressing human TRPA1 (hTRPA1), mouse TRPA1 (mTRPA1), human TRPV1 (hTRPV1) or mouse TRPV1 (mTRPV1) in response to propofol (Prop, 100 or 300 μ M) application. AITC (100 μ M) or capsaicin (Cap, 1 μ M) was applied after propofol. Ramp-pulses from -100 to +100 mV in 300 msec were applied every 3 sec, and current-voltage curves at the time points a, b and c are shown in insets. (B) Dose-dependencies of the effects of propofol on hTRPA1-, mTRPA1-, hTRPV1- and mTRPV1-mediated currents at -60 mV (n = 5-6). *, p < 0.01, analyzed with Mann-Whitney *U* test. (C) Dose-dependencies of the effects of propofol on hTRPA1-mediated currents at -60 mV in the presence and absence of extracellular Ca²⁺ (n = 4-18). (D) Dose-dependent inhibition of propofol-activated hTRPA1 currents by HC-030031 at -60 mV (n = 2-8).

Figure 2.

Propofol-evoked hTRPA1 activation at a single-channel level

(A) A representative single-channel current trace at +60 mV in response to propofol (30 μ M) and AITC (30 μ M). Currents at (a) and (b) are expanded and shown with open channel histograms fitted with a Gaussian equation (red line). C: closed level, O1-3: open levels. (B) Mean unitary amplitudes of the propofol-activated single channels at -60 and +60 mV (n = 3).

Figure 3.

Effects of propofol on intracellular Ca²⁺ concentrations in isolated DRG cells from wild-type (Wt), *Trpa1*-knockout (A1KO), *Trpv1*-knockout (V1KO) and *Trpv1/Trpa1*

double-knockout (V1A1DKO) mice

(A and B) Effects of propofol on intracellular Ca^{2+} concentrations in Wt DRG cells in the presence (A) or absence (B) of extracellular Ca^{2+} . **(C)** Venn-diagrams of the effects of propofol, AITC and capsaicin in Wt, A1KO, V1KO and V1A1DKO DRG cells. The number in each box indicates the percentage of cells responding to each agonist. The number in parentheses in each box indicates the percentage of cells responding to only KCl. **(D and E)** Percentages of propofol-responsive cells (D) and normalized Fura-2 ratios in the propofol-responsive cells (E) in Wt, A1KO, V1KO and V1A1DKO DRG cells. *, $p < 0.05$; **, $p < 0.01$, analyzed with Chi-square test (D) and non-parametric multiple comparison followed by Steel-Dwass test (E). **(F)** Comparison of the propofol-responsive cell sizes between Wt and V1A1DKO DRG. P value was calculated by performing the unpaired *t*-test.

Figure 4.

Effects of antagonists at GABA_A receptors and voltage-gated Ca^{2+} channels on the propofol-evoked changes in intracellular Ca^{2+} concentrations in V1A1DKO DRG cells

(A, B and C) Averaged changes in intracellular Ca^{2+} concentrations (indicated by ratios normalized to that caused by ionomycin) upon propofol application in the presence (colored traces) and absence (black trace) of the indicated compounds in V1A1DKO DRG cells. **(D)** Ratios of the second propofol (Prop_{2nd})-evoked responses (with the indicated compounds) to the first propofol (Prop_{1st})-evoked responses (without the compounds). **, $p < 0.01$ vs. Cont.; ##, $p < 0.01$ vs. Pic, Bic and Ver.; §§, $p < 0.01$ vs. Nif, Flu, and NNC; ††, $p < 0.01$ vs. Pic and Ver, analyzed with non-parametric multiple comparison followed by Steel-Dwass test.

Figure 5.

GABA and propofol induce depolarization and action potential generation in V1A1DKO

DRG cells

(A) A representative trace of GABA- and propofol-induced inward currents in V1A1DKO DRG (n = 4, $C_m = 25.9 \pm 3.8$ pF). Picrotoxin inhibited the propofol-induced inward currents. $V_m = -60$ mV. (B) GABA- and propofol-induced depolarization and action potentials in V1A1DKO DRG cells (n = 6, $C_m = 19.5 \pm 1.3$ pF). Picrotoxin inhibited the propofol-induced action potentials (n = 4, $C_m = 17.0 \pm 0.6$ pF). (C) Traces indicated as (a) and (b) in (B) are expanded as (a) and (b), respectively.

Figure 6.

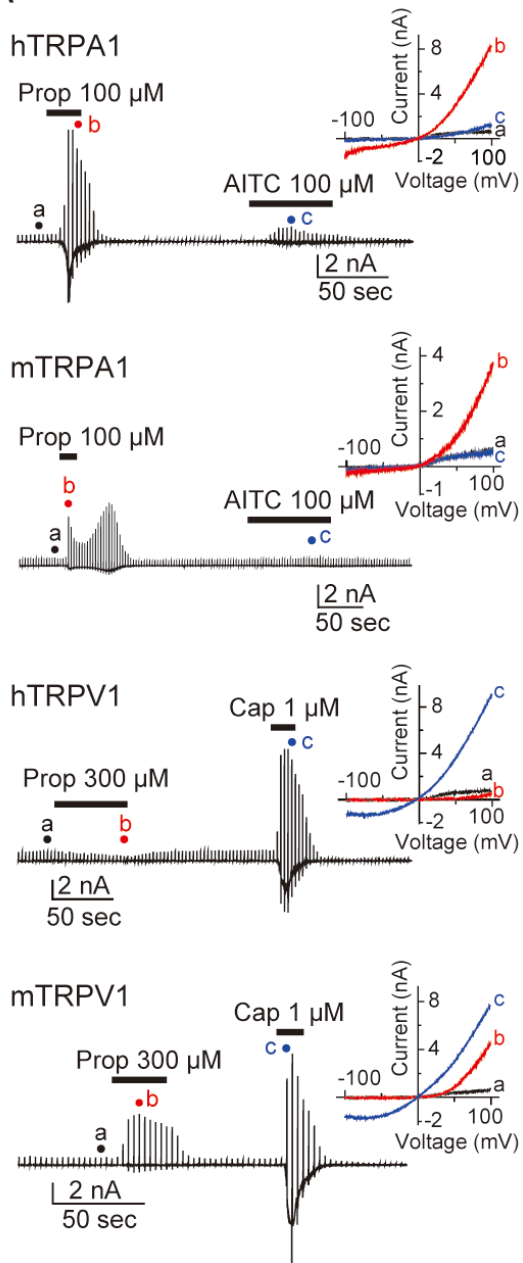
Pain-related behaviors induced by propofol injection into mouse hind paws

The time spent licking or biting induced by injection of 50 mM propofol or 10% DMSO for 2 min in wild-type (Wt) or *Trpv1/Trpa1* double-knockout (V1A1DKO) mice. Wt-DMSO n = 13, Wt-Prop n = 14, V1A1DKO-DMSO n = 7 and V1A1DKO-Prop n = 7. Data represent mean \pm SEM. *, $p < 0.05$, Wt-DMSO versus Wt-Prop, Student *t*-test.

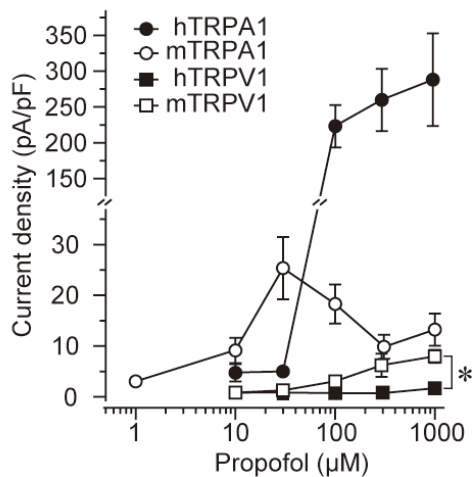
I-6. Figures

Figure 1

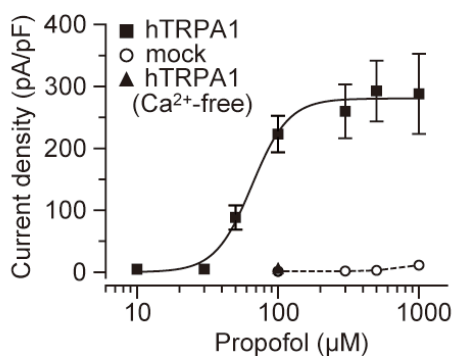
A



B



C



D

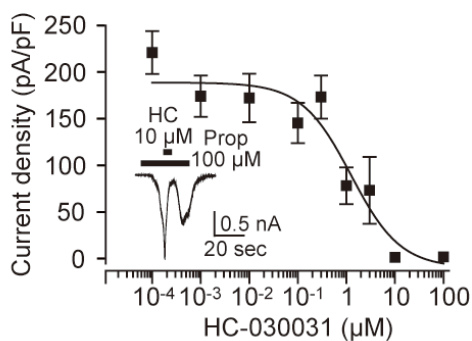


Figure 2

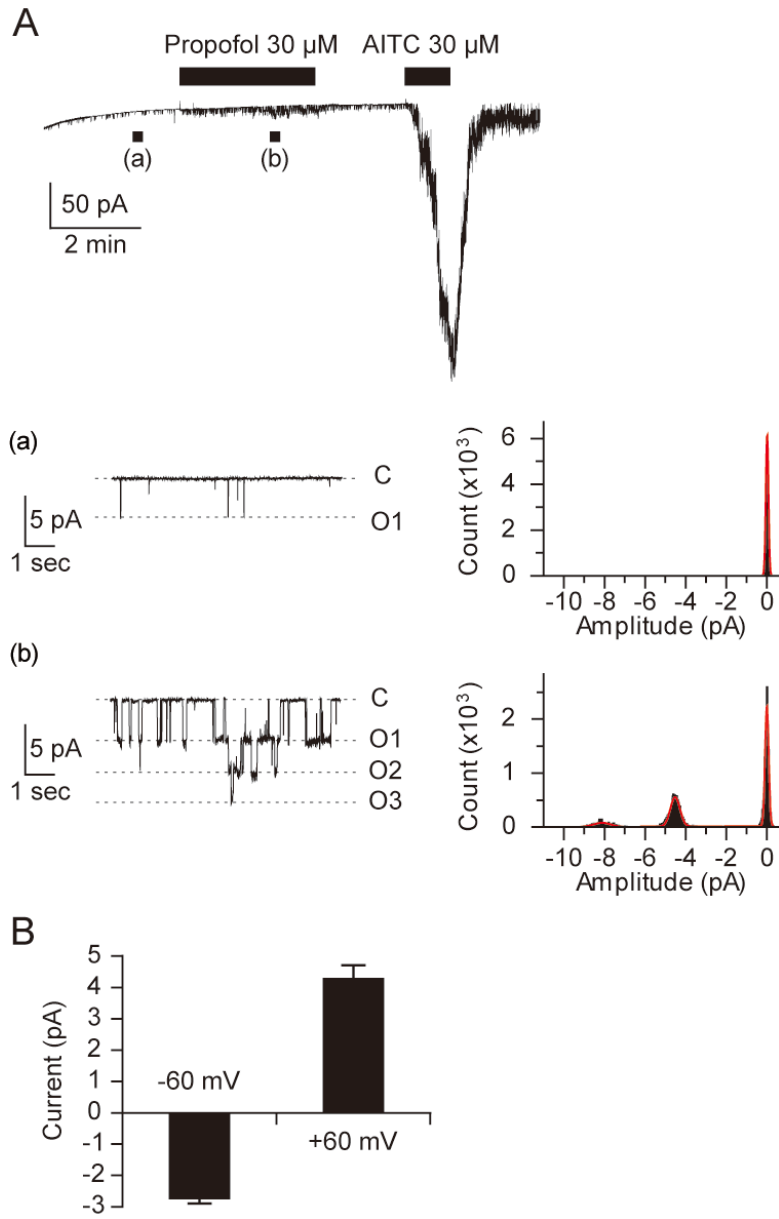


Figure 3

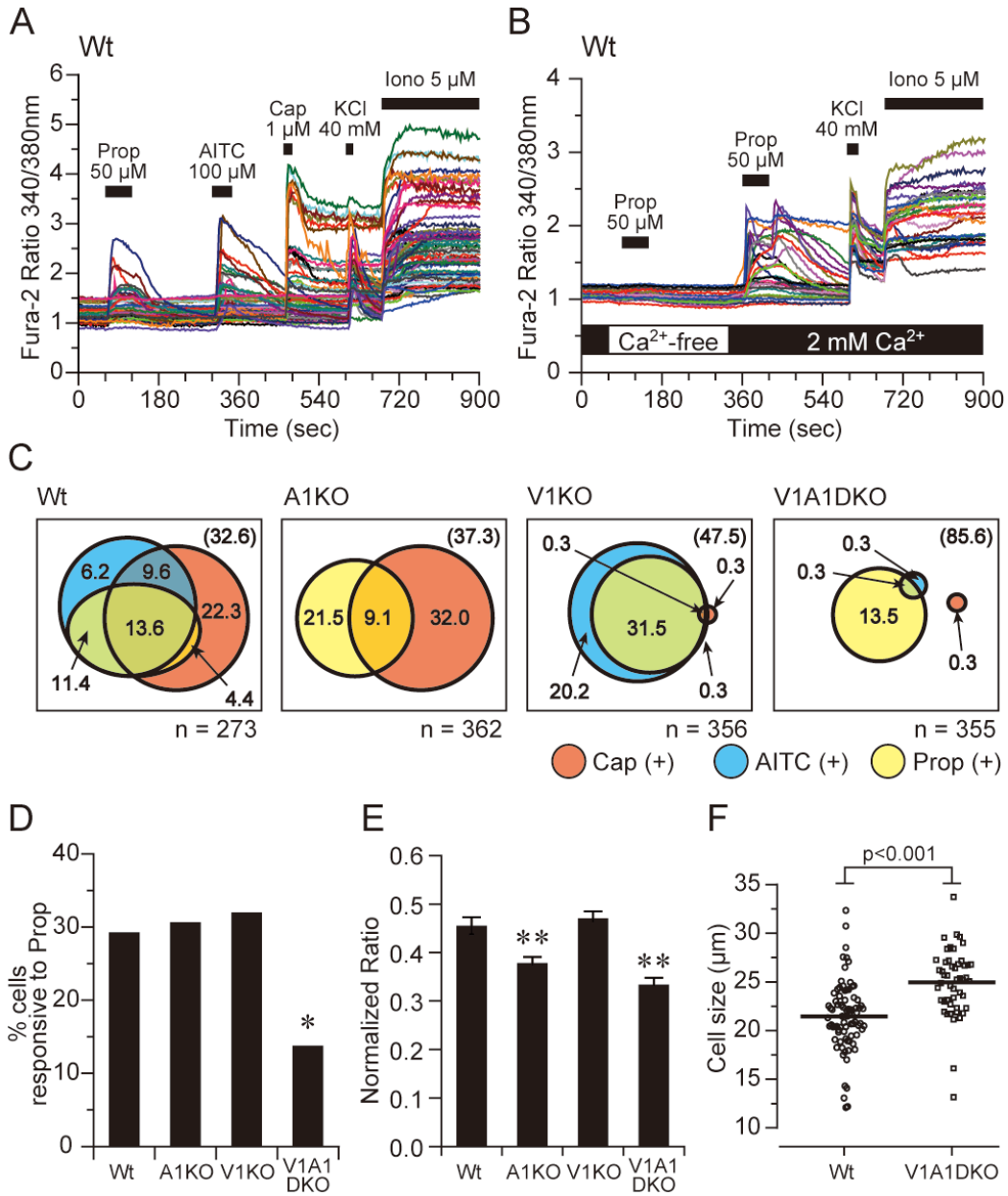


Figure 5

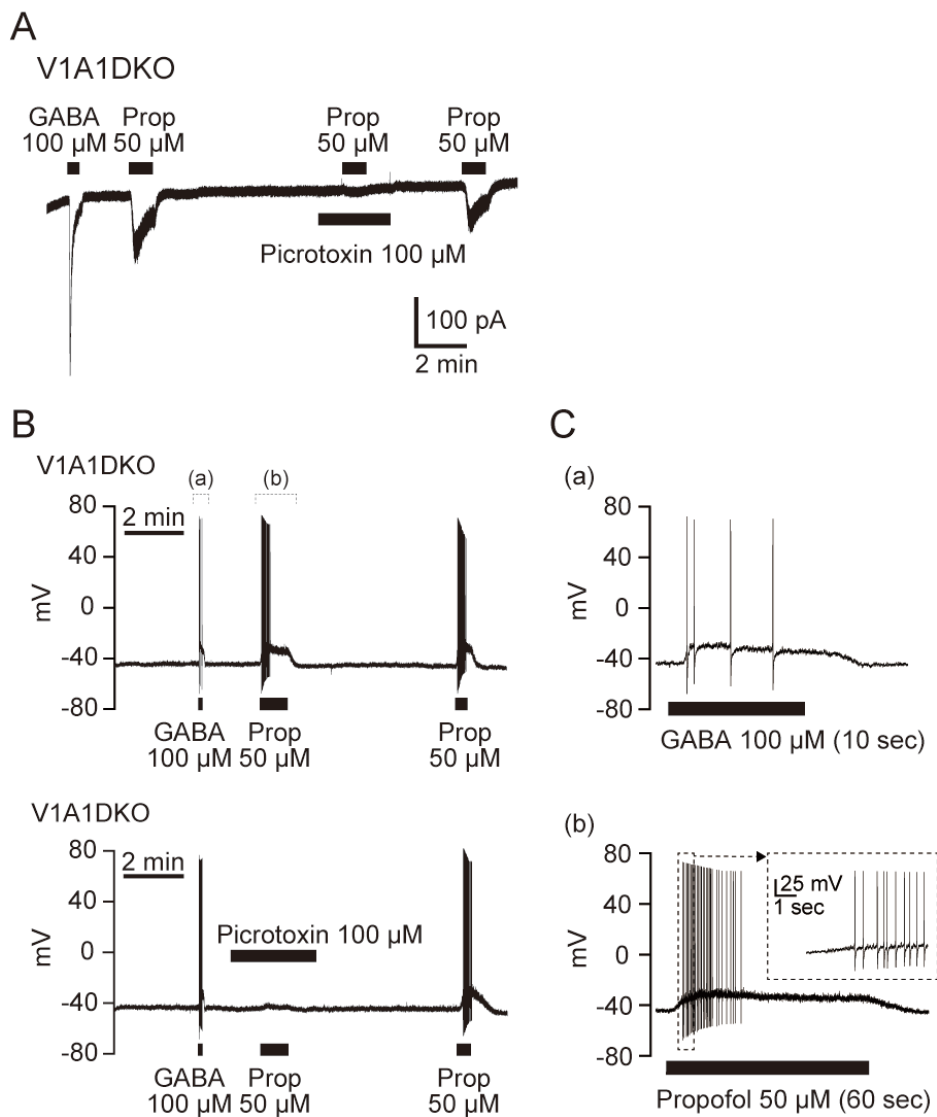
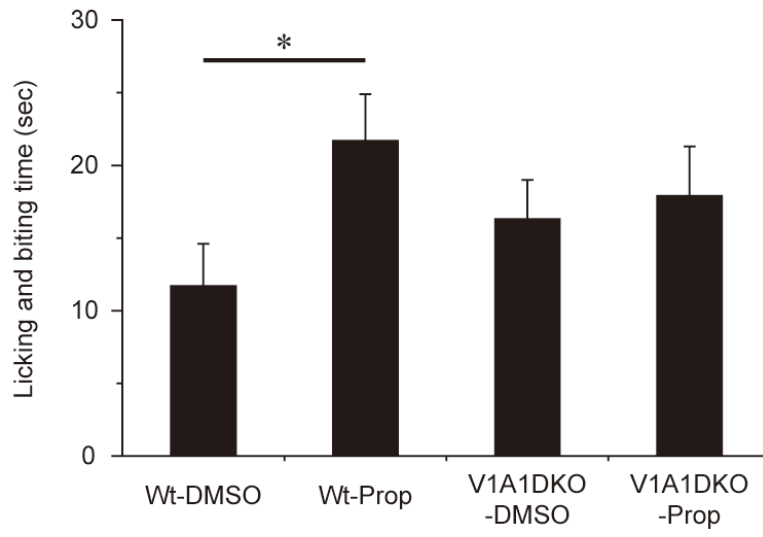


Figure 6



Chapter II

Temperature-dependent microglia movement and the involvement of thermosensitive TRP channels

II-1. Introduction

Microglia as immune cells in the brain are highly motile

Microglia, which are resident immune cells in the brain, play important roles in the maintenance of the brain by responding to the environmental changes caused by neurons, other glial cells (astrocytes and oligodendrocytes) and supporting cells (Ransohoff *et al.*, 2009; Prinz *et al.*, 2014). In terms of their origin, they are distinct from peripheral tissue immune cells such as macrophages, as they are derived from hematopoietic stem cells in the yolk sac, which intrude to the brain at the embryonic stage (Prinz *et al.*, 2014). Microglia *in vivo* show a highly-branched morphology and the territories of neighboring microglia do not overlap each other in the healthy brain (Nimmerjahn *et al.*, 2005). These highly-branched microglia serve as surveillants of the brain, monitoring their surrounding area with motile processes (Nimmerjahn *et al.*, 2005; Tremblay *et al.*, 2014). In addition to the dynamic activity of surveillant microglia, they rapidly develop activated phenotypes transforming into larger cell bodies with shorter and thicker processes and migrate in response to signs of damage, injury or inflammation in the brain (Tremblay *et al.*, 2014). Moreover, changes in the expression patterns of various types of cytosolic proteins also allow microglia to efficiently respond to their environment. That is, the alterations promote migration and phagocytosis with extreme cytoskeletal rearrangements (Davalos *et al.*, 2005; Ransohoff *et al.*, 2009; Tremblay *et al.*, 2014). The dynamic motility of microglia is a fundamental feature that characterizes microglial activities in both physiological and pathological conditions.

The receptors related to microglial motility

In order to detect the environmental changes in the brain, microglia express a wide variety of receptors on the plasma membrane for converting their surrounding inputs into the initiations of

receptor-mediated signaling in the cytoplasm (Kettenmann *et al.*, 2011). As for microglial motility, purinergic receptors play important roles in chemotaxis. For example, metabotropic P2Y₆ and P2Y₁₂ receptors are crucial for the recognition of brain damage (Haynes *et al.*, 2006; Kettenmann *et al.*, 2011). P2Y₆ receptors are coupled to G_{q/11} proteins that lead to the initiation of phospholipase C (PLC)-inositol trisphosphate (InsP3)-endoplasmic reticulum (ER) Ca²⁺ release signaling. This pathway is involved in uridine-5'-diphosphate (UDP)-induced microglial translocation and phagocytosis without membrane ruffles. This characteristic morphology is observed in adenosine diphosphate- (ADP) and adenosine triphosphate (ATP)-induced chemotaxis of microglia through P2Y₁₂ receptor activation (Sasaki *et al.*, 2003; Haynes *et al.*, 2006; Koizumi *et al.*, 2007). Increases in intracellular Ca²⁺ concentrations ([Ca²⁺]_i) downstream from P2Y₆ receptor activation can trigger the activation of Ca²⁺-dependent molecules related to cell motility such as integrin (Stock *et al.*, 2013; Madry *et al.*, 2015). On the other hand, ATP (released or leaked from surrounding reactive astrocytes or damaged neurons) activates P2Y₁₂ receptors associated with G_i protein. This process increases microglial chemotaxis during the acute state through activation of phosphoinositide 3-kinase (PI3K) and the phosphorylation of protein kinase B (Akt) resulting in actin rearrangements in microglia followed by downregulation of its expression during later states (Haynes *et al.*, 2006; Madry *et al.*, 2015). Although P2Y₁₂ receptors mediate stimulus-evoked microglial migration, it appears that they are not involved in surveillant motility of microglia since the motile properties of P2Y₁₂ knockout microglia were unaltered compared with wild-type (Haynes *et al.*, 2006). Another candidate involved in microglial surveillant motility is CXC3R1, a G_i-coupled fractalkine receptor that is expressed specifically in microglia in the central nervous system. CXC3R1 is known as a cell adhesion-mediating receptor activated by its unique ligand, chemokine (C-X3-C motif) ligand 1 (CX3CL1), a membrane-bound form of which is present in

neurons (Imai *et al.*, 1997; Tremblay *et al.*, 2014). Genetic ablation of CXC3R1 led to partial (~30%) reduction of microglial motility compared with that of wild-type, indicating the existence of other candidates or pathways (Liang *et al.*, 2009; Madry *et al.*, 2015).

The dynamic changes of ion concentrations via ion channels also participate in microglial motility (Stock *et al.*, 2013). Intracellular Ca^{2+} modulation contributes to Ca^{2+} -dependent morphological and functional transformation of microglia (Hoffmann *et al.*, 2003). In addition, Ca^{2+} influx itself can activate other Ca^{2+} -activated ion channels such as $\text{K}_{\text{Ca}3.1}$ involved in microglial chemotaxis (Schilling *et al.*, 2004) and cause depolarization of the plasma membrane in the vicinity of those channels, possibly triggering activation of voltage-gated channels such as $\text{K}_{\text{v}1.3}$ that are involved in cell motility conserved in other motile cells in whole body (Stock *et al.*, 2013). The P2X_4 receptor, one of the Ca^{2+} -permeable ionotropic purinergic receptors, is expressed in microglia and thought to be involved in morphine-induced enhancement of ADP-induced microglial chemotaxis through phosphatidylinositol 3,4,5-trisphosphate (PIP_3)- and phosphorylated Akt-mediated pathways. It is not known how Ca^{2+} influx through P2X_4 receptor activation could contribute to that enhancement (Horvath *et al.*, 2009). With regard to the contribution of Na^+ ions to microglia function, it has been reported that $\text{Nav}1.6$ expressed in microglia is involved in ATP-induced microglial transformation via RAS-related C3 *botulinum* toxin substrate 1 (Rac1) and extracellular-signal-regulated kinase (ERK) 1/2 pathways (Persson *et al.*, 2014; Kettenmann *et al.*, 2011). Rac1 is a small GTPase that is important for lamellipodium protrusion. Its activation is due to intracellular Ca^{2+} mobilization (Stock *et al.*, 2013). Na^+ influx by activation of Na^+ -permeable channels is thought to contribute to cell motility through the induction of Ca^{2+} influx via the reverse mode of NCX, a Na^+ - Ca^{2+} exchanger, although the significance of depolarization itself has not been well studied.

TRP channels: candidates for involvement in microglial motility

Due to their Ca^{2+} permeability, TRP channels are widely believed to be involved in cell motility. TRPV1 reportedly contributes to the retraction of the growth cone of DRG neurons and scratch-induced astrocyte migration through Ca^{2+} influx-induced disassembly of microtubules (Goswami *et al.*, 2007; Ho *et al.*, 2014). It has also been reported that the Ca^{2+} influx induced by TRPV1 activation mediates microglial cell death via mitochondrial disruption and caspase-3 activation (Kim *et al.*, 2006). TRPV2, which is expressed in murine macrophages at the leading edge, is involved in chemotaxis and phagocytosis through the modulation of actin dynamics via depolarization by TRPV2 activation (Link *et al.*, 2010; Stock *et al.*, 2013). TRPV4 was reported to be expressed in microglia, and its activation suppresses lipopolysaccharide (LPS)-induced microglial activation through the reduction in tumor necrosis factor α (TNF α) release and the attenuation of driving force of Ca^{2+} influx via the depolarization by its activation (Konno *et al.*, 2012). It has also been reported that TRPV4 interacts with actin and microtubules and its activation regulates the disassembly of microtubules in the growth cone of cultured DRG neurons similar to TRPV1, but its time course seems to be slower than that caused by TRPV1 activation (Goswami *et al.*, 2010). It is conceivable that TRPV4 as well as TRPV1 could be involved in microglial motility. TRPM2 is also functionally expressed in microglia (Kraft *et al.*, 2004). The temperature sensitivity of TRPM2 is modulated by redox signals such as hydrogen peroxide downstream from nicotinamide adenine dinucleotide phosphate (NADPH) oxidase activity. Moreover, zymosan-induced macrophage function such as cytokine release is attenuated by knockout of the *Trpm2* gene (Kashio *et al.*, 2012). Blockade of TRPM2 activation leads to the inhibition of neutrophil chemotaxis, which seems to depend on chemoattractant (Stock *et al.*, 2013). TRPM4 is a Ca^{2+} -activated monovalent cation permeable channel that plays important roles in

mobilization of intracellular Ca^{2+} via depolarization induced by its activation especially in non-excitable cells such as T-lymphocytes (Launay *et al.*, 2002; Launay *et al.*, 2004; Gees *et al.*, 2012). Dendritic cells from *Trpm4*-knockout mice showed impairment of chemotaxis due to the downregulation of PLC β 2 by Ca^{2+} overload (Barbet *et al.*, 2008). The impact of TRPM4 activity contributing to cell motility depends on its expression levels because the phenotypes after knockdown of the *Trpm4* gene yielded opposite results in the migration assay (Weber *et al.*, 2010). Thus, TRP channels take part in the modulation of cell motility in various types of cells through their channel activity although the endogenous molecules that directly regulate the activation of TRP channels involved in the migration mechanism are still under investigation.

Therapeutic hypothermia affects microglial function

The brain temperature is known to fluctuate over a range of $\sim 3^{\circ}\text{C}$ depending on brain homeostasis. It is also modulated by the application of neuroactive pharmacologic agents such as general anesthetic drugs (Kiyatkin, 2013). Extreme hyperthermia ($>40^{\circ}\text{C}$) leads to destructive damages to brain cells such as neurons and glial cells and the disruption of the blood brain barrier whereas brain hypothermia causes the impairment of neurophysiological activities such as neuronal synaptic transmission (Wang *et al.*, 2014). In spite of the varied effects of temperature on the brain, cooling tissues for their preservation is a time-honored clinical concept in the field of organ transplantation (Yenari *et al.*, 2012). Therapeutic hypothermia has been established in the patients undergoing cardiopulmonary resuscitation from cardiac arrest (Hypothermia-After-Cardiac-Arrest-Study-Group., 2002) and is also applicable in cardiac surgery for the protection of brain functions. It is thought that the lowering of brain temperature down to 34°C (mild hypothermia) in patients achieved within several hours (up to 4 hrs) after resuscitation and maintained for 24 hrs improves neurological outcome. However,

it is difficult for clinicians to use hypothermia because of the limited number of equipped medical facilities and available staff. There are several possible mechanisms of hypothermia-induced neuroprotection reported such as reduction in oxygen consumption and lactate production, which leads to improvements of brain metabolism in the acute phase and prevention of apoptotic neuronal death in the subacute phase via inhibition of caspase 3-dependent and independent pathways (Yenari *et al.*, 2012). Such mechanisms are expected to work in the period of therapeutic hypothermia. However, it is poorly understood how the brain detects the temperature changes. Although many studies regarding therapeutic hypothermia have focused on neurons, the functions of other cell types in the brain such as microglia could also be affected by therapeutic hypothermia. The fact that some of the TRP channels, especially ones activated by temperature changes, are involved in the microglial functions and that cytokine release from lipopolysaccharide (LPS)-stimulated microglia was suppressed at low temperature prompted me to pursue the possibility that temperature-sensitive ion channels, including thermosensitive TRP channels, play a pivotal role in therapeutic hypothermia through regulation of microglia function.

II-2. Materials and Methods

All procedures involving the care and use of animals were approved by the Institutional Animal Care and Use Committee of the National Institutes of Natural Sciences and carried out in accordance with the National Institutes of Health Guide for the care and use of laboratory animals (NIH publication no. 85-23. Revised 1985).

II-2-1. Animals

C57BL/6NCr (Wt) mice (SLC, Hamamatsu, Japan) were used. *Trpm2*-knockout (M2KO) mice and *Trpv4*-knockout (V4KO) mice were generously provided by Dr. Yasuo Mori (Kyoto University, Kyoto, Japan) (Yamamoto *et al.*, 2008) and Dr. Makoto Suzuki (Jichi Medical School, Tochigi, Japan) (Suzuki *et al.*, 2003), respectively. The genotyping of the parents of M2KO and V4KO pups was performed by PCR. They were housed in a controlled environment (12 hrs light/12 hrs dark cycle; room temperature, 22 to 24°C; 50 to 60% relative humidity) with free access to food and water.

II-2-2. Construction of expression vectors

Myc-tagged mouse TRPM4 (mTRPM4) cDNA in the pcDNA3 expression vector was generously provided by Dr. Veit Flockerzi (Universität des Saarlandes, Hamburg, Germany). Mouse Hv1 (mHv1) cDNA in the pIRES2-EGFP expression vector was generously provided by Dr. Yasushi Okamura (Osaka University, Osaka, Japan). The entire sequence was confirmed. The mTRPM4-expression vector and mHv1-expression vector were transfected to human embryonic kidney-derived 293T (HEK293T) cells for patch-clamp recordings or immunocytochemistry.

II-2-3. Cell culture

HEK293T cells were maintained in D-MEM (DMEM, Wako) supplemented with 10% (v/v) fetal bovine serum (BioWest or Gibco), penicillin-streptomycin (50 units/mL and 50 mg/mL, respectively, Gibco) and GlutaMAX (2 mM, Gibco) and seeded at densities of 5×10^5 , 2×10^5 or 1×10^5 cells per 35-mm dish 24, 48 or 72 hrs before transfection, respectively. For patch-clamp recordings, 1 μ g of expression vector and 0.1 μ g pGreen-Lantern 1 cDNA (pGL) in OPTI-MEM I medium (Invitrogen) were transfected to HEK293T cells cultured on 35-mm dishes using Lipofectamine and Plus reagents (Invitrogen). pGL was not used in the experiments with HEK293T cells expressing mHv1. After incubation for 3 to 5 hrs, cells were reseeded on cover glasses (for patch-clamp recordings) or 35-mm glass bottom dishes (for immunocytochemistry) and further incubated at 37°C in a humidified 5% CO₂ incubator. Cells were used for experiments 20 to 36 hrs after transfection.

Primary mouse microglia were obtained according to the method described previously (Koizumi *et al.*, 2007; Doering, 2010) with modification. A glial mixed culture was prepared from postnatal (P0-P1) pups. The brain was carefully isolated from each pup. The meninges with olfactory bulbs and hippocampi were removed in chilled phosphate buffered saline (PBS). Cerebral hemispheres were collected and then minced with a sterile feather. The minced tissue was transferred into a 50 mL tube to which was added trypsin (a final concentration of 0.2%) followed by incubation at 37°C for 8 min with rigorous shaking. After incubation, DNaseI (a final concentration of 0.1 mg/mL, Roche) was added and triturated using a 10 mL pipette. An equal volume of horse serum (Biowest) was added to stop the reaction of trypsin. Cells were centrifuged at 800 rpm for 6 min and resuspended in D-MEM (D6046, Sigma-Aldrich) containing 10% (v/v) heat-inactivated bovine serum (Sigma-Aldrich), penicillin-streptomycin (10 units/mL and 10 mg/mL, respectively, Gibco), bovine insulin (5 μ g/mL, Sigma-Aldrich)

and glucose solution (2 mg/mL, Otsuka Pharmaceutical Co., Ltd.) (microglia medium) followed by trituration using a fire-polished Pasteur glass pipette and filtration through 100 μ m pore mesh (BD Falcon). The number of viable cells was determined using the trypan blue exclusion test: an equal volume of trypan blue (0.5% in PBS) was added to a cell suspension and incubated a few minutes at room temperature, after which the number of unstained cells was counted. Cells were cultured in 75-cm² tissue flasks at 4×10^6 to 8×10^6 cells/flask in fresh microglia medium and cultured for 10 to 20 days at 37°C in a humidified CO₂ incubator (glia mixed culture). The medium was replaced 48 hrs later and subsequently once every 3 to 4 days. Glia mixed cultures were plated onto 35-mm glass bottom dishes (Matsunami) at an approximate density and incubated at 37°C in a humidified CO₂ incubator until used for immunocytochemistry. Microglia defined as cells weakly attached or floating were isolated by shaking the flasks of glia mixed cultures at 37°C at 80 rpm for 60 to 120 min on an orbital shaker. Cells were resuspended in microglia medium and seeded on 35-mm glass bottom dishes or cover glasses (Matsunami) at a density of 1×10^4 cells/dish or cover glass and incubated at 37°C in a humidified CO₂ incubator. After 30 min, the medium was replaced to remove the unattached cells. Cells were used within 6 days after isolation for each experiment and the medium was changed every 3 days for further incubation.

For astrocyte-enriched culture, a glia mixed culture was prepared from P0 pups as described above and cultured in a 25-cm² tissue flask. When the culture reached almost 100% confluency, cells were washed with PBS and PBS containing EDTA (a final concentration of 1 mM) and then incubated with PBS containing trypsin (a final concentration of 0.05%) and 1 mM EDTA for 2.5 min at 37°C. After incubation, the microglia medium was added to end the trypsin reaction and cells were detached by pipetting. Cells were centrifuged at 1000 rpm for 6 min and the approximate volume of microglia medium was added. After trituration with a

fire-polished Pasteur glass pipette, cells were plated onto a 10-cm petri dish and incubated at 37°C for 1 hr to remove the attached cells including microglia. After cultivation, the floating cells were collected and centrifuged at 800 rpm for 6 min. The collected cells were resuspended in microglia medium and reseeded on 35-mm glass bottom dishes (Matsunami) coated with poly-L-lysine (a final concentration of 100 µg/mL, Sigma) at an approximate density. The cells were cultured at 37°C for immunocytochemistry.

For hippocampal neuron culture, the hippocampi of ten E18 mouse embryos were dissected and meninges were removed. Hippocampi were cut into pieces with a sterile scalpel and transferred into a 50 mL tube followed by the incubation with trypsin (a final concentration of 0.25%) at 37°C for 16 min with rigorous shaking. After incubation, DNaseI (a final concentration of 0.1 mg/mL) was added and the pieces of hippocampi were triturated using a 10 mL pipette. An equal volume of horse serum was added to stop the reaction of trypsin. Dissociated cells were centrifuged at 800 rpm for 6 min and resuspended in D-MEM/F12 medium (10565-018, Gibco) containing 10% FBS (D-MEM/F12+FBS) followed by trituration using a fire-polished Pasteur glass pipette. The cell suspension was transferred into a 15 mL tube containing horse serum. The suspension was centrifuged at 800 rpm for 5min and the upper layer of D-MEM/F12+FBS medium was removed. An equal volume of D-MEM/F12+FBS medium was added and the suspension was triturated again. After centrifugation at 800 rpm for 1 min, the cells were resuspended with D-MEM/F12+FBS. Cells were seeded on poly-L-lysine-coated 35-mm glass bottom dishes (Matsunami) that were prepared prior to isolation of hippocampi at a density of 2.5×10^4 cells/dish. Cells were incubated at 37°C in a humidified CO₂ incubator overnight. The next day, an equal volume of Neurobasal medium (Gibco) containing B27 supplement (a final concentration of 2%, Gibco) and GlutaMAX (a final concentration of 2 mM, Gibco) was added to each dish and then further

incubated. After 24 hrs incubation, the medium was replaced with Neurobasal medium containing B27 and GlutaMAX and changed every 5 days until used for immunocytochemistry.

II-2-4. Time-lapse imaging and quantitative analysis of microglia movement

Primary mouse microglia on glass bottom dishes were incubated for 2 to 6 days before use. The glass bottom dish was placed on the stage of an inverted fluorescence microscope, Keyence BZ-9000 (Keyence) fitted with a temperature-controlled stage incubator (Tokai Hit) under a circulating mixture of gases (20% O₂/5% CO₂/75% N₂). The temperatures of the stage/the cover were set at 33/33, 37/40 or 40/41°C for each experiment at least 1 hr before taking cell images except for the experiment for the sequential change of the temperature. The temperature setting in each condition was determined in advance by measuring the medium temperature with a wire probe (OM210-004a, Unique Medical) and a digital thermometer (PTC-301, Unique Medical). Cells were imaged at intervals of 3 min with 20x phase contrast objective lens (S PL FL ELWD ADM 20xC, Nikon Instech) and the image acquisition was performed using BZ-9000 software with a Z-stack function. The focused image taken with a Z-stack function was automatically selected by BZ-II analyzer in each frame correction and then reconstructed into a series of stacking images along the time axis. In the experiments using inhibitors, the images were captured for 2 hrs for the control (Con) and then the inhibitors were added into the medium at the appropriate dilution of 1:1000. In some experiments, the medium was replaced twice by a new one which was incubated in advance at 37°C in a humidified CO₂ incubator.

For assays of microglia movement, the stacking images were processed as described in the former paragraph. Their migration distances during the set time were quantified by a newly developed cell-tracking program based on template matching, a digital processing technique

used for pattern recognition and object searching. In brief, prior to the analysis by the program, the contrast of the stacking images was enhanced using morphological image processing to extract the structural features of the cells (Kimori, 2011). At the first image, the cells that migrated within the captured region were selected. Then, a certain region within one cell was marked and the centroid of the marked region (x, y) was defined as the position of the cell. The region with a range surrounding the cell of interest was cropped as the first template. At the second image, template matching was performed and a region with xy coordinates of the centroid was selected as the best-matched one that was most similar to the first template in a searching window of a larger size around the template that was set in advance. The template used for template matching was updated every image. With this updated template, the best-matched region in the subsequent image was chosen with xy coordinates of the centroid. The process of template matching was repeated in every stacking image until a series of the stacking images was completed. Cells (up to 10 %) were excluded when tracking by the program failed. Then, xy coordinates elicited from the cell-tracking program were further analyzed using ImageJ software (National Institutes of Health), its plugin of Chemotaxis and Migration tool and Excel software (Microsoft) to calculate the migrating distances of an individual cell. Data defining the migrating distances of microglia were collected from at least 2 individual glass bottom dishes in 2 different preparations.

The directionality of each cell was determined by calculating the value with the following formula using Chemotaxis and Migration tool (ImageJ software plugin): the directionality value = (the rectilinear distance between the coordinate in the first image and that in the last image) / (the accumulated distance). The directionality value equal to 1 indicates straight migration traveled by an analyzed cell.

II-2-5. Electrophysiology

Transfected HEK293T cells or primary mouse microglia on cover glasses were incubated in culture medium at 37°C. The cover glasses were mounted in a chamber (RG26G, Warner Instruments) connected to a gravity flow system to deliver various stimuli and heated bath solutions. The cover glasses were washed with a standard bath solution containing 140 mM NaCl, 5 mM KCl, 1 mM MgCl₂, 2 mM CaCl₂, 10 mM HEPES and 10 mM glucose at pH 7.4 adjusted with NaOH. After achievement of a whole cell configuration, the solution was replaced with K⁺-free bath solution containing 145 mM NaCl, 1 mM MgCl₂, 2 mM CaCl₂, 10 mM HEPES and 10 mM glucose at pH 7.4 adjusted with NaOH. The intracellular solution for whole-cell recording contained 20 mM NaCl, 120 mM Na gluconate, 1 mM MgCl₂, 5 mM EGTA, 10 mM HEPES at pH 7.3 adjusted with NaOH. For the experiments in which the concentration of intracellular free calcium ([Ca²⁺]_i) was fixed to 1 μM, 4.53 mM CaCl₂ was added (calculated by Maxchelator, standard version, <http://maxchelator.stanford.edu/downloads.htm>) and then the pH was adjusted. Data for analyses were sampled at 10 kHz and filtered at 5 kHz for whole-cell recordings (Axon 200B amplifier with pCLAMP software, Molecular Devices). Thermal stimulation was applied by increasing the bath temperature with a preheated solution through an inline heater (SH-27B, Warner Instruments). The bath temperature in a chamber during recordings was monitored with a thermocouple (TA-29, Warner Instruments) and sampled with an analog-to-digital converter with pCLAMP software (Molecular Devices). Membrane potential was clamped at 0 mV for HEK293T cells or -70 mV for primary microglia. Ramp pulses from -100 to +100 mV for 500 msec were applied every 5 sec. All the experiments were performed at room temperature except for the experiments of thermal stimulation.

II-2-6. siRNA knockdown of TRPM4 expression in primary microglia

Primary mouse microglia on glass bottom dishes were transfected with StealthTM RNAi Negative Control Medium GC Duplex (GC siRNA) or Stealth RNAiTM siRNA duplex for mouse TRPM4 (Invitrogen) using HiPerFect transfection reagent (Qiagen) according to the manufacturer's protocols. The sequences of the Stealth RNAiTM siRNA duplex for mouse TRPM4 were as follows: 5'-CCUCUGCGUGUGGCUUGUAGCUUAU-3' (siRNA1), 5'-GCGUCCCAUGCUAGUAGCAGCAAAU-3' (siRNA2) and 5'-CCGAAAGGAGUUGCUGACGGUCUAU-3' (siRNA3), respectively. The final concentration of siRNA was 100 nM and a fluorescein-labeled Block-iTTM Fluorescent Oligo dsRNA duplex (a final concentration of 20 nM, Invitrogen) was co-transfected for visualization of the transfected cells. After 16 hrs treatment with siRNA, the medium was replaced and incubated for 48 to 72 hrs until assay by qRT-PCR or time-lapse imaging. As for the analysis of microglia movement, the intensity of the fluorescein signal in each cell was obtained prior to the measurement of microglia movement. The fluorescent signals were excited with a 480 nm wavelength and emission was monitored at a wavelength of 510 nm. The exposure time of the excitation and emission was the same for each measurement. The fluorescein signals were quantified using ImageJ software and cells in which the fluorescein signal was higher than the threshold value (defined below) were analyzed. The intensity of the fluorescein signal in the cytoplasmic region of one cell was averaged and the subtracted value between the minimum and maximum in one data set of a stacking image was calculated. The threshold value was determined by the following correction: (the threshold value) = (the maximum average) - 0.25 x (the subtracted value).

II-2-7. Immunostaining

Primary mouse microglia were used within 6 days of culture on a glass bottom dish. HEK293T cells expressing mTRPM4 were prepared as described above. Cells were washed twice with PBS (-) and fixed by using ice-cold 4% paraformaldehyde (PFA) for 10 min. After rinsing 3 times with PBS (-), cells were permeabilized with 0.1% Triton X-100-containing PBS (-) (PBST) for 5 min. Non-specific immunoreactive sites were blocked with 1% bovine serum albumin (Sigma-Aldrich) in PBST (PBST-BSA) for 1 hr. Primary and secondary antibodies were diluted in PBST-BSA. Cells were incubated overnight at 4°C with primary antibodies against ionized calcium binding adaptor molecule 1 (Iba1, Wako, 1:500), integrin β 2 (CD11b, AbD Serotec, 1:50), glial fibrillary acidic protein (GFAP, Sigma-Aldrich, 1:500), class III β -tubulin (Tuj1, Covance, 1:500), oligodendrocyte transcription factor 2 (Olig2, Millipore, 1:500), Myc (Sigma-Aldrich, 1:1000) and TRPM4 (a gift from Dr. Naruse, Okayama university, Alomone, 1:100). After washing 3 times with PBST, cells were incubated for 1 hr with goat anti-rabbit Alexa Fluor 488 or 594, goat anti-rat Alexa Fluor 568 and/or goat anti-mouse Alexa Fluor 488 or 594 (Thermo Fisher Scientific, 1:2000). Cells were incubated with 4', 6-diamidino-2-phenylindole (DAPI, Dojindo, 1:1000) in PBST for 10 to 15 min to stain the nucleus and then washed twice with PBS (-). All the procedures were conducted at room temperature except for the reaction of primary antibodies. The image acquisition was performed with an inverted fluorescence microscope (Keyence BZ-9000 or Olympus IX-71). The images were analyzed with a BZ-II analyzer (Keyence) or ImageJ software (National Institutes of Health). The purity of microglia culture was determined by counting the number of Iba1- or CD11b-positive cells compared with GFAP-, Tuj1- or Olig2-positive cells among DAPI-positive cells in at least 4 different areas from 2 individual samples of Wt microglia culture.

II-2-8. RT-PCR and quantitative RT-PCR

Total RNA was purified from primary mouse microglia using an RNeasy Plus Mini kit (RT-PCR) or an RNeasy Micro Kit (qRT-PCR) (Qiagen) with DNase I treatment for elimination of genomic DNA according to the manufacturer's protocols. cDNA was synthesized from total RNAs (up to 1 µg) using reverse transcription with a Superscript III first-strand synthesis system for reverse transcription (RT)-PCR (Invitrogen). To examine the expressions of genes of interest in mouse microglia, PCR was performed using rTaq polymerase (TaKaRa) in the iCycler (Bio-Rad) with specific primer sets. The primers for *Gapdh*, *Trpv1*, *Trpv2*, *Trpv4*, *Trpm2*, *Trpm4*, *Trpm5* and *Hv1* were the same as those reported previously (Inada *et al.*, 2006; Sasaki *et al.*, 2006). The sequences of the sense and antisense primers and the predicted size of the amplified cDNA in parenthesis were as follows: 5'-TGAAGGGTGGAGCCAAAAGG-3' and 5'-GGAAGAGTGGGAGTTGCTGTTG-3' for *Gapdh* (545 bp), 5'-CGGCTTCAGAGATGACCAG-3' and 5'-GCTTCATTCATCATGTCCTTG-3' for *Cd11b* (607 bp), 5'-AACTCCACCCACACTGAAG-3' and 5'-TCGCCTCTGCAGGAAATACT-3' for *Trpv1* (548 bp), 5'-ACCGCATGGTGGTTTTAGAG-3' and 5'-CTACAGCAAAGCCGAAAAGG-3' for *Trpv2* (552 bp), 5'-TGACAGAGACCCCATCCAAT-3' and 5'-GGGTGTCTCGCCAAAATAGA-3' for *Trpv3* (518 bp), 5'-ACAACACCCGAGAGAACACC-3' and 5'-CCCAAACCTTACGCCACTTGT-3' for *Trpv4* (404 bp), 5'-ACAACCCTGAAGGACAGTGG-3' and 5'-CATCACTAGCACCTCCAGCA-3' for *Trpm2* (543 bp), 5'-TGACCAAGGAATGGCAACTG-3' and 5'-ATGCCAGGATGTCGGATG-3' for *Trpm3* (609 bp), 5'-TGGATGCTCTGCTGAATGAC-3' and 5'-GACTCTAGGCGAGCCATCAC-3' for *Trpm4* (520 bp), 5'-CTGATCGCCATGTTTCAGCTA-3' and 5'-GGAGCCAGTGTATCCGTCAT-3'

for *Trpm5* (455 bp), 5'-TCGAAGCTCTAGGGCTGCTG-3' and 5'-AGATCTGCCGTTCTGAGCGT-3' for *Hv1* (102 bp). PCR conditions were as follows: 1 cycle at 94°C for 2 min; 35 cycles at 94°C for 10 sec, 58°C for 10 sec and 72°C for 30 sec; and 1 cycle at 72°C for 2 min. The specificity of the amplified fragments was confirmed by sequencing. For qRT-PCR, total RNA from microglia on a glass bottom dish was purified and cDNA was synthesized the same as with RT-PCR. The sequences of the sense and antisense primers were as follows: 5'-ATTTCTGGGAGAAGGGCTCCAACT-3' and 5'-TGCTCGCTCTTCACTGTTGTGGTA-3' for *Trpm4* (185 bp), 5'-CATCCTGCACCACCAACTG-3' and 5'-TGGATGCAGGGATGATGTTC-3' for *Gapdh* (183 bp). The qRT-PCR reaction volume contained 1 µL cDNA solution (5-fold dilution of the RT sample), 10 µL of KAPA SYBR Reagent (Nihon Genetics), 0.4 µL of 10 µM sense primer and 0.4 µL of 10 µM antisense primer and was brought to a final volume of 20 µL with nuclease-free water. qRT-PCR conditions were as follows: 1 cycle at 95°C for 10 min; 40 cycles at 95°C for 15 sec and 60°C for 1 min. Data were collected during each extension phase of the PCR reaction and analyzed using ABI-7700 SDS software (Applied Biosystems).

II-2-9. Chemicals

9-phenanthrol (9-phe) was purchased from Tocris and dissolved in dimethyl sulfoxide (DMSO) as a stock solution. Zinc chloride (ZnCl₂) as 0.1 M solution was from Kanto chemical. The dissolved 9-phe and 0.1 M ZnCl₂ were diluted 1:1000 into the medium and solution for time-lapse imaging and patch-clamp experiments, respectively. The concentration of DMSO did not exceed 0.1%.

II-2-10. Statistical analysis

Data are presented as means \pm standard error of mean (SEM). The abbreviation n indicates the number of data points. The one-way analysis of variance (ANOVA) with Tukey-Kramer test and non-parametric multiple comparison with Shirley-Williams test were applied for statistical analyses. P values less than 0.05 were considered significant. Data related to the inhibitory effect of 9-phenanthrol on microglia movement observed at 37°C in Fig. 10A were fitted by a logistic curve to calculate the IC₅₀ value. All statistical analyses were performed using OriginPro software (OriginLab) or Excel add-in software, Statcel 4 (OMS, Ltd.).

II-3. Results

II-3-1. Confirmation of the purity of microglia cultures

First, the purity of the microglia culture was evaluated by immunocytochemistry using antibodies against ionized calcium binding adaptor molecule 1 (Iba1) or integrin β 2 (CD11b) for microglia, glial fibrillary acidic protein (GFAP) for astrocytes, class III β -tubulin (Tuj1) for neurons or oligodendrocyte transcription factor 2 (Olig2) for oligodendrocytes (Akiyama *et al.*, 1990; Ito *et al.*, 1998; Zhou *et al.*, 2000; Kubo *et al.*, 2008; Shibasaki *et al.*, 2013). In Fig. 1, representative figures of microglia culture are shown with control cultures for GFAP (Fig. 1A), Tuj1 (Fig. 1B) or Olig2 (Fig. 1C). The whole cell number in a sample culture was determined by counting the 4', 6-diamidino-2-phenylindole (DAPI) signals (data not shown). The populations of GFAP-, Tuj1- or Olig2-positive cells in microglia culture were 0.12% (the actual numbers: 3 GFAP-positive/2710 counted cells), 0.42% (11/2962) and 0.02% (1/3291), respectively, while remaining cells were Iba1- or CD11 β -positive. With regard to the analysis of Olig2-immunoreactivity, faint signals were observed sparsely in the nuclear regions of almost all the cells in microglia culture, although typical strong signals identical to the nucleus found in glia-mixed culture were not observed. Such cells showing faint signals of Olig2 in microglia culture presented visible signals of CD11b that were coincident with those in glia-mixed culture and distinct from Olig2-positive signals in the same sample (the right panel in Fig. 1C). Olig2-immunoreactivity in microglia culture was judged by appearance of signals identical to the nucleus stained by DAPI. Therefore, microglia cultures prepared in this study appeared to exhibit a high purity of microglia (>99%).

II-3-2. Temperature-dependent microglia movement revealed by time-lapse imaging

To address whether microglia movement was affected by temperature, microglia movements

were monitored at a single-cell level with a time-lapse phase-contrast microscopy. Fig. 2A shows the experimental protocol used in this particular observation shown in Fig. 2B. The temperature of microglia culture was changed continuously by changing the temperature of the incubator set on the microscope. After isolation and 2 days of cultivation as shown in Fig. 2B (a) and (b), microglia exhibited motility and a fan-shaped cell body with an elastic tail that seemed to be polarized (Fig. 2B (a)), even without chemoattractants as reported in a previous study of chemotaxis (Haynes *et al.*, 2006). During observation at 37°C, they had a highly-mobile lamellipodium structure at the leading edge of the fan-shaped cell body as reported previously (Siddiqui *et al.*, 2012). Each cell migrated randomly. Some of them presented a rod and bipolar shape (Tam *et al.*, 2014) with a lower mobility than those that were fan-shaped ones during the observation. However, such rod/bipolar microglia rapidly changed their shape to that of a fan and started to move more quickly. Conversely, a fan-shaped cell could transform to a less mobile rod/bipolar or round phenotype as they slowed or stopped at a certain position. Hence, cultured microglia were morphologically heterogeneous and a fan-shaped microglia tended to be motile although the transforming mechanism was not evaluated in this study.

After the temperature was changed to 33°C (Fig. 2B (c) and (d)), the rectilinear distance of the pointed microglia at 33°C was clearly shorter than that at 37°C even though the time duration between images at 33°C was longer than that at 37°C, indicating that microglia moved more slowly at 33°C than at 37°C. Some microglia changed their shapes to smaller cell bodies with shorter branches in response to the lowering of the temperature. As shown in Fig. 2B (e) and (f), the pointed microglia moved more at 37°C than at 33°C after rewarming to 37°C. The temperature was then changed to 40°C. Microglia at 40°C apparently moved in a manner similar to that at 37°C but looked more complex, suggesting that microglia at 40°C might move

more than at 37°C. These results indicated that temperature may affect microglia movement. However, more attention should be paid to the method of analysis because simply measuring the rectilinear distance over time did not reflect the complicated movement.

The distances traveled by microglia during adjacent images captured every 3 min were accumulated by measuring the distance between *xy* coordinates of the cell at each image by using an automatic cell tracking program based on a template-matching method. The trajectory of microglia from an image at 0 min to 57 min as colored lines at 37°C was overlaid to images at each captured time with a colored circle at the cell position recognized by the tracking program (Fig. 3A). These figures indicated that the microglia migration was not straight but rather complex. Fig. 3B shows the trajectories of microglia measured in *xy* dimensions every 3min for 2hrs at 33°C, 37°C and 40°C. The direction of each cell was random and the directionality value (defined in II-2-4) was 0.28 ± 0.02 at 33°C, 0.39 ± 0.02 at 37°C and 0.34 ± 0.03 at 40°C, indicating that microglia moved in a random fashion. The average values of the accumulated distances for 2 hrs were $125.73 \pm 4.85 \mu\text{m}$ at 33°C, $213.27 \pm 5.19 \mu\text{m}$ at 37°C and $251.45 \pm 9.77 \mu\text{m}$ at 40°C, with significant differences among 3 different temperature conditions (Fig. 3C). This result suggested that the migrating distance of microglia could increase in a temperature-dependent manner at least from 33°C to 40°C, which is within a physiological range. Altogether, microglia movement can be affected by temperature.

II-3-3. The screening of thermosensitive TRP channels expressed in microglia

The results of time-lapse imaging suggested that a molecule that responded to temperature changes might exist in microglia *in vitro*. This suggested the possibility of the expression of thermosensitive membrane-bound proteins. Some thermosensitive TRP channels have been

reported to be expressed in microglia although it is still unclear that they have temperature sensitivity (Kraft *et al.*, 2004; Konno *et al.*, 2012; Miyake *et al.*, 2015). To assess the expression of thermosensitive TRP channels in microglia, RT-PCR was performed using microglia culture. The mRNAs of *Trpm2*, *Trpm4*, *Trpv4* and *Trpv2* were detected as shown in Fig. 4. With regards to *Trpm2* and *Trpv4*, the result of RT-PCR in this study supported the evidence reported previously. However, *Trpv1* mRNA was not observed although recent work reported the functional expression of *Trpv1* in microglia (Kim *et al.*, 2006; Miyake *et al.*, 2015). Concerning *Trpv2* mRNA, it is conceivable that microglia could express TRPV2 for some reasons because some groups reported that TRPV2 was functionally expressed in macrophages (Nagasawa *et al.*, 2007; Link *et al.*, 2010). Owing to the high temperature threshold for activation of TRPV2 (above 52°C), which is beyond the physiological range (Caterina *et al.*, 1999), the involvement of TRPV2 in the temperature-dependent microglia movement was not likely, and was not evaluated accordingly. Thus, I used time-lapse imaging to investigate whether TRPM2, TRPV4 or TRPM4 were involved in the mechanism of the temperature-dependent microglia movement.

II-3-4. Time-lapse imaging using *Trpm2*- and *Trpv4*-knockout microglia

To address whether TRPM2 or TRPV4 was involved in the temperature-dependent microglia movement, microglia prepared from *Trpm2*-knockout (M2KO) or *Trpv4*-knockout (V4KO) were assessed by time-lapse imaging. The results of wild-type (Wt) assessment are shown in Fig. 3C. The accumulated average distance of M2KO or V4KO microglia at 3 different temperature conditions were as follows: (M2KO) 119.28 ± 5.73 μm at 33°C, 196.76 ± 9.57 μm at 37°C, 221.70 ± 8.20 μm at 40°C, (V4KO) 110.10 ± 4.05 μm at 33°C, 201.59 ± 6.01 μm at 37°C and 216.58 ± 7.31 μm at 40°C (Fig. 5). The average distance of M2KO and V4KO

microglia movement over 2hrs was not significantly different from that of Wt microglia at 33°C and 37°C. On the other hand, at 40°C, the average distance of V4KO microglia movement was significantly smaller than that of Wt microglia ($p < 0.01$, ANOVA with Tukey-Kramer test) whereas the average distance of M2KO microglia movement was not different from that of Wt microglia. With regard to the temperature-dependency, there was no significant difference between the distances at 37°C and 40°C in M2KO and V4KO microglia whereas the difference was significant in Wt microglia, indicating that TRPM2 and TRPV4 may be involved in microglia movement at higher temperature. However, no significant differences in microglia movement at 37°C were observed among 3 genotypes. Altogether, these results suggested that TRPM2 and TRPV4 were not involved in microglia movement around the normal temperature condition of 37°C.

II-3-5. The expression of TRPM4 in microglia assessed by immunocytochemistry

TRPM4 is a Ca^{2+} -activated temperature-sensitive channel expressed broadly in various tissues such as heart, kidney and pancreas (Launay *et al.*, 2002; Talavera *et al.*, 2005). TRPM4 activation mediates membrane depolarization due to its monovalent cation permeability and contributes to intracellular Ca^{2+} mobilization in T lymphocytes and mast cells (Launay *et al.*, 2004; Vennekens *et al.*, 2007; Shimizu *et al.*, 2009). Few papers so far have reported the possible existence of TRPM4 in microglia by electrophysiological analysis although TRPM4 mRNA was detectable in the brain (Inada *et al.*, 2006; Beck *et al.*, 2008). To investigate the expression of TRPM4 at the protein level, immunocytochemistry was performed using an antibody against TRPM4 (Piao *et al.*, 2015). The TRPM4-positive signals in HEK293T cells expressing myc-tagged mouse TRPM4 (mTRPM4) were obvious and coincident with the signals obtained with anti-Myc antibody (Fig. 6A). In microglia culture, TRPM4-positive

signals were observed in CD11b-positive cells, while no detectable signals were seen in the sample without the first antibodies (Fig. 6B). Thus, TRPM4 might be expressed in microglia at the protein level *in vitro*.

II-3-6. The channel properties of TRPM4 in a heterologous expression system

I characterized the channel properties of TRPM4 using a patch-clamp method with HEK293T cells expressing mouse TRPM4 (mTRPM4). It was reported that intracellular free Ca^{2+} or warm temperatures around 35°C can activate TRPM4 and that there are no chemical ligands capable of activating TRPM4 from the extracellular side (Launay *et al.*, 2002; Talavera *et al.*, 2005). After the establishment of the whole-cell configuration at 0 sec in Fig. 7A, currents with strong outward rectification were observed in a time-dependent manner in response to dialysis with $1\ \mu\text{M}$ intracellular free Ca^{2+} ($[\text{Ca}^{2+}]_i = 1\ \mu\text{M}$) in a HEK293T cell expressing mTRPM4 as reported previously (Fig. 7A and C) (Nilius *et al.*, 2005; Ullrich *et al.*, 2005). These Ca^{2+} -activated currents gradually declined, showing a TRPM4 property of desensitization (Nilius *et al.*, 2005). Such currents were not observed in a HEK293T cell expressing mTRPM4 without the stimulus of intracellular free Ca^{2+} (Fig. 7B), in a HEK293T cell without a fluorescent signal of Green-Lantern1 or in a HEK293T cell transfected with pcDNA3.1 vector (data not shown). Surprisingly, large currents were evoked by heat application in a HEK293T cell expressing mTRPM4 after desensitization (Fig. 7A and C), whereas heat-evoked currents without intracellular free Ca^{2+} were negligible (Fig. 7B). These results suggested that a high concentration of intracellular free Ca^{2+} was necessary for heat-evoked mTRPM4 currents, though its mechanism seems not to be related to the desensitization of TRPM4.

9-phenanthrol (9-phe) is a phenanthrene derivative and a potent inhibitor of TRPM4 (Wang *et al.*, 1994; Guinamard *et al.*, 2014). Indeed, the intracellular Ca^{2+} -induced mTRPM4 currents

were inhibited rapidly by the application of 100 μM 9-phe (Fig. 7D and E). Furthermore, I found that heat-evoked mTRPM4 currents with intracellular free Ca^{2+} were also inhibited by the application of 100 μM 9-phe followed by partial recovery, which has never been reported (Fig. 7F and G). As shown in Fig. 7H, I analyzed the heat-evoked mTRPM4 currents in the presence of intracellular free Ca^{2+} during the application of 9-phe. The average current densities at -100 and +100 mV were as follows: 41.87 ± 8.94 pA/pF (Con at -100 mV) / 188.81 ± 32.17 pA/pF (Con at +100 mV), 37.60 ± 14.17 pA/pF (with 1 μM 9-phe at -100 mV) / 159.29 ± 45.90 pA/pF (with 1 μM 9-phe at +100 mV), 12.85 ± 3.70 pA/pF (with 10 μM 9-phe at -100 mV) / 68.03 ± 20.37 pA/pF (with 10 μM 9-phe at +100 mV), and 10.46 ± 2.71 pA/pF (with 100 μM 9-phe at -100 mV) / 26.56 ± 7.14 pA/pF (with 100 μM 9-phe at +100 mV). I found that the inhibition of heat-evoked mTRPM4 currents by 9-phe was dose-dependent (*, $p < 0.05$ and **, $p < 0.01$, non-parametric multiple comparison with Shirley-Williams test, Fig. 7H). Thus, these observations indicated that 9-phe inhibited TRPM4 activity caused by both intracellular free Ca^{2+} and heat.

II-3-7. 9-phenanthrol inhibits heat-evoked currents in microglia in the presence of high intracellular free Ca^{2+}

Given that 9-phe inhibits TRPM4 activation by its activators in the heterologous expression system, further analysis was conducted using primary mouse microglia prepared from Wt mice to examine the functional expression of TRPM4 by a whole-cell patch-clamp method.

In response to repeated applications of heat, large heat-evoked currents were observed in microglia in the presence of 1 μM intracellular free Ca^{2+} with a strong outward rectification (Fig. 8A and B), which is similar to the currents observed in HEK293T cells expressing mTRPM4. When 9-phe was co-applied with heat, heat-evoked currents were decreased followed by the

recovery after washout of 9-phe (Fig. 8C). The decrease of the heat-evoked currents during 9-phe application at +100 mV was larger than that at -100 mV (Fig. 8D). Under conditions in which 9-phe was applied prior to heat, heat-evoked currents in microglia were also smaller than those after washout of 9-phe (Fig. 8E). Then, I examined the dose-dependency of 9-phe-induced inhibition of heat-evoked currents in microglia in the presence or absence of intracellular free Ca^{2+} (Fig. 8F). Thus, the heat-evoked currents during 9-phe application were normalized to those after washout. The normalized ratios of heat-evoked currents in microglia in the presence of intracellular free Ca^{2+} at -100 and +100 mV were as follows: 1.09 ± 0.04 (without 9-phe at -100 mV) / 1.05 ± 0.05 (without 9-phe at +100 mV), 1.07 ± 0.13 (with 1 μM 9-phe at -100 mV) / 0.80 ± 0.07 (with 1 μM 9-phe at +100 mV), 1.01 ± 0.13 (with 10 μM 9-phe at -100 mV) / 0.68 ± 0.05 (with 10 μM 9-phe at +100 mV) and 1.13 ± 0.13 (with 100 μM 9-phe at -100 mV) / 0.63 ± 0.04 (with 100 μM 9-phe at +100 mV), respectively. The normalized ratios of heat-evoked currents in microglia in the absence of intracellular free Ca^{2+} at -100 and +100 mV were as follows: 0.94 ± 0.09 (with 1 μM 9-phe at -100 mV) / 0.90 ± 0.03 (with 1 μM 9-phe at +100 mV), 1.14 ± 0.09 (with 10 μM 9-phe at -100 mV) / 1.02 ± 0.05 (with 10 μM 9-phe at +100 mV) and 1.02 ± 0.13 (with 100 μM 9-phe at -100 mV) / 0.96 ± 0.05 (with 100 μM 9-phe at +100 mV), respectively. The ratios of heat-evoked currents at +100 mV were significantly reduced by the application of 9-phe in a dose-dependent manner in comparison to those without 9-phe application in the presence of 1 μM intracellular free Ca^{2+} (*, $p < 0.05$ and **, $p < 0.01$, ANOVA with Tukey-Kramer test). However, there were no significant changes in heat-evoked currents at -100 mV in any concentration of 9-phe. On the other hand, the ratios of heat-evoked currents did not decrease regardless of 9-phe concentrations both at -100 mV or +100 mV in the absence of 1 μM intracellular free Ca^{2+} (Fig. 8F). These data suggested that the components of the heat-evoked currents inhibited by 9-phe in microglia require high

intracellular free Ca^{2+} .

II-3-8. The 9-phenanthrol effects on microglia movement

Because *Trpm4*-knockout mice were not available, I performed time-lapse imaging using 9-phe to evaluate the involvement of TRPM4 in temperature-dependent microglia movement. As shown in Fig. 9A and B, time-lapse imaging with 30 μM 9-phe followed by washout was conducted at 37°C. A fan-shaped microglia with an elongated tail (yellow arrow in Fig. 9B) changed its shape to a rod-like shape in response to application of 30 μM 9-phe and did not migrate a significant distance. After washout of 9-phe by changing the whole medium, the microglia started to move gradually and adopted a fan-shape with a tail, indicating that 30 μM 9-phe affected microglial morphology and inhibited microglia movement reversibly. Some of the microglia showed the same tendency as that above, whereas others became immobile even after washout of 9-phe, but few cells became detached from the glass coverslip. These observations suggested that 9-phe could reversibly repress microglia movement.

Thus, I examined the dose-dependency and temperature-dependency of 9-phe-induced inhibition of microglia movement (Fig. 10A and B). The actual average distances (the average before application of 9-phe (Con) / the average distance with each concentration of 9-phe) were as follows; $189.52 \pm 9.97 \mu\text{m} / 172.90 \pm 10.02 \mu\text{m}$ (1 μM 9-phe), $225.94 \pm 10.25 \mu\text{m} / 230.70 \pm 13.18 \mu\text{m}$ (3 μM 9-phe), $228.59 \pm 10.11 \mu\text{m} / 180.40 \pm 9.25 \mu\text{m}$ (10 μM 9-phe), $208.77 \pm 6.68 \mu\text{m} / 86.28 \pm 3.37 \mu\text{m}$ (30 μM 9-phe) and $210.67 \pm 7.15 \mu\text{m} / 59.78 \pm 2.78 \mu\text{m}$ (100 μM 9-phe). Although the average accumulated distance of migrating microglia before application of 9-phe varied, the average distances traveled by microglia in the presence of 10, 30 or 100 μM 9-phe were significantly shorter than those before application of 9-phe. The IC_{50} value of 9-phe-induced inhibition fitted by a logistic curve was 17.10 μM comparable with that reported

previously (Guinamard *et al.*, 2014). With regard to the temperature-dependency, the average distances of microglia before (Con) / after application of 10 μM (Fig. 10B (a)) or 30 μM (Fig. 10B (b)) 9-phe at 33°C, 37°C or 40°C were as follows: 108.37 \pm 2.62 μm / 96.96 \pm 2.04 μm (at 33°C, 10 μM 9-phe), 184.05 \pm 4.85 μm / 152.10 \pm 4.20 μm (at 37°C, 10 μM 9-phe), 188.56 \pm 4.65 μm / 147.92 \pm 4.01 μm (at 40°C, 10 μM 9-phe), 101.59 \pm 2.33 μm / 65.77 \pm 1.59 μm (at 33°C, 30 μM 9-phe), 141.34 \pm 4.98 μm / 69.52 \pm 2.43 μm (at 37°C, 30 μM 9-phe) and 216.85 \pm 5.89 μm / 87.12 \pm 3.34 μm (at 40°C, 30 μM 9-phe). The average distances traveled by microglia during 9-phe applications were significantly shorter than those of Con with 10 μM at 37°C and 40°C temperature conditions and with 30 μM at 33°C, 37°C and 40°C temperature conditions (**, $p < 0.01$, one-way ANOVA with Tukey-Kramer test). Notably, 10 μM 9-phe did not show the inhibitory effect at 33°C. In addition, temperature-dependency of microglia movement was absent in the presence of 30 μM 9-phe. These data suggested that 9-phe has an inhibitory effect on temperature-dependent microglia movement in a dose-dependent manner.

To further confirm the involvement of TRPM4 in temperature-dependent microglia movement, gene silencing of TRPM4 in primary microglia was performed using 3 individual specific siRNAs for *Trpm4*. The efficacy of the siRNA transfection was tested at the mRNA level (Fig. 11A). Cells transfected with 3 different siRNAs for *Trpm4* resulted in significant reductions of the *Trpm4* mRNA level compared to those transfected with GC siRNA as a negative control (GC siRNA) (the average relative values: 0.13 \pm 0.02 in GC siRNA, 0.08 \pm 0.01 in siRNA1, 0.07 \pm 0.01 in siRNA2, 0.06 \pm 0.004 in siRNA3). In order to assess cellular movement, microglia with a higher fluorescein signal than the threshold were analyzed (Fig. 11B). The average accumulated distances traveled by siRNA-transfected microglia at 37°C were as follows: 112.78 \pm 7.72 μm (GC siRNA), 100.84 \pm 16.51 μm (siRNA1), 119.60 \pm 13.55 μm (siRNA2) and 146.15 \pm 9.65 μm (siRNA3). The accumulated distances of microglia at 37°C in

each *Trpm4* siRNA-transfected group did not show significant differences compared with that in a GC siRNA group, although the average distances of GC siRNA microglia themselves looked shorter than those measured in the experiments before at 37°C, indicating the possibility that the transfection procedure itself might have affected microglia movement.

II-3-9. Evaluation of the involvement of voltage-gated proton channels in microglia movement

Voltage-gated proton channels (Hv1) are reportedly expressed in microglia, and they contribute to the enhancement of brain damage in the ischemic model (Eder *et al.*, 2001; Wu *et al.*, 2012). Additionally, Hv1 is a temperature-sensitive channel (Fujiwara *et al.*, 2012). To address the question whether Hv1 is involved in temperature-dependent microglia movement, I performed whole-cell patch-clamp experiments, RT-PCR and time-lapse imaging using primary microglia and HEK293T cells expressing mouse Hv1 (mHv1). In the presence of 1 μM intracellular free Ca^{2+} , heat-evoked outwardly rectifying currents in primary microglia were inhibited rapidly by application of 100 μM ZnCl_2 , an inhibitor of mHv1, followed by recovery upon washout (Fig. 12A and B). As shown in Fig. 12C, the mRNA of mHv1 was detected in the sample prepared from microglia culture. As to the action of ZnCl_2 on the heat response mediated by mHv1, large heat-evoked currents were observed in a HEK293T cell expressing mHv1 (Fig. 12D (a)) and those currents were greatly inhibited by 100 μM ZnCl_2 application whose effect lasted at least for several tens of seconds after washout (Fig. 12D (b)). Then, I examined the inhibitory effect of ZnCl_2 on microglial movement by time-lapse imaging (Fig. 12E). The average values of the accumulated distances before (Con)/after 100 μM ZnCl_2 application at 3 different temperatures were as follows: 121.94 \pm 4.01 μm / 131.27 \pm 4.69 μm (at 33°C), 179.44 \pm 4.16 μm / 176.57 \pm 3.92 μm (at 37°C), 201.13 \pm 7.10 μm / 191.91 \pm 6.60 μm (at 40°C).

ZnCl₂-mediated inhibition of migration was not observed at any temperature setting. Taken together, it is not likely that Hv1 activation is involved in temperature-dependent microglia movement.

II-4. Discussion

In the present study, I found that microglia movement is clearly temperature-dependent within the range of human body temperature and that TRPM4 channels among thermosensitive TRP channels are possibly involved in the temperature-dependent microglia movement.

The assay system of microglia movement

I established the temperature-controlled time-lapse imaging system to analyze the temperature-dependent microglia movement that allowed me to evaluate the moving distance at different temperatures as small as 3°C even for the cells showing a zigzag path (Fig. 3). This is the first study to clearly demonstrate temperature-dependent single-cell movement with the system. Cell motility is essential for the development and maintenance of living organisms in terms of differentiation, proliferation, embryonic development, tissue repair processes and immune responses (Stock *et al.*, 2013). It has been well studied using microscopic tools such as Transwell migration assays and time-lapse imaging. The Transwell migration assay is conducted over several hours to days, whereas time-lapse imaging allows us to quantitate distance, speed and morphological changes. Thus, I chose time-lapse imaging to evaluate the effect of temperature changes on microglia because I wanted to examine the basic properties of microglia from a point of view of cell motility, which is an essential feature for all living cells. As for the temperature control system, few papers reported temperature-dependency in cell motility because the maintenance of temperature in culture at 37°C is a common parameter among the people who work in the field of cell motility at least in mammals. The fact that the surface expression of some ion channels can increase by cultivation at low temperature (Vanoye *et al.*, 2013) led me to perform time-lapse imaging under different temperature conditions. I successfully established the system to observe temperature-dependent microglia movement at a

single-cell level.

Microglial motility is temperature-dependent

The present study focused on the modulation of microglial motility by temperature. In the brain, microglia as resident immune cells exhibit a robust motile feature that characterizes them as cells distinct from other glial cells such as astrocytes and oligodendrocytes (Hanisch *et al.*, 2007). In response to the brain damage or inflammation, surveillant microglia transform into the activated phenotype to migrate toward the damaged area and release various molecules including cytokines. Although there is a work showing that microglial motility was different between 33°C and 37°C conditions with regard to speed of microglia process movement, the difference was reported to be caused by the temperature-dependence of neuronal activity. Moreover, the temperature-dependency was lost in the presence of tetrodotoxin (TTX) (Wake *et al.*, 2009). Though the functions of many proteins could be affected by temperature changes, I found that microglia movement was strongly affected by the temperature changes through 33°C to 40°C *in vitro* (Figs. 2 and 3). Thus, microglial functions could be regulated by the multiple mechanisms, including one involving microglia themselves as well in cooperation with neurons. However, the observations in the above report did not determine whether temperature itself affected microglial motility because a recent study reported that Nav 1.6 is expressed functionally in microglia and contributes to the mechanism of lamellipodial protrusion in microglia (Persson *et al.*, 2014). As to the influence of temperature on microglia functions, some studies reported that the production of pro-inflammatory cytokines such as tumor necrosis factor α (TNF α) and nitrite oxide (NO) in stimulated microglia were temperature-dependent between 33°C and 39°C (Matsui *et al.*, 2012; Seo *et al.*, 2012). In the ischemic situation, hypothermia protects neuronal functions by suppressing the immune responses stimulated by

ischemic damage (Yenari *et al.*, 2012). Microglia migrate to the damaged area and release pro-inflammatory cytokines and reactive oxygen species (ROS) that can activate immune cells invading the brain. My analysis of temperature-dependent microglia movement suggests that therapeutic hypothermia can suppress the microglia movement as well as cytokine production. On the other hand, hypothermia can impair the immune system by suppressing the cytokine response of T-lymphocytes and worsen the outcome and mortality in the patients treated with therapeutic hypothermia (Han *et al.*, 2015). Given that microglia share basic properties with immune cells such as macrophages (Ransohoff *et al.*, 2009), my results also can explain the mechanism underlying the side effects observed in clinical trials of therapeutic hypothermia wherein suppression of immune cell functions accompanies the lowering of temperature. Thus, my results in this study will help to understand the basis of cell motility for the establishment of better applications in therapeutic hypothermia while avoiding the side effects.

Involvement of thermosensitive TRP channels

Given that microglia movement was temperature-dependent, I examined the mRNA expression levels of several thermosensitive TRP channels whose temperature thresholds are within the body temperature range, and found three candidate channels: TRPM2, TRPM4 and TRPV4 (Fig. 4). Although the expression and several functions of TRPM2 and TRPV4 in microglia have been studied, the functions of TRPM4 have not been well analyzed. Furthermore, the temperature-dependence of the three channels has never been studied in microglia. I analyzed the temperature-dependency of the candidates using a pharmacological approach and gene-knockout mice with a patch-clamp method and time-lapse imaging technique. The results showed that there was no difference in migration distance between 37°C and 40°C in both M2KO and V4KO microglia, suggesting that TRPM2 and TRPV4 are involved in the

temperature-dependent microglia movement to some extent although the distance was significantly different only between Wt and V4KO microglia at 40°C (Fig. 5). Because it is well known that some thermosensitive TRP channels can be synergistically activated by temperature with other effective stimuli, involvement of TRPM2 and TRPV4 in the temperature-dependent microglia movement could be more clearly seen in other experimental conditions.

The remaining candidate thermosensitive TRP channel is TRPM4. In addition to immunocytochemistry, I conducted experiments with patch-clamp recordings and time-lapse imaging using a TRPM4 inhibitor and siRNA-mediated gene knockdown. I observed the expression of TRPM4 in isolated microglia at the protein level using an anti-TRPM4 antibody applicable in the heterologous expression system (Fig. 6). In my analysis of TRPM4 function, 9-phenanthrol inhibited both heat-evoked currents with high intracellular free Ca^{2+} concentration in isolated microglia (Fig. 8) and temperature-dependent microglia movement (Figs. 9 and 10), although microglia movement at 37°C was not significantly affected by siRNA-mediated gene knockdown partly because of the inefficiency of the siRNAs used (Fig. 11). These results suggest the involvement of TRPM4 in the temperature-dependent microglia movement. However, more supporting data would be necessary to confirm the TRPM4 involvement. There is an apparent discrepancy between the effects on heat-evoked currents in microglia and the effects on temperature-dependent microglia movement. Although I have currently no clear idea to explain the discrepancy, several ion channels may be activated by heat in microglia and 9-phenanthrol could inhibit ion channels other than TRPM4 in microglia. As to the specificity of 9-phenanthrol inhibition on TRPM4 activation, 9-phenanthrol does not inhibit TRPM5, TRPC3, TRPC6 or cystic fibrosis transmembrane conductance regulator (CFTR) channel activities at the concentration of 30 μ M at which the temperature-dependency of microglia

movement was not observed (Fig. 10) (Guinamard *et al.*, 2014). In primary cerebral artery smooth muscle cells, 9-phenanthrol does not inhibit the activation of Ca^{2+} -activated K^+ channels, inward rectifying K^+ channels or voltage-gated K^+ channels at the same range used in my study (Guinamard *et al.*, 2014). Although I should consider the possibility that 9-phenanthrol inhibits such ion channels at higher concentrations, the involvement of K^+ -permeable ion channels is unlikely because I did not use K^+ -containing solutions in patch-clamp recordings in which I observed heat-evoked currents in microglia inhibited by 9-phenanthrol (Fig. 8).

As to the methodology of knockdown, microglia are known to be strongly refractory to gene transfer (Su *et al.*, 2015). Indeed, the efficiency of knockdown was around 50% in this study (Fig. 11). Such a low efficiency could be one reason for the lack of significant differences in microglia movement between GC siRNA (negative control) and *Trpm4*-specific siRNAs groups. Gene transfer with lentiviral or recombinant adeno-associated viral vectors is a useful tool for microglia with a high efficiency and worth trying to verify the involvement of TRPM4 in microglia movement with high cell variability. Virus-mediated siRNA incorporation into microglia or analysis of *Trpm4*-knockout microglia could provide clearer evidence for the involvement of TRPM4.

Other candidate ion channels involved in the temperature-dependent microglia movement

Other ion channels or ion channel-related proteins activated by temperature changes could also be involved in temperature-dependent microglia movement. Hv1 is one such candidate because a recent work reported that Hv1 is necessary for ROS generation in microglia and deletion of *Hv1* attenuated the ischemic-induced brain damage in mice (Wu *et al.*, 2012). Additionally, it is strongly temperature-sensitive (Fujiwara *et al.*, 2012). Indeed, I observed strongly outwardly rectifying heat-evoked currents in microglia and the property of such

currents looked similar to that of Hv1. The results of the inhibition of heat-evoked currents by 100 μM ZnCl_2 in microglia suggests that Hv1 may be involved in temperature-dependent microglia movement more than TRPM4 because the extent of 100 μM ZnCl_2 inhibition on heat-evoked currents in microglia was greater than that of 100 μM 9-phe (Figs. 8 and 12). However, in comparison to the effects of 9-phenanthrol on microglia movements (Fig. 10), ZnCl_2 had no effect on microglia movement at all (Fig. 12). Thus, the involvement of Hv1 looks unlikely (Fig. 12).

Heat stimulus is also known to activate stromal interaction molecule 1 (STIM1)/calcium release-activated calcium channel protein (Orai) complex which is well expressed in microglia (Michaelis *et al.*, 2015), suggesting its involvement in the temperature-dependent microglia movement. It has been reported that STIM1 activation is temperature-dependent and heat leads to Orai-mediated Ca^{2+} influx through STIM1 clustering (Xiao *et al.*, 2011). In that report, STIM1/Orai-mediated Ca^{2+} responses showed an off-response property. In other words, a large Ca^{2+} influx responding to the lowering of temperature after heat application was observed in Ca^{2+} -imaging experiments using HEK293T cells expressing STIM1/Orai. In contrast, my results of heat-evoked currents in microglia showed a property of the reaction parallel to heat application. Additionally, the experimental condition in the paper is different from that in this study. Although it is difficult to compare them, it is possible that STIM1/Orai-mediated Ca^{2+} influx could be upstream of TRPM4 activation because TRPM4 activation by heat requires intracellular Ca^{2+} as discussed below (Fig. 7). Other unknown temperature-dependent ion channels could be working in microglia, and identification of such proteins would clarify the complicated temperature dependency of microglia.

A possible scheme for temperature-dependent microglia movement involving TRPM4

If TRPM4 is involved in temperature-dependent microglia movement, how is TRPM4 activated? As shown in Fig. 7, heat-evoked TRPM4 activation requires an increase in intracellular free Ca^{2+} . Although I did not determine the dose-dependency of intracellular free Ca^{2+} for TRPM4 activation, heat-evoked TRPM4-mediated currents were never observed if the pipette solution lacked Ca^{2+} . Therefore, increases in intracellular free Ca^{2+} are essential for heat-evoked TRPM4 activation in HEK293T cells expressing mTRPM4. The result that 9-phenanthrol-dependent components in the heat-evoked currents in microglia were observed only in the presence of intracellular free Ca^{2+} could support the notion of a Ca^{2+} requirement for TRPM4 activation in microglia. Increases in intracellular free Ca^{2+} could be caused in several ways, including downstream G_q -coupled receptor activation. Ca^{2+} influx through Ca^{2+} -permeable channels such as TRPC channels could also lead to TRPM4 activation (Kettenmann *et al.*, 2011). Membrane phospholipids such as PIP_2 are also known to regulate TRPM4 function (Nilius *et al.*, 2006) and the amount of PIP_2 or its binding to the channel is reported to be affected by threshold temperature changes in another TRPM channel, TRPM8 (Fujita *et al.*, 2013). Thus, TRPM4 channel activity can be regulated in physiological conditions.

One can also ask how TRPM4 activation increases microglia movement. As described in the Introduction, mobilization of intracellular free Ca^{2+} can regulate cell motility through actin cytoskeleton rearrangement. However, Ca^{2+} does not permeate TRPM4. Na^+ influx through TRPM4 could lead to the inhibition of other Na^+ influx pathways such as NCX and sodium/hydrogen exchanger 1 (NHE), both of which are well expressed in microglia, which could cause increases in intracellular free Ca^{2+} (Liu *et al.*, 2010; Stock *et al.*, 2013). Such increases in intracellular free Ca^{2+} might further activate TRPM4. Such global increases in intracellular free Ca^{2+} and local increases in intracellular free Ca^{2+} could be differentially

regulated. Alternatively, Na⁺ influx through TRPM4 could contribute to microglial motility via the activation of the reverse mode of NCX as reported in other cell types (Persson *et al.*, 2014; Hilge, 2013; Shi *et al.*, 2013). Recently, an interesting paper has reported that depolarization itself can regulate the two anionic phospholipids, phosphatidylserine (PS) and PIP₂, via the acceleration of their clustering on the plasma membrane. PS enhances Kirsten rat sarcoma viral oncogene homolog (K-Ras)-related-MAPK signaling involved in cell proliferation (Zhou *et al.*, 2015). The depolarization through TRPM4 activation could influence unknown signal pathways in the cytoplasm. Thus, TRPM4 can be a modulator downstream of Ca²⁺-dependent signaling in the mechanism of temperature-dependent cell motility.

In conclusion, I identified TRPM4 as an important molecule involved in the temperature-dependent movement of mouse microglia. Although further studies are necessary to confirm this concept, modulation of TRPM4 function in microglia could lead to the development of therapeutic ways to treat various diseases that involve TRPM4.

II-5. Figure Legends

Figure 1.

Characterization of microglia culture by immunocytochemistry

(A, B and C) Representative images of microglia cultures (left, A-C) and each control culture (right, astrocyte-enriched culture (A), hippocampal neuron culture (B) and glia-mixed culture (C)) are shown. The following antibodies were used: Iba1 and GFAP (A), Iba1 and Tuj1 (B) and CD11b and Olig2 (C). Scale bar represents 50 μm .

Figure 2.

Temperature affected microglia movement

(A) The experimental method of time-lapse imaging using microglia culture in different temperature conditions. The letters in parenthesis and arrows indicate the time at which each image was taken. (B) The images of microglia culture in different temperature conditions taken at the time from (a) to (h). An open yellow circle indicates the xy coordinate of a representative target at each time and a red-filled circle indicates the coordinate in the previous image. A red dotted-arrow indicates the rectilinear distance of the target from the previous place. Scale bar represents 50 μm .

Figure 3.

Quantitative analysis of microglia movement in different temperature conditions

(A) The trajectories of microglia at 37°C traced by a cell-tracking program using the algorithm of template matching. Dots in the center of the open circles represent the coordinates of cells and colored lines indicate the trajectory of those cells moving from 0 min to 57 min. (B) The trajectories of microglia movement over 2hrs in different temperature conditions (33°C, 37°C

and 40°C). The paths were arranged to show their origins at $x = y = 0$. Each line indicates a trajectory of each cell. (C) The accumulated distances of migrating microglia in different temperature conditions. The number in parenthesis indicates the analyzed cell number of microglia whose paths are shown in (B). **, $p < 0.01$, one-way ANOVA with Tukey-Kramer test.

Figure 4.

Expression patterns of thermosensitive TRP channel genes in isolated microglia

Expression patterns of eight TRP channel genes in isolated microglia and two controls (*Gapdh* and *Cd11b*, a microglia marker) are shown. The mRNAs of *Trpm2*, *Trpm4*, *Trpv4* and *Trpv2* were detectable. C indicates the amplified fragments using each cDNAs as a template.

Figure 5.

Comparison of the moving distances of microglia from Wt, *Trpm2*-knockout (M2KO) or *Trpv4*-knockout (V4KO) mice in different temperature conditions

The moving distances of each cell during a 2 hr incubation are shown as filled circles. The horizontal line indicates the average distance calculated from the accumulated distances of microglia in each temperature condition. The number in parenthesis shows the cell number analyzed. **, $p < 0.01$, one-way ANOVA with Tukey-Kramer test.

Figure 6.

Immunocytochemical analysis using an anti-TRPM4 antibody

(A) Representative images of HEK293T cells expressing mTRPM4 stained with anti-Myc and anti-TRPM4 antibodies. (B) Representative images of primary microglia stained with

anti-CD11b and anti-TRPM4 antibodies. Nuclei were stained with DAPI. Images without the first antibodies are shown in the far right. Scale bar represents 50 μm .

Figure 7.

TRPM4 is a Ca^{2+} -activated and heat-sensitive channel inhibited by 9-phenanthrol

(A, B and C) Representative whole-cell current traces in HEK293T cells expressing mTRPM4 in the presence (A) or absence (B) of 1 μM intracellular free Ca^{2+} ($[\text{Ca}^{2+}]_i = 1\mu\text{M}$) followed by heat stimulation. The lower traces indicate the temperature transition of the extracellular solution applied into the chamber. Ramp-pulses from -100 to +100 mV in 500 msec were applied every 5 sec. Current-voltage curves at the time points a, b and c are shown in (C). **(D and E)** The mTRPM4-mediated currents activated by 1 μM intracellular free Ca^{2+} decreased rapidly after 100 μM 9-phenanthrol (9-phe) application. **(F and G)** 9-phe reversibly inhibited the mTRPM4-mediated heat responses. HEK293T cells expressing mTRPM4 dialyzed with 1 μM intracellular free Ca^{2+} were stimulated by ramp-pulses (-100 to +100 mV in 500 msec, every 5 sec) and repeated heat application. The mTRPM4-mediated currents responding to the second heat stimulation were recorded in the absence (F) or presence (G) of 100 μM 9-phe. **(H)** Dose-dependent inhibition of heat-evoked mTRPM4-mediated currents by 9-phe at -100 or +100 mV (n = 5 or 6). *, p < 0.05 and **, p < 0.01 at +100 mV; #, p < 0.05 and ##, p < 0.01 at -100 mV, non-parametric multiple comparison with Shirley-Williams test.

Figure 8.

9-phenanthrol inhibited heat-evoked currents in primary microglia

(A and B) A representative whole-cell current trace in primary microglia in the presence of 1 μM intracellular free Ca^{2+} stimulated by repeated heat application (A). The lower trace

indicates the temperature transition of the extracellular solution applied into the chamber. Ramp-pulses from -100 to +100 mV in 500 msec were applied every 5 sec. Current-voltage curves at the time points a and b are shown in (B). **(C and D)** The partial and reversible inhibition of heat-evoked currents in microglia by 100 μM 9-phe (C). The lower trace indicates the temperature transition. Current-voltage curves at the time points a, b and c are shown in (D). **(E)** A representative whole-cell current trace in microglia in the presence of 1 μM intracellular free Ca^{2+} with application of 100 μM 9-phe prior to heat stimulus. The lower trace indicates the temperature transition. **(F)** The comparative inhibition of heat-evoked currents by 9-phe in microglia in the presence or absence of 1 μM intracellular free Ca^{2+} at -100 or +100 mV ($n = 6$ or 7). *, $p < 0.05$ and **, $p < 0.01$ versus the normalized currents without 9-phe at +100mV, one-way ANOVA with Tukey-Kramer test.

Figure 9.

9-phenanthrol reversely inhibited microglia movement

(A) The experimental method of time-lapse imaging with 30 μM 9-phenanthrol (9-phe). After incubation at 37°C for 2hrs, 9-phe was added in a final concentration of 30 μM . **(B)** Representative images showing the reversible inhibition of microglia movement by 9-phenanthrol. The images were taken at the indicated time points. A yellow arrow in each image indicates the target. Scale bar represents 50 μm .

Figure 10.

9-phenanthrol inhibited microglia movement in a dose-dependent manner

The inhibitory effects of 9-phenanthrol (9-phe) on microglia movement were tested using time-lapse imaging of microglia cultures. Each filled circle indicates the moving distance of

one cell and a horizontal line indicates the average distance in each group. Control (Con) represents the moving distance of each cell in 2 hrs before application of 9-phe as a black filled circle. The distance of the corresponding microglia in 2 hrs after application of 9-phe is shown as a red filled circle. The number in parenthesis indicates the cell number analyzed. **(A)** Dose-dependent inhibition of microglia movement at 37°C by 9-phe. **, $p < 0.01$, one-way ANOVA with Tukey-Kramer test. **(B)** Analysis of temperature-dependent inhibition of microglia movement by 10 μM (a) or 30 μM (b) 9-phe at 33°C, 37°C and 40°C. **, $p < 0.01$, one-way ANOVA with Tukey-Kramer test.

Figure 11.

Effects of *Trpm4*-specific siRNA treatment on microglia movement

(A) Relative expression of *Trpm4* mRNA treated with three different siRNAs and GC siRNA ($n = 6$ in each group). **(B)** Effects of siRNAs on microglia movement at 37°C were tested using time-lapse imaging of microglia cultures. Each filled circle indicates the moving distance of one cell and the horizontal line indicates the average distance in each group. GC siRNA represents the distance moved in 2 hrs by each cell treated with GC siRNA (black filled circle). The distance moved in 2 hrs by microglia treated with three different *Trpm4*-specific siRNAs (red filled circle). The number in parenthesis indicates the cell number analyzed.

Figure 12.

Zinc chloride, a proton channel inhibitor, inhibited heat-evoked currents in primary microglia but did not affect temperature-dependent microglia movement

(A and B) A representative whole-cell current trace from primary microglia in the presence of 1 μM intracellular free Ca^{2+} stimulated by heat application followed by 100 μM zinc chloride

(ZnCl₂, A). The lower trace indicates the temperature transition of the extracellular solution applied into the chamber. Ramp-pulses from -100 to +100 mV in 500 msec were applied every 5 sec. Current-voltage curves at the time points a, b and c are shown in (B). (C) Expression of the *Hv1* gene in primary microglia (RT-PCR). Con indicates the amplified fragment obtained using a plasmid DNA as a DNA template. The predicted band was not amplified in the sample of RT (-) that was not subjected to the RT reaction. (D) Representative whole-cell current traces of heat responses in HEK293T cells expressing mHv1 in the absence (a) or presence (b) of 100 μM ZnCl₂. The pipette solution contained 1 μM intracellular free Ca²⁺. (E) ZnCl₂ did not inhibit temperature-dependent microglia movement. The accumulated distances of migrating microglia in three different temperature conditions before (black filled circles) and after (red filled circles) application of 100 μM ZnCl₂ are shown with a horizontal line indicating the average distance in each group. **, p < 0.01, one-way ANOVA with Tukey-Kramer test.

II-6. Figures

Figure 1

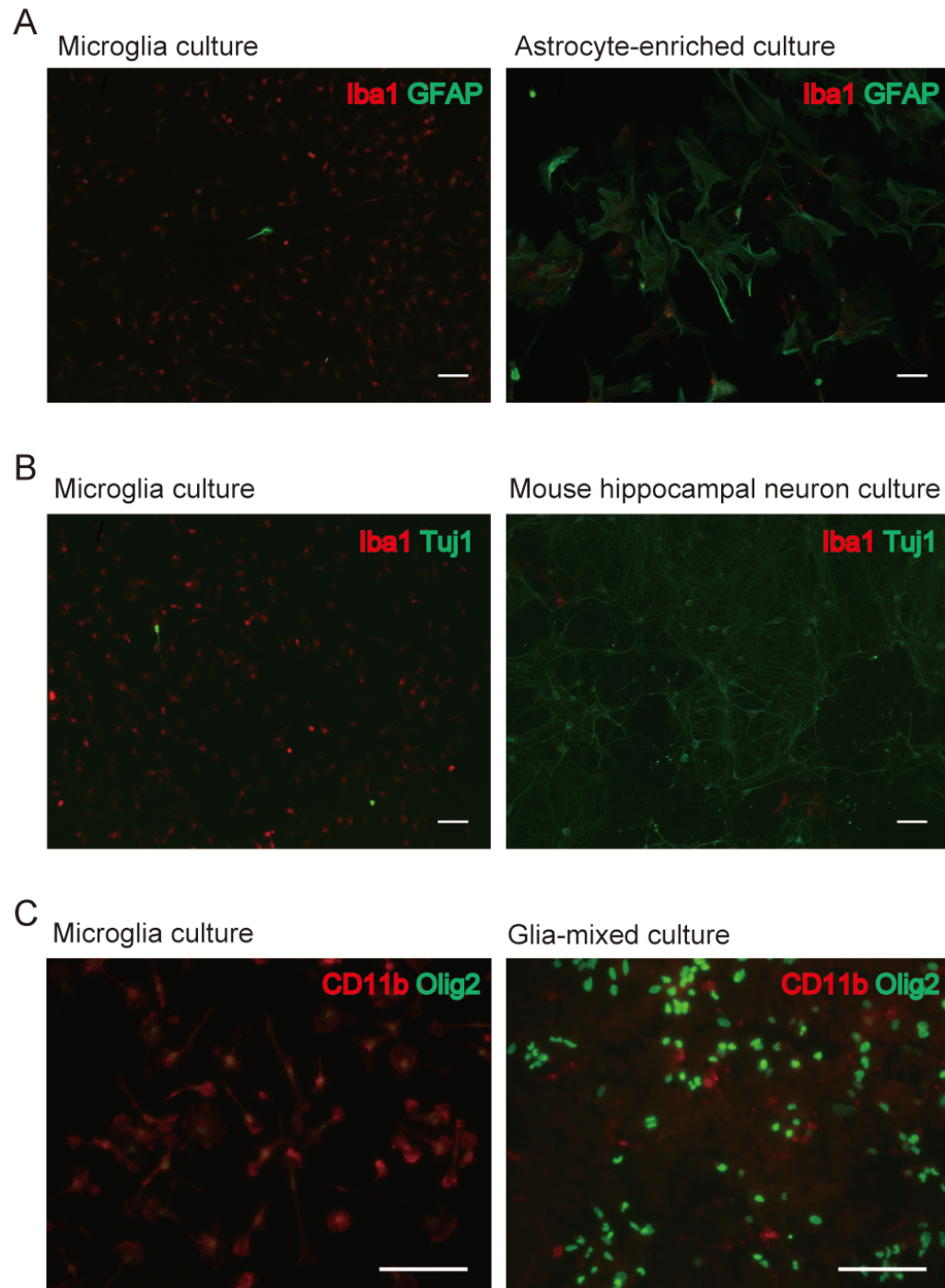


Figure 2

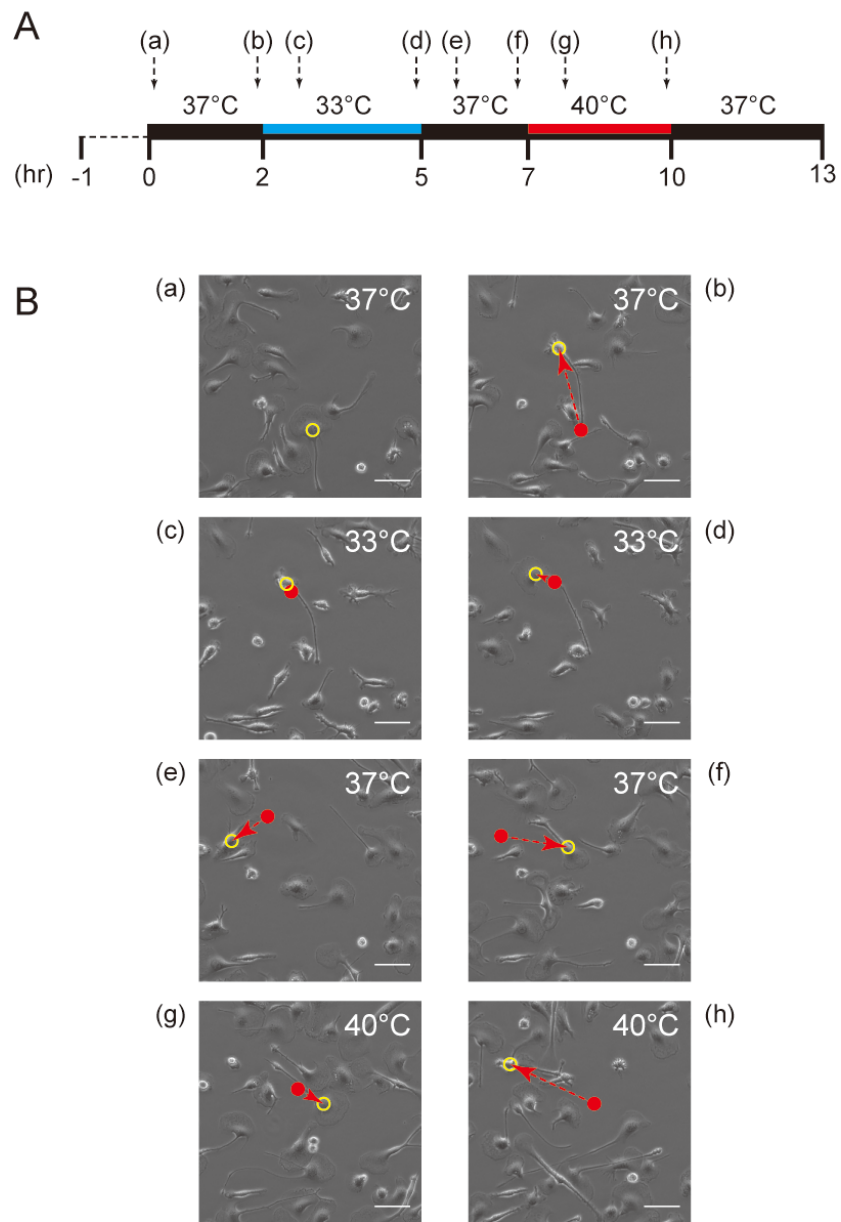
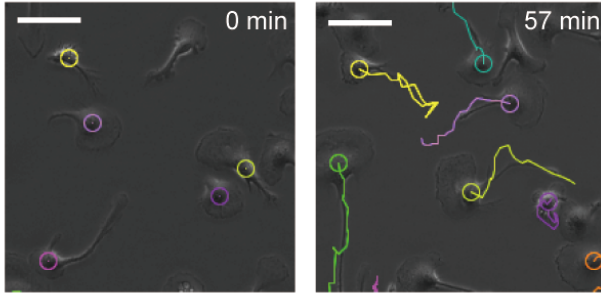
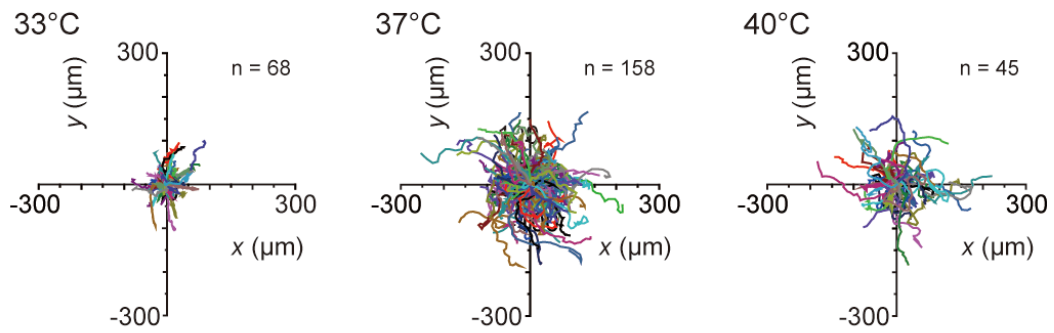


Figure 3

A



B



C

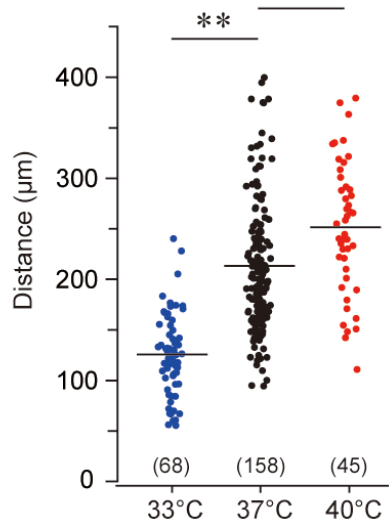


Figure 4

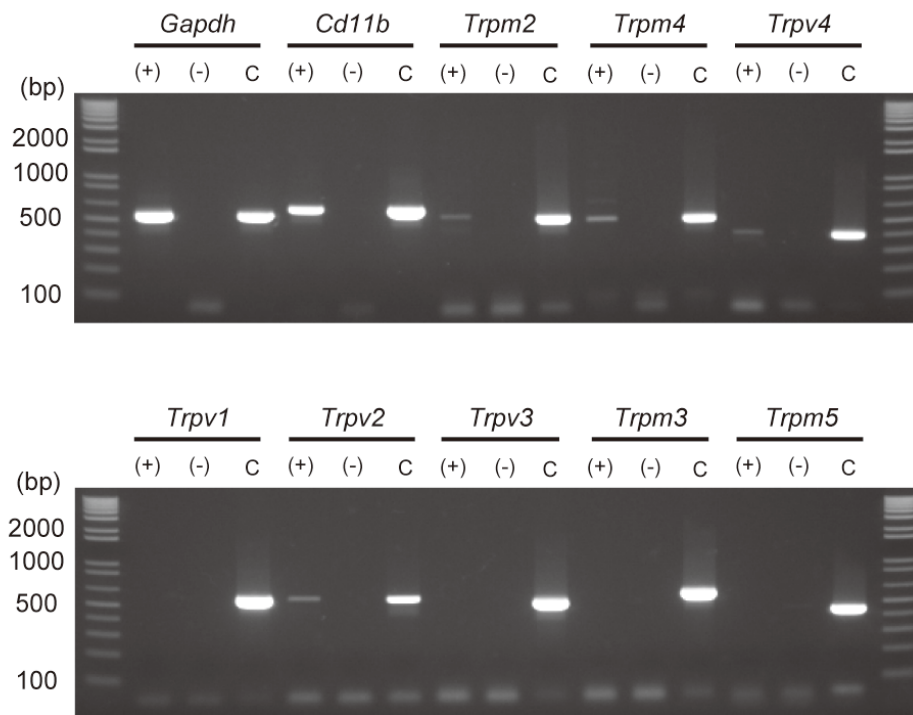


Figure 5

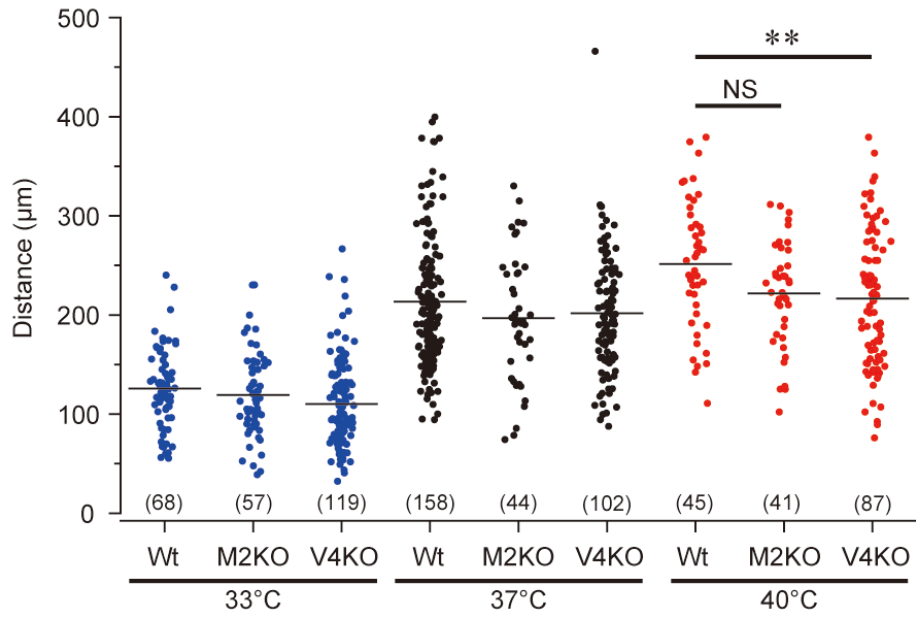
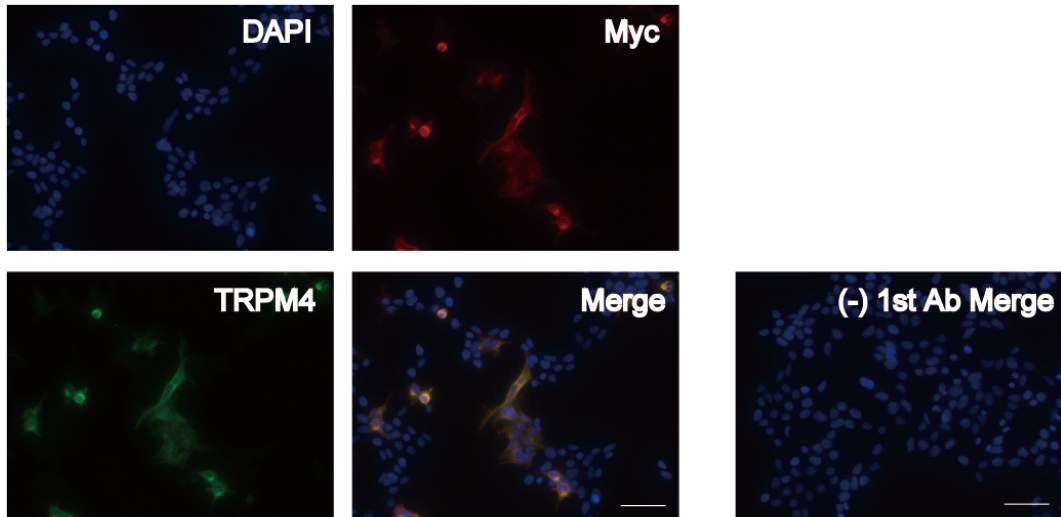


Figure 6

A HEK293T cells expressing myc-tagged mTRPM4



B Microglia culture

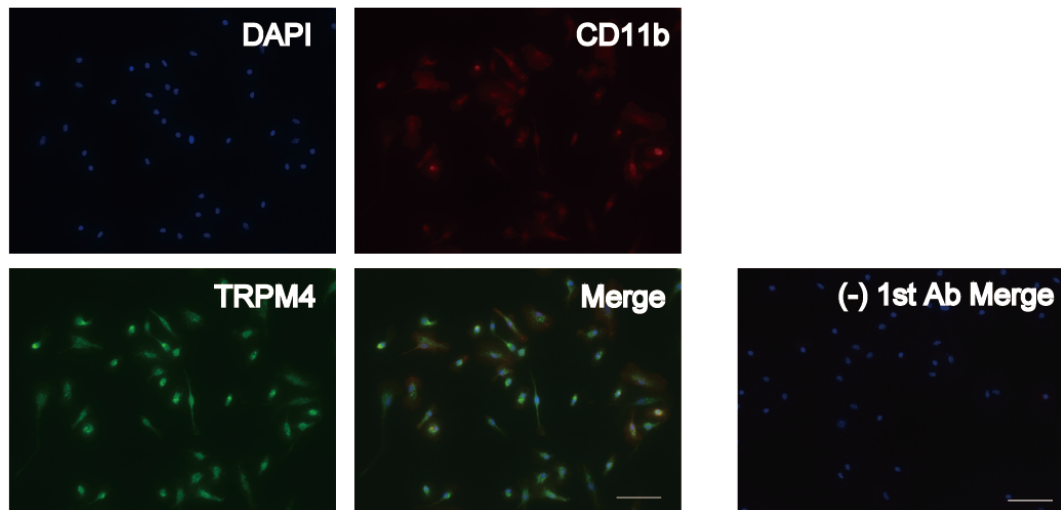


Figure 7

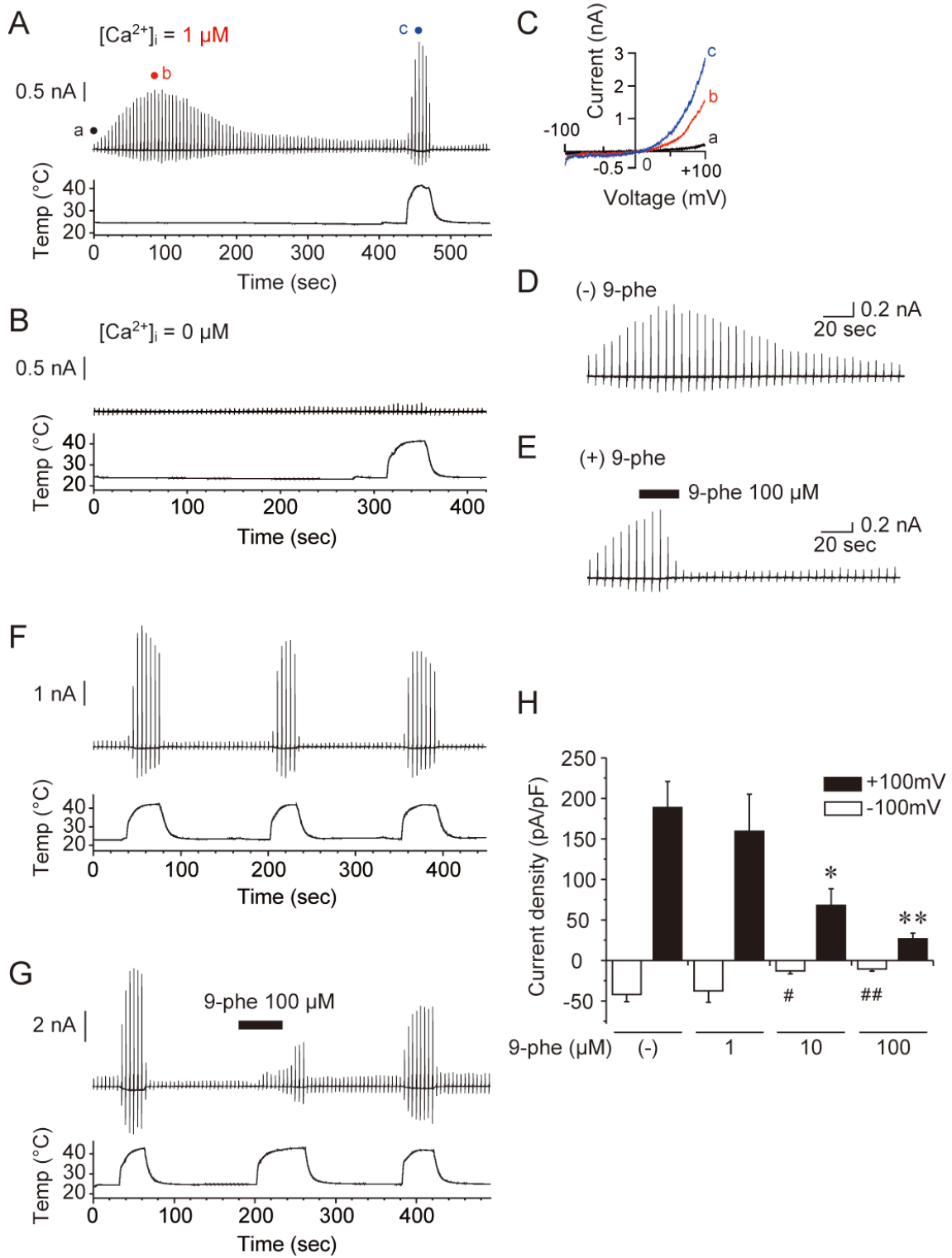


Figure 8

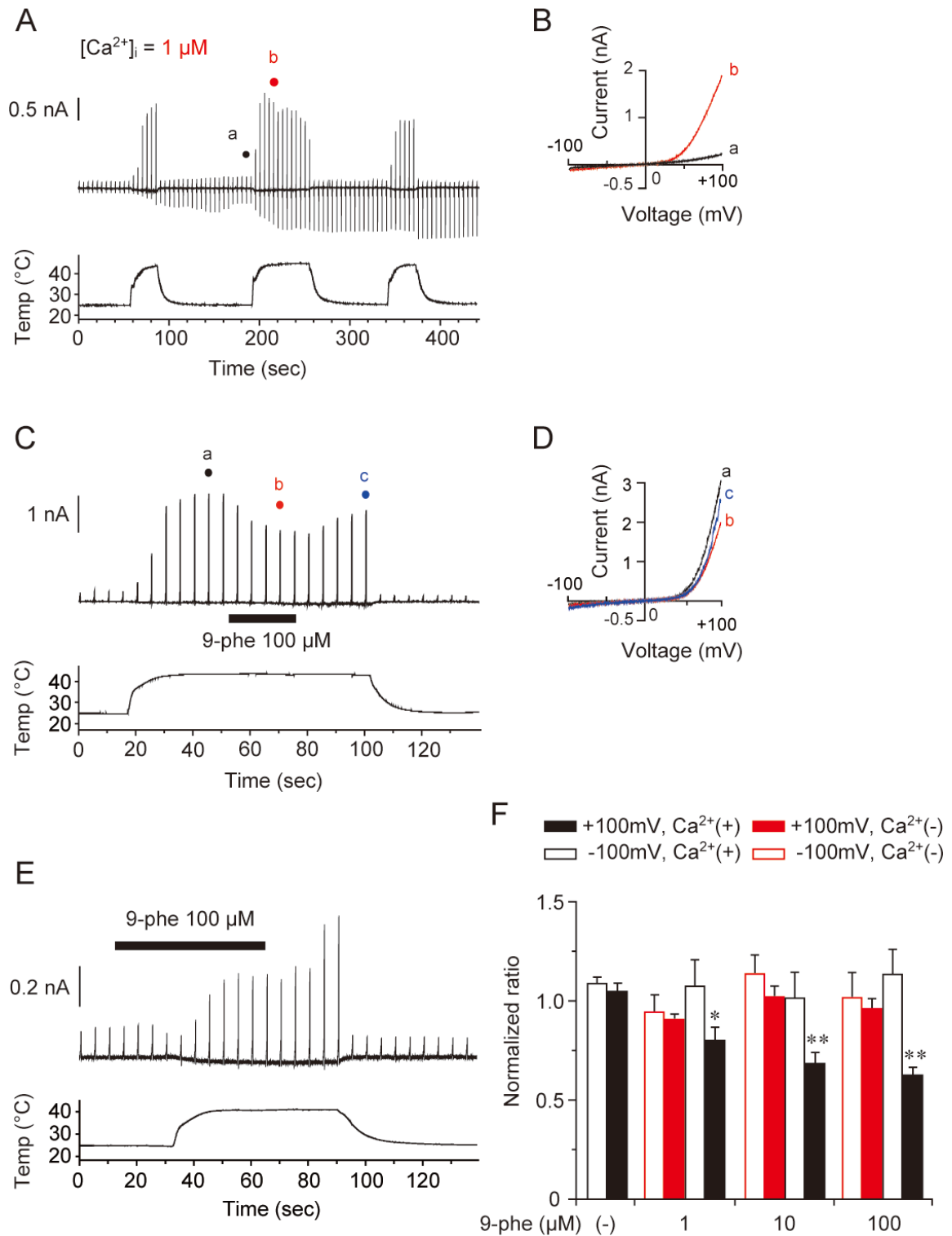


Figure 9

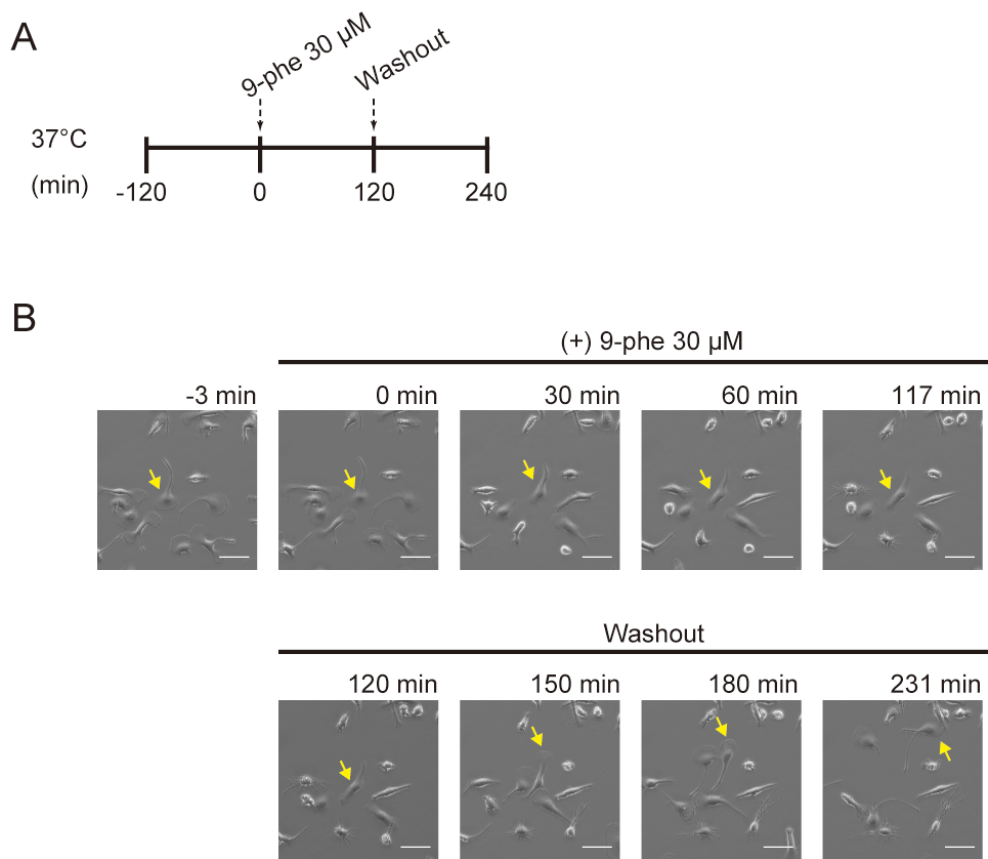
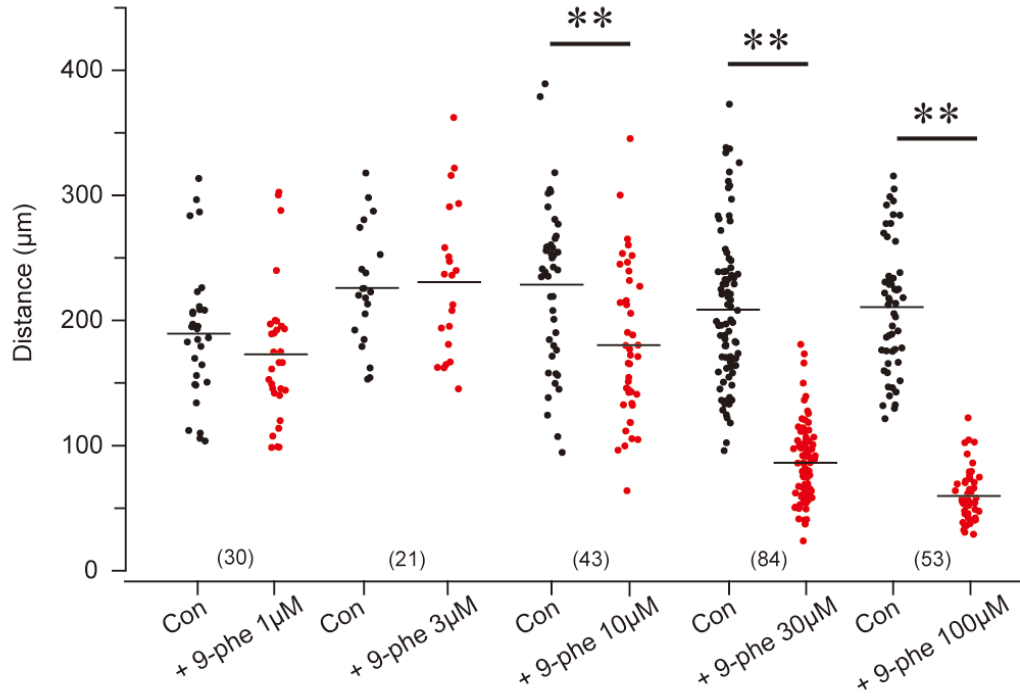


Figure 10

A



B

(a) 9-phenanthrol 10 µM

(b) 9-phenanthrol 30 µM

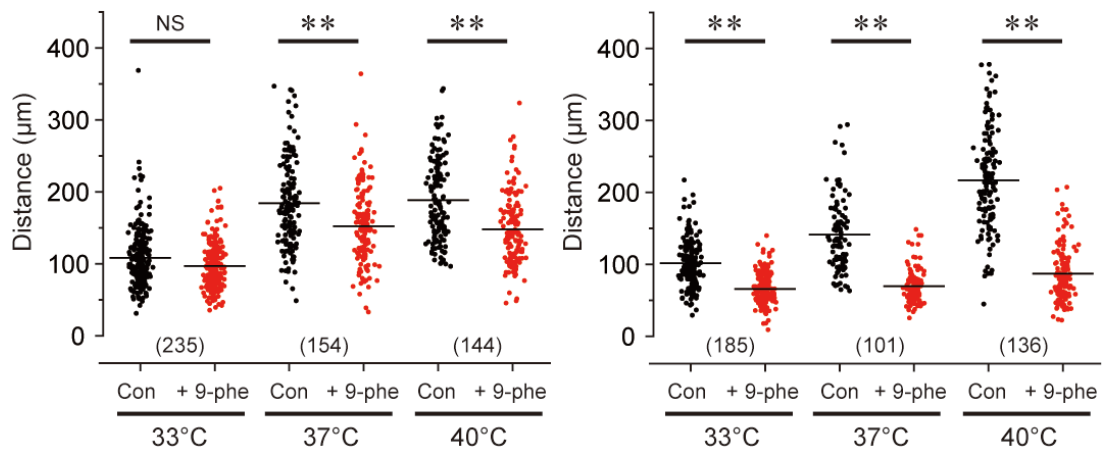


Figure 11

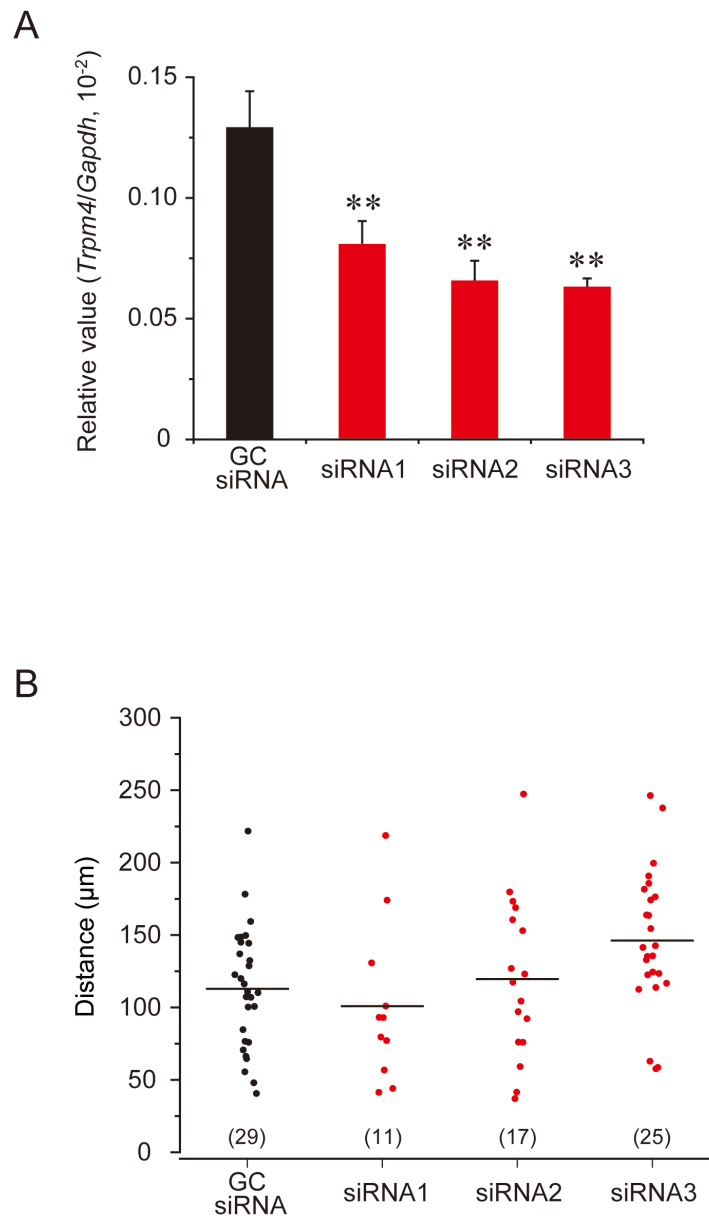
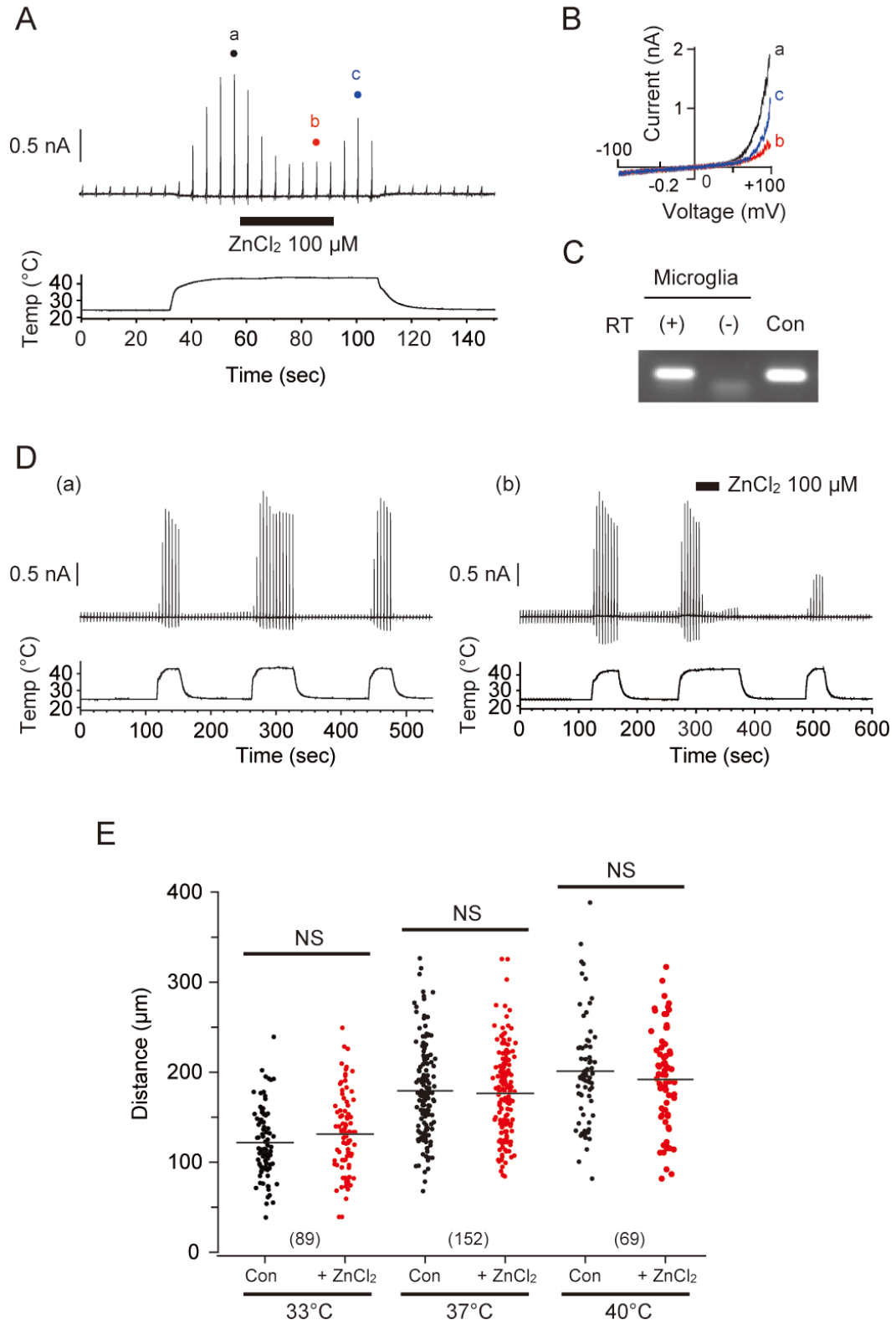


Figure 12



3. Abbreviations

A1KO, *Trpa1*-knockout
ADP, adenosine diphosphate
AITC, allyl isothiocyanate
Akt, protein kinase B
ANOVA, analysis of variance
ATP, adenosine triphosphate
ATP, adenosine triphosphate
Bic, (+)-bicuculline
BSA, bovine serum albumin
[Ca²⁺]_i, intracellular Ca²⁺ concentration
Cap, capsaicin
CD11b, integrin β2
cDNA, complementary DNA
Con, control
CX3CL1, chemokine (C-X3-C motif) ligand 1
CXC3R1, G_i-coupled fractalkine receptor
DAPI, 4', 6-diamidino-2-phenylindole
DMSO, dimethyl sulfoxide
DNA, deoxyribonucleic acid
DRG, dorsal root ganglion
ER, endoplasmic reticulum
ERK, extracellular-signal-regulated kinase
Flu, flunarizine dihydrochloride
GABA, γ-amino butyric acid
GABA_A receptor, type A γ-amino butyric acid receptor
Gapdh, glyceraldehyde 3-phosphate dehydrogenase
GFAP, glial fibrillary acidic protein
HEK293T cell, human embryonic kidney 293T cell
hr, hour
hTRPA1, human TRPA1
hTRPV1, human TRPV1

Hv1, voltage-gated proton channel Hv1/VSOP
Iba1, ionized calcium binding adaptor molecule 1
InsP₃, inositol trisphosphate
Iono, ionomycin
K-Ras, Kirsten rat sarcoma viral oncogene homolog
KCC2, potassium chloride cotransporter 2
K_v1.3, voltage-gated potassium channel shaker-related 1.3,
LPS, lipopolysaccharide
M2KO, *Trpm2*-knockout
mHv1, mouse Hv1
min, minute
mM, mili molar
mTRPA1, mouse TRPA1
mTRPM4, mouse TRPM4
mTRPV1, mouse TRPV1
NADPH, nicotinamide adenine dinucleotide phosphate
Nav1.6, voltage-gated sodium channel 1.6
NCX, sodium calcium exchanger
NHE, sodium hydrogen exchanger
Nif, nifedipine
NNC, NNC 55-0396 dihydrochloride
NO, nitrite oxide
Olig2, oligodendrocyte transcription factor 2
Orai, calcium release-activated calcium modulator
P2X, purinergic receptor ionotropic
P2Y, purinergic receptor G protein-coupled
9-phe, 9-phenanthrol
PCR, polymerase chain reaction
pGL, pGreen Lantan1
PI(4,5)P₂, phosphatidylinositol 4,5-bisphosphate
PI3K, phosphoinositide 3-kinase
Pic, picrotoxin
PIP₂, phosphatidylinositol 4,5-bisphosphate

PIP₃, phosphatidylinositol-3,4,5-trisphosphate
PKC ϵ , protein kinase C epsilon
PLC, phospholipase C
Propofol, 2,6-diisopropylphenol
PS, phosphatidylserine
RNA, ribonucleic acid
ROS, reactive oxygen species
RT-PCR, reverse transcription polymerase chain reaction
sec, second
siRNA, small interfering RNA
STIM1, stromal interaction molecule 1
TNF α , tumor necrosis factor α
TRP channels, transient receptor potential channels
TRPA1, transient receptor potential ankyrin 1
TRPC, transient receptor potential canonical
TRPM2, transient receptor potential melastatin 2
TRPM4, transient receptor potential melastatin 4
TRPV1, transient receptor potential vanilloid 1
TRPV2, transient receptor potential vanilloid 2
TRPV4, transient receptor potential vanilloid 4
TTX, tetrodotoxin
Tuj1, class III β -tubulin
UDP, uridine-5'-diphosphate
V1A1DKO, *Trpv1/Trpa1* double-knockout
V1KO, *Trpv1*-knockout
V4KO, *Trpv4*-knockout
Ver, verapamil hydrochloride
Wt, wild-type
ZnCl₂, zinc chloride
 μ L, micro liter
 μ M, micro molar

4. Acknowledgements

I would like to thank Dr. Makoto Tominaga for leading me to the physiological sciences and also for his continuous encouragement and helpful advice throughout my doctoral thesis study. I also would like to thank Dr. Makiko Kashio (Kyoto Prefectural Univ.) for her mentorship, encouragement and kind advice throughout my study. I would like to thank Dr. Yoshitaka Kimori for developing the cell-tracking program and analyzing the data of cell coordinates. I would like to thank Dr. Junichi Nabekura, Dr. Hiroaki Wake (National Institutes of Physiological Sciences (NIPS)), Dr. Motohiro Nishida (NIPS), Dr. Hidemasa Furue (NIPS), Dr. Hitoshi Ishibashi (Kitasato Univ.), Dr. Tenpei Akita (Hamamatsu Univ. School of Medicine), Dr. Masaki Fukata and Dr. Yuko Fukata (NIPS) for their technical help and helpful suggestions and comments. I would like to thank Dr. David Julius (Univ. of California, San Francisco), Dr. Yasuo Mori (Kyoto Univ.), Dr. Makoto Suzuki (Jichi Medical School) for providing *Trpv1*-knockout, *Trpa1*-knockout, *Trpm2*-knockout and *Trpv4*-knockout mice, respectively. I would like to thank Dr. Michael Zhu (Univ. of Texas School of Medicine) for providing mTRPV1-inserted vector, Dr. Kenji Naruse and Dr. Ken Takahashi (Okayama Univ.) for their generous gift of anti-TRPM4 antibodies, Dr. Veit Flockerzi (Universität des Saarlandes) for providing mTRPM4-inserted vectors and Dr. Yasushi Okamura (Osaka Univ.) for providing mHv1-inserted vector. I would like to thank Naomi Fukuta and Claire Saito for their technical assistance. I would like to thank Dr. Makoto Tanaka and Dr. Sumii Yamamoto (Tsukuba Univ.) for their kind suggestions. I would like to thank Dr. Kunitoshi Uchida, Dr. Yoshiro Suzuki, Dr. Sigeru Saito and all of the laboratory members for their input. Finally, I would like to thank my father, mother and brother for their continuous encouragement.

5. References

- Akiyama H, McGeer PL (1990) Brain microglia constitutively express beta-2 integrins. *J Neuroimmunol* 30:81-93.
- Alkire MT, Hudetz AG, Tononi G (2008) Consciousness and anesthesia. *Science* 322:876-80.
- Aptel H, Hilaire C, Pieraut S, Boukhaddaoui H, Mallie S, Valmier J, Scamps F (2007) The Cav3.2/alpha1H T-type Ca²⁺ current is a molecular determinant of excitatory effects of GABA in adult sensory neurons. *Mol Cell Neurosci* 36:293-303.
- Ault B, Hildebrand LM (1994) GABA_A receptor-mediated excitation of nociceptive afferents in the rat isolated spinal cord-tail preparation. *Neuropharmacology* 33:109-14.
- Barbet G, Demion M, Moura IC, Serafini N, Leger T, Vrtovsnik F, Monteiro RC, Guinamard R, Kinet JP, Launay P (2008) The calcium-activated nonselective cation channel TRPM4 is essential for the migration but not the maturation of dendritic cells. *Nat Immunol* 9:1148-56.
- Bautista DM, Jordt SE, Nikai T, Tsuruda PR, Read AJ, Poblete J, Yamoah EN, Basbaum AI, Julius D (2006) TRPA1 mediates the inflammatory actions of environmental irritants and proalgesic agents. *Cell* 124:1269-82.
- Beck A, Penner R, Fleig A (2008) Lipopolysaccharide-induced down-regulation of Ca²⁺ release-activated Ca²⁺ currents (I_{CRAC}) but not Ca²⁺-activated TRPM4-like currents (I_{CAN}) in cultured mouse microglial cells. *J Physiol* 586:427-39.
- Benham CD, Gunthorpe MJ, Davis JB (2003) TRPV channels as temperature sensors. *Cell Calcium* 33:479-487.
- Cao E, Cordero-Morales JF, Liu B, Qin F, Julius D (2013) TRPV1 channels are intrinsically heat sensitive and negatively regulated by phosphoinositide lipids. *Neuron* 77:667-79.
- Carlton SM, Zhou S, Coggeshall RE (1999) Peripheral GABA_A receptors: evidence for peripheral primary afferent depolarization. *Neuroscience* 93:713-22.
- Caterina MJ, Rosen TA, Tominaga M, Brake AJ, Julius D (1999) A capsaicin-receptor homologue with a high threshold for noxious heat. *Nature* 398:436-41.
- Caterina MJ, Schumacher MA, Tominaga M, Rosen TA, Levine JD, Julius D (1997) The capsaicin receptor: a heat-activated ion channel in the pain pathway. *Nature* 389:816-24.
- Caterina MJ, Leffler A, Malmberg AB, Martin WJ, Trafton J, Petersen-Zeitz KR, Koltzenburg M, Basbaum AI, Julius D (2000) Impaired nociception and pain sensation in mice

- lacking the capsaicin receptor. *Science* 288:306-13.
- Chung MK, Jung SJ, Oh SB (2011) Role of TRP channels in pain sensation. *Adv Exp Med Biol* 704:615-36.
- Coull JA, Boudreau D, Bachand K, Prescott SA, Nault F, Sik A, De Koninck P, De Koninck Y (2003) Trans-synaptic shift in anion gradient in spinal lamina I neurons as a mechanism of neuropathic pain. *Nature* 424:938-42.
- Davalos D, Grutzendler J, Yang G, Kim JV, Zuo Y, Jung S, Littman DR, Dustin ML, Gan WB (2005) ATP mediates rapid microglial response to local brain injury in vivo. *Nat Neurosci* 8:752-8.
- Doenicke AW, Roizen MF, Rau J, Kellermann W, Babl J (1996) Reducing pain during propofol injection: the role of the solvent. *Anesth Analg* 82:472-4.
- Doering L (2010) *Protocols for Neural Cell Culture*. Humana Press.
- Dong XP, Wang X, Xu H (2010) TRP channels of intracellular membranes. *J Neurochem* 113:313-28.
- Dundee JW (1979) New i.v. anaesthetics. *Br J Anaesth* 51:641-8.
- Eder C, DeCoursey TE (2001) Voltage-gated proton channels in microglia. *Prog Neurobiol* 64:277-305.
- Fischer MJ, Leffler A, Niedermirtl F, Kistner K, Eberhardt M, Reeh PW, Nau C (2010) The general anesthetic propofol excites nociceptors by activating TRPV1 and TRPA1 rather than GABA_A receptors. *J Biol Chem* 285:34781-92.
- Franks NP (2006) Molecular targets underlying general anaesthesia. *Br J Pharmacol* 147 Suppl 1:S72-81.
- Fujita F, Uchida K, Takaishi M, Sokabe T, Tominaga M (2013) Ambient temperature affects the temperature threshold for TRPM8 activation through interaction of phosphatidylinositol 4,5-bisphosphate. *J Neurosci* 33:6154-9.
- Fujiwara Y, Kurokawa T, Takeshita K, Kobayashi M, Okochi Y, Nakagawa A, Okamura Y (2012) The cytoplasmic coiled-coil mediates cooperative gating temperature sensitivity in the voltage-gated H⁺ channel Hv1. *Nat Commun* 3:816.
- Funk K, Woitecki A, Franjic-Wurtz C, Gensch T, Mohrlen F, Frings S (2008) Modulation of chloride homeostasis by inflammatory mediators in dorsal root ganglion neurons. *Mol Pain* 4:32.
- Garcia PS, Kolesky SE, Jenkins A (2010) General anesthetic actions on GABA_A receptors. *Curr Neuropharmacol* 8:2-9.

- Gees M, Colsoul B, Nilius B (2010) The role of transient receptor potential cation channels in Ca^{2+} signaling. *Cold Spring Harb Perspect Biol* 2:a003962.
- Gees M, Owsianik G, Nilius B, Voets T (2012) TRP channels. *Compr Physiol* 2:563-608.
- Goswami C, Schmidt H, Hucho F (2007) TRPV1 at nerve endings regulates growth cone morphology and movement through cytoskeleton reorganization. *FEBS J* 274:760-72.
- Goswami C, Kuhn J, Heppenstall PA, Hucho T (2010) Importance of non-selective cation channel TRPV4 interaction with cytoskeleton and their reciprocal regulations in cultured cells. *PLoS One* 5:e11654.
- Guinamard R, Hof T, Del Negro CA (2014) The TRPM4 channel inhibitor 9-phenanthrol. *Br J Pharmacol* 171:1600-13.
- Guler AD, Lee H, Iida T, Shimizu I, Tominaga M, Caterina M (2002) Heat-evoked activation of the ion channel, TRPV4. *J Neurosci* 22:6408-14.
- Han Z, Liu X, Luo Y, Ji X (2015) Therapeutic hypothermia for stroke: Where to go? *Exp Neurol* 272:67-77.
- Hanisch UK, Kettenmann H (2007) Microglia: active sensor and versatile effector cells in the normal and pathologic brain. *Nat Neurosci* 10:1387-94.
- Haynes SE, Hollopeter G, Yang G, Kurpius D, Dailey ME, Gan WB, Julius D (2006) The P2Y₁₂ receptor regulates microglial activation by extracellular nucleotides. *Nat Neurosci* 9:1512-9.
- Hilge M (2013) Ca^{2+} regulation in the $\text{Na}^+/\text{Ca}^{2+}$ exchanger features a dual electrostatic switch mechanism. *Adv Exp Med Biol* 961:27-33.
- Hinman A, Chuang HH, Bautista DM, Julius D (2006) TRP channel activation by reversible covalent modification. *Proc Natl Acad Sci U S A* 103:19564-8.
- Ho KW, Lambert WS, Calkins DJ (2014) Activation of the TRPV1 cation channel contributes to stress-induced astrocyte migration. *Glia* 62:1435-51.
- Hoffmann A, Kann O, Ohlemeyer C, Hanisch UK, Kettenmann H (2003) Elevation of basal intracellular calcium as a central element in the activation of brain macrophages (microglia): suppression of receptor-evoked calcium signaling and control of release function. *J Neurosci* 23:4410-9.
- Horvath RJ, DeLeo JA (2009) Morphine enhances microglial migration through modulation of P2X₄ receptor signaling. *J Neurosci* 29:998-1005.
- Hypothermia-After-Cardiac-Arrest-Study-Group. (2002) Mild therapeutic hypothermia to improve the neurologic outcome after cardiac arrest. *N Engl J Med* 346:549-56.

- Imai T, Hieshima K, Haskell C, Baba M, Nagira M, Nishimura M, Kakizaki M, Takagi S, Nomiya H, Schall TJ, Yoshie O (1997) Identification and molecular characterization of fractalkine receptor CX3CR1, which mediates both leukocyte migration and adhesion. *Cell* 91:521-30.
- Inada H, Iida T, Tominaga M (2006) Different expression patterns of TRP genes in murine B and T lymphocytes. *Biochem Biophys Res Commun* 350:762-7.
- Islam M (2012) Calcium signaling. *Adv Exp Med Biol* 740.
- Ito D, Imai Y, Ohsawa K, Nakajima K, Fukuuchi Y, Kohsaka S (1998) Microglia-specific localisation of a novel calcium binding protein, Iba1. *Brain Res Mol Brain Res* 57:1-9.
- Jalota L, Kalira V, George E, Shi YY, Hornuss C, Radke O, Pace NL, Apfel CC (2011) Prevention of pain on injection of propofol: systematic review and meta-analysis. *BMJ* 342:d1110.
- Jurd R, Arras M, Lambert S, Drexler B, Siegwart R, Crestani F, Zaugg M, Vogt KE, Ledermann B, Antkowiak B, Rudolph U (2003) General anesthetic actions in vivo strongly attenuated by a point mutation in the GABA_A receptor beta3 subunit. *FASEB J* 17:250-2.
- Kakazu Y, Akaike N, Komiyama S, Nabekura J (1999) Regulation of intracellular chloride by cotransporters in developing lateral superior olive neurons. *J Neurosci* 19:2843-51.
- Kashio M, Tominaga M (2015) Redox Signal-mediated Enhancement of the Temperature Sensitivity of Transient Receptor Potential Melastatin 2 (TRPM2) Elevates Glucose-induced Insulin Secretion from Pancreatic Islets. *J Biol Chem* 290:12435-42.
- Kashio M, Sokabe T, Shintaku K, Uematsu T, Fukuta N, Kobayashi N, Mori Y, Tominaga M (2012) Redox signal-mediated sensitization of transient receptor potential melastatin 2 (TRPM2) to temperature affects macrophage functions. *Proc Natl Acad Sci U S A* 109:6745-50.
- Kettenmann H, Hanisch UK, Noda M, Verkhratsky A (2011) Physiology of microglia. *Physiol Rev* 91:461-553.
- Kim SR, Kim SU, Oh U, Jin BK (2006) Transient Receptor Potential Vanilloid Subtype 1 Mediates Microglial Cell Death In Vivo and In Vitro via Ca²⁺-Mediated Mitochondrial Damage and Cytochrome c Release. *The Journal of Immunology* 177:4322-4329.
- Kimori Y (2011) Mathematical morphology-based approach to the enhancement of morphological features in medical images. *J Clin Bioinforma* 1:33.
- Kiyatkin EA (2013) The hidden side of drug action: brain temperature changes induced by

- neuroactive drugs. *Psychopharmacology (Berl)* 225:765-80.
- Klein RM, Ufret-Vincenty CA, Hua L, Gordon SE (2008) Determinants of molecular specificity in phosphoinositide regulation. Phosphatidylinositol (4,5)-bisphosphate (PI(4,5)P₂) is the endogenous lipid regulating TRPV1. *J Biol Chem* 283:26208-16.
- Klement W, Arndt JO (1991) Pain on injection of propofol: effects of concentration and diluent. *Br J Anaesth* 67:281-4.
- Koizumi S, Shigemoto-Mogami Y, Nasu-Tada K, Shinozaki Y, Ohsawa K, Tsuda M, Joshi BV, Jacobson KA, Kohsaka S, Inoue K (2007) UDP acting at P2Y₆ receptors is a mediator of microglial phagocytosis. *Nature* 446:1091-5.
- Konno M, Shirakawa H, Iida S, Sakimoto S, Matsutani I, Miyake T, Kageyama K, Nakagawa T, Shibasaki K, Kaneko S (2012) Stimulation of transient receptor potential vanilloid 4 channel suppresses abnormal activation of microglia induced by lipopolysaccharide. *Glia* 60:761-70.
- Kraft R, Grimm C, Grosse K, Hoffmann A, Sauerbruch S, Kettenmann H, Schultz G, Harteneck C (2004) Hydrogen peroxide and ADP-ribose induce TRPM2-mediated calcium influx and cation currents in microglia. *Am J Physiol Cell Physiol* 286:C129-37.
- Kubo T, Endo M, Hata K, Taniguchi J, Kitajo K, Tomura S, Yamaguchi A, Mueller BK, Yamashita T (2008) Myosin IIA is required for neurite outgrowth inhibition produced by repulsive guidance molecule. *J Neurochem* 105:113-26.
- Kurganov E, Zhou Y, Saito S, Tominaga M (2014) Heat and AITC activate green anole TRPA1 in a membrane-delimited manner. *Pflugers Arch* 466:1873-84.
- Launay P, Fleig A, Perraud AL, Scharenberg AM, Penner R, Kinet JP (2002) TRPM4 is a Ca²⁺-activated nonselective cation channel mediating cell membrane depolarization. *Cell* 109:397-407.
- Launay P, Cheng H, Srivatsan S, Penner R, Fleig A, Kinet JP (2004) TRPM4 regulates calcium oscillations after T cell activation. *Science* 306:1374-7.
- Lee SP, Buber MT, Yang Q, Cerne R, Cortes RY, Sprous DG, Bryant RW (2008) Thymol and related alkyl phenols activate the hTRPA1 channel. *Br J Pharmacol* 153:1739-49.
- Liang KJ, Lee JE, Wang YD, Ma W, Fontainhas AM, Fariss RN, Wong WT (2009) Regulation of dynamic behavior of retinal microglia by CX3CR1 signaling. *Invest Ophthalmol Vis Sci* 50:4444-51.
- Liao M, Cao E, Julius D, Cheng Y (2013) Structure of the TRPV1 ion channel determined by electron cryo-microscopy. *Nature* 504:107-12.

- Link TM, Park U, Vonakis BM, Raben DM, Soloski MJ, Caterina MJ (2010) TRPV2 has a pivotal role in macrophage particle binding and phagocytosis. *Nat Immunol* 11:232-9.
- Liu Y, Kintner DB, Chanana V, Algharabli J, Chen X, Gao Y, Chen J, Ferrazzano P, Olson JK, Sun D (2010) Activation of microglia depends on Na⁺/H⁺ exchange-mediated H⁺ homeostasis. *J Neurosci* 30:15210-20.
- Macpherson LJ, Dubin AE, Evans MJ, Marr F, Schultz PG, Cravatt BF, Patapoutian A (2007) Noxious compounds activate TRPA1 ion channels through covalent modification of cysteines. *Nature* 445:541-5.
- Madry C, Attwell D (2015) Receptors, ion channels, and signaling mechanisms underlying microglial dynamics. *J Biol Chem* 290:12443-50.
- Mandadi S, Tominaga T, Numazaki M, Murayama N, Saito N, Armati PJ, Roufogalis BD, Tominaga M (2006) Increased sensitivity of desensitized TRPV1 by PMA occurs through PKCepsilon-mediated phosphorylation at S800. *Pain* 123:106-16.
- Mao S, Garzon-Muvdi T, Di Fulvio M, Chen Y, Delpire E, Alvarez FJ, Alvarez-Leefmans FJ (2012) Molecular and functional expression of cation-chloride cotransporters in dorsal root ganglion neurons during postnatal maturation. *J Neurophysiol* 108:834-52.
- Matsui T, Motoki Y, Inomoto T, Miura D, Kato Y, Suenaga H, Hino K, Nojima J (2012) Temperature-related effects of adenosine triphosphate-activated microglia on pro-inflammatory factors. *Neurocrit Care* 17:293-300.
- Matta JA, Cornett PM, Miyares RL, Abe K, Sahibzada N, Ahern GP (2008) General anesthetics activate a nociceptive ion channel to enhance pain and inflammation. *Proc Natl Acad Sci U S A* 105:8784-9.
- McKemy DD, Neuhauser WM, Julius D (2002) Identification of a cold receptor reveals a general role for TRP channels in thermosensation. *Nature* 416:52-8.
- Michaelis M, Nieswandt B, Stegner D, Eilers J, Kraft R (2015) STIM1, STIM2, and Orai1 regulate store-operated calcium entry and purinergic activation of microglia. *Glia* 63:652-63.
- Miyake T, Shirakawa H, Nakagawa T, Kaneko S (2015) Activation of mitochondrial transient receptor potential vanilloid 1 channel contributes to microglial migration. *Glia* 63:1870-82.
- Mohammadi B, Haeseler G, Leuwer M, Dengler R, Krampfl K, Bufler J (2001) Structural requirements of phenol derivatives for direct activation of chloride currents via GABA(A) receptors. *Eur J Pharmacol* 421:85-91.

- Moriyama T, Iida T, Kobayashi K, Higashi T, Fukuoka T, Tsumura H, Leon C, Suzuki N, Inoue K, Gachet C, Noguchi K, Tominaga M (2003) Possible involvement of P2Y₂ metabotropic receptors in ATP-induced transient receptor potential vanilloid receptor 1-mediated thermal hypersensitivity. *J Neurosci* 23:6058-62.
- Nagasawa M, Nakagawa Y, Tanaka S, Kojima I (2007) Chemotactic peptide fMetLeuPhe induces translocation of the TRPV2 channel in macrophages. *J Cell Physiol* 210:692-702.
- Nilius B, Mahieu F, Prenen J, Janssens A, Owsianik G, Vennekens R, Voets T (2006) The Ca²⁺-activated cation channel TRPM4 is regulated by phosphatidylinositol 4,5-bisphosphate. *Embo j* 25:467-78.
- Nilius B, Prenen J, Tang J, Wang C, Owsianik G, Janssens A, Voets T, Zhu MX (2005) Regulation of the Ca²⁺ sensitivity of the nonselective cation channel TRPM4. *J Biol Chem* 280:6423-33.
- Nimmerjahn A, Kirchhoff F, Helmchen F (2005) Resting microglial cells are highly dynamic surveillants of brain parenchyma in vivo. *Science* 308:1314-8.
- Nishimoto R, Kashio M, Tominaga M (2015) Propofol-induced pain sensation involves multiple mechanisms in sensory neurons. *Pflugers Arch* 467:2011-20.
- Numazaki M, Tominaga T, Toyooka H, Tominaga M (2002) Direct phosphorylation of capsaicin receptor VR1 by protein kinase C epsilon and identification of two target serine residues. *J Biol Chem* 277:13375-8.
- Numazaki M, Tominaga T, Takeuchi K, Murayama N, Toyooka H, Tominaga M (2003) Structural determinant of TRPV1 desensitization interacts with calmodulin. *Proc Natl Acad Sci U S A* 100:8002-6.
- Orser BA, Wang LY, Pennefather PS, MacDonald JF (1994) Propofol modulates activation and desensitization of GABA_A receptors in cultured murine hippocampal neurons. *J Neurosci* 14:7747-60.
- Paulsen CE, Armache JP, Gao Y, Cheng Y, Julius D (2015) Structure of the TRPA1 ion channel suggests regulatory mechanisms. *Nature* 520:511-7.
- Peier AM, Moqrich A, Hergarden AC, Reeve AJ, Andersson DA, Story GM, Earley TJ, Dragoni I, McIntyre P, Bevan S, Patapoutian A (2002a) A TRP channel that senses cold stimuli and menthol. *Cell* 108:705-15.
- Peier AM, Reeve AJ, Andersson DA, Moqrich A, Earley TJ, Hergarden AC, Story GM, Colley S, Hogenesch JB, McIntyre P, Bevan S, Patapoutian A (2002b) A heat-sensitive TRP

- channel expressed in keratinocytes. *Science* 296:2046-9.
- Persson AK, Estacion M, Ahn H, Liu S, Stamboulian-Platel S, Waxman SG, Black JA (2014) Contribution of sodium channels to lamellipodial protrusion and Rac1 and ERK1/2 activation in ATP-stimulated microglia. *Glia* 62:2080-95.
- Piao H, Takahashi K, Yamaguchi Y, Wang C, Liu K, Naruse K (2015) Transient receptor potential melastatin-4 is involved in hypoxia-reoxygenation injury in the cardiomyocytes. *PLoS One* 10:e0121703.
- Prinz M, Priller J (2014) Microglia and brain macrophages in the molecular age: from origin to neuropsychiatric disease. *Nat Rev Neurosci* 15:300-12.
- Ransohoff RM, Perry VH (2009) Microglial physiology: unique stimuli, specialized responses. *Annu Rev Immunol* 27:119-45.
- Rosenbaum T, Gordon-Shaag A, Munari M, Gordon SE (2004) Ca^{2+} /calmodulin modulates TRPV1 activation by capsaicin. *J Gen Physiol* 123:53-62.
- Rudolph U, Antkowiak B (2004) Molecular and neuronal substrates for general anaesthetics. *Nat Rev Neurosci* 5:709-20.
- Sasaki M, Takagi M, Okamura Y (2006) A voltage sensor-domain protein is a voltage-gated proton channel. *Science* 312:589-92.
- Sasaki Y, Hoshi M, Akazawa C, Nakamura Y, Tsuzuki H, Inoue K, Kohsaka S (2003) Selective expression of $G_{i/o}$ -coupled ATP receptor P2Y₁₂ in microglia in rat brain. *Glia* 44:242-50.
- Schilling T, Stock C, Schwab A, Eder C (2004) Functional importance of Ca^{2+} -activated K^+ channels for lysophosphatidic acid-induced microglial migration. *Eur J Neurosci* 19:1469-74.
- Scroggs RS, Fox AP (1992) Calcium current variation between acutely isolated adult rat dorsal root ganglion neurons of different size. *J Physiol* 445:639-58.
- Seo JW, Kim JH, Kim JH, Seo M, Han HS, Park J, Suk K (2012) Time-dependent effects of hypothermia on microglial activation and migration. *J Neuroinflammation* 9:164.
- Shi Y, Kim D, Caldwell M, Sun D (2013) The role of Na^+/H^+ exchanger isoform 1 in inflammatory responses: maintaining H^+ homeostasis of immune cells. *Adv Exp Med Biol* 961:411-8.
- Shibasaki K, Ishizaki Y, Mandadi S (2013) Astrocytes express functional TRPV2 ion channels. *Biochem Biophys Res Commun* 441:327-32.
- Shimizu T, Owsianik G, Freichel M, Flockerzi V, Nilius B, Vennekens R (2009) TRPM4

- regulates migration of mast cells in mice. *Cell Calcium* 45:226-32.
- Siddiqui TA, Lively S, Vincent C, Schlichter LC (2012) Regulation of podosome formation, microglial migration and invasion by Ca^{2+} -signaling molecules expressed in podosomes. *J Neuroinflammation* 9:250.
- Smith GD, Gunthorpe MJ, Kelsell RE, Hayes PD, Reilly P, Facer P, Wright JE, Jerman JC, Walhin JP, Ooi L, Egerton J, Charles KJ, Smart D, Randall AD, Anand P, Davis JB (2002) TRPV3 is a temperature-sensitive vanilloid receptor-like protein. *Nature* 418:186-90.
- Sokabe T, Fukumi-Tominaga T, Yonemura S, Mizuno A, Tominaga M (2010) The TRPV4 channel contributes to intercellular junction formation in keratinocytes. *J Biol Chem* 285:18749-58.
- Stein AT, Ufret-Vincenty CA, Hua L, Santana LF, Gordon SE (2006) Phosphoinositide 3-kinase binds to TRPV1 and mediates NGF-stimulated TRPV1 trafficking to the plasma membrane. *J Gen Physiol* 128:509-22.
- Stein V, Nicoll RA (2003) GABA generates excitement. *Neuron* 37:375-8.
- Stock C, Ludwig FT, Hanley PJ, Schwab A (2013) Roles of ion transport in control of cell motility. *Compr Physiol* 3:59-119.
- Story GM, Peier AM, Reeve AJ, Eid SR, Mosbacher J, Hricik TR, Earley TJ, Hergarden AC, Andersson DA, Hwang SW, McIntyre P, Jegla T, Bevan S, Patapoutian A (2003) ANKTM1, a TRP-like channel expressed in nociceptive neurons, is activated by cold temperatures. *Cell* 112:819-29.
- Su W, Kang J, Sopher B, Gillespie J, Aloï MS, Odom GL, Hopkins S, Case A, Wang DB, Chamberlain JS, Garden GA (2015) Recombinant adeno-associated viral (rAAV) vectors mediate efficient gene transduction in cultured neonatal and adult microglia. *J Neurochem*.
- Suzuki M, Mizuno A, Kodaira K, Imai M (2003) Impaired pressure sensation in mice lacking TRPV4. *J Biol Chem* 278:22664-8.
- Takayama Y, Uta D, Furue H, Tominaga M (2015) Pain-enhancing mechanism through interaction between TRPV1 and anoctamin 1 in sensory neurons. *Proc Natl Acad Sci U S A* 112:5213-8.
- Talavera K, Yasumatsu K, Voets T, Droogmans G, Shigemura N, Ninomiya Y, Margolskee RF, Nilius B (2005) Heat activation of TRPM5 underlies thermal sensitivity of sweet taste. *Nature* 438:1022-5.

- Tam WY, Ma CH (2014) Bipolar/rod-shaped microglia are proliferating microglia with distinct M1/M2 phenotypes. *Sci Rep* 4:7279.
- Tan CH, Onsiong MK (1998) Pain on injection of propofol. *Anaesthesia* 53:468-476.
- Togashi K, Hara Y, Tominaga T, Higashi T, Konishi Y, Mori Y, Tominaga M (2006) TRPM2 activation by cyclic ADP-ribose at body temperature is involved in insulin secretion. *Embo j* 25:1804-15.
- Tominaga M, Caterina MJ, Malmberg AB, Rosen TA, Gilbert H, Skinner K, Raumann BE, Basbaum AI, Julius D (1998) The cloned capsaicin receptor integrates multiple pain-producing stimuli. *Neuron* 21:531-43.
- Tremblay M, Sierra A (2014) *Microglia in Health and Disease*. Springer New York.
- Uchida K, Tominaga M (2013) Extracellular zinc ion regulates transient receptor potential melastatin 5 (TRPM5) channel activation through its interaction with a pore loop domain. *J Biol Chem* 288:25950-5.
- Ullrich ND, Voets T, Prenen J, Vennekens R, Talavera K, Droogmans G, Nilius B (2005) Comparison of functional properties of the Ca²⁺-activated cation channels TRPM4 and TRPM5 from mice. *Cell Calcium* 37:267-78.
- Usala M, Thompson SA, Whiting PJ, Wafford KA (2003) Activity of chlormethiazole at human recombinant GABA_A and NMDA receptors. *Br J Pharmacol* 140:1045-50.
- Vanoye CG, Kunic JD, Ehring GR, George AL, Jr. (2013) Mechanism of sodium channel NaV1.9 potentiation by G-protein signaling. *J Gen Physiol* 141:193-202.
- Vennekens R, Menigoz A, Nilius B (2012) TRPs in the Brain. *Rev Physiol Biochem Pharmacol* 163:27-64.
- Vennekens R, Olausson J, Meissner M, Bloch W, Mathar I, Philipp SE, Schmitz F, Weissgerber P, Nilius B, Flockerzi V, Freichel M (2007) Increased IgE-dependent mast cell activation and anaphylactic responses in mice lacking the calcium-activated nonselective cation channel TRPM4. *Nat Immunol* 8:312-20.
- Wake H, Moorhouse AJ, Jinno S, Kohsaka S, Nabekura J (2009) Resting microglia directly monitor the functional state of synapses in vivo and determine the fate of ischemic terminals. *J Neurosci* 29:3974-80.
- Wang BH, Ternai B, Polya GM (1994) Specific inhibition of cyclic AMP-dependent protein kinase by the antimalarial halofantrine and by related phenanthrenes. *Biol Chem Hoppe Seyler* 375:527-35.
- Wang H, Wang B, Normoyle KP, Jackson K, Spitler K, Sharrock MF, Miller CM, Best C,

- Llano D, Du R (2014) Brain temperature and its fundamental properties: a review for clinical neuroscientists. *Front Neurosci* 8:307.
- Wang YY, Chang RB, Waters HN, McKemy DD, Liman ER (2008) The nociceptor ion channel TRPA1 is potentiated and inactivated by permeating calcium ions. *J Biol Chem* 283:32691-703.
- Watanabe H, Vriens J, Suh SH, Benham CD, Droogmans G, Nilius B (2002) Heat-evoked activation of TRPV4 channels in a HEK293 cell expression system and in native mouse aorta endothelial cells. *J Biol Chem* 277:47044-51.
- Watanabe M, Suzuki Y, Uchida K, Miyazaki N, Murata K, Matsumoto S, Kakizaki H, Tominaga M (2015) Trpm7 Protein Contributes to Intercellular Junction Formation in Mouse Urothelium. *J Biol Chem* 290:29882-92.
- Waxman SG, Zamponi GW (2014) Regulating excitability of peripheral afferents: emerging ion channel targets. *Nat Neurosci* 17:153-63.
- Weber KS, Hildner K, Murphy KM, Allen PM (2010) Trpm4 differentially regulates Th1 and Th2 function by altering calcium signaling and NFAT localization. *J Immunol* 185:2836-46.
- Wu LJ, Wu G, Akhavan Sharif MR, Baker A, Jia Y, Fahey FH, Luo HR, Feener EP, Clapham DE (2012) The voltage-gated proton channel Hv1 enhances brain damage from ischemic stroke. *Nat Neurosci* 15:565-73.
- Xiao B, Coste B, Mathur J, Patapoutian A (2011) Temperature-dependent STIM1 activation induces Ca²⁺ influx and modulates gene expression. *Nat Chem Biol* 7:351-8.
- Xu H, Ramsey IS, Kotecha SA, Moran MM, Chong JA, Lawson D, Ge P, Lilly J, Silos-Santiago I, Xie Y, DiStefano PS, Curtis R, Clapham DE (2002) TRPV3 is a calcium-permeable temperature-sensitive cation channel. *Nature* 418:181-6.
- Yamamoto S, Shimizu S, Kiyonaka S, Takahashi N, Wajima T, Hara Y, Negoro T, Hiroi T, Kiuchi Y, Okada T, Kaneko S, Lange I, Fleig A, Penner R, Nishi M, Takeshima H, Mori Y (2008) TRPM2-mediated Ca²⁺ influx induces chemokine production in monocytes that aggravates inflammatory neutrophil infiltration. *Nat Med* 14:738-47.
- Yenari MA, Han HS (2012) Neuroprotective mechanisms of hypothermia in brain ischaemia. *Nat Rev Neurosci* 13:267-78.
- Yevenes GE, Zeilhofer HU (2011) Allosteric modulation of glycine receptors. *Br J Pharmacol* 164:224-36.
- Zeller A, Arras M, Lazaris A, Jurd R, Rudolph U (2005) Distinct molecular targets for the

- central respiratory and cardiac actions of the general anesthetics etomidate and propofol. *FASEB J* 19:1677-9.
- Zheng J (2013) Molecular mechanism of TRP channels. *Compr Physiol* 3:221-42.
- Zhou Q, Wang S, Anderson DJ (2000) Identification of a novel family of oligodendrocyte lineage-specific basic helix-loop-helix transcription factors. *Neuron* 25:331-43.
- Zhou Y, Suzuki Y, Uchida K, Tominaga M (2013) Identification of a splice variant of mouse TRPA1 that regulates TRPA1 activity. *Nat Commun* 4:2399.
- Zhou Y, Wong CO, Cho KJ, van der Hoeven D, Liang H, Thakur DP, Luo J, Babic M, Zinsmaier KE, Zhu MX, Hu H, Venkatachalam K, Hancock JF (2015) Membrane potential modulates plasma membrane phospholipid dynamics and K-Ras signaling. *Science* 349:873-6.
- Zurborg S, Yurgionas B, Jira JA, Caspani O, Heppenstall PA (2007) Direct activation of the ion channel TRPA1 by Ca^{2+} . *Nat Neurosci* 10:277-9.